

3

Ceramic Microforming Process

by

Matthew E. Rosenthal

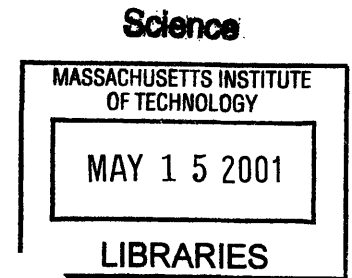
B.S. Aerospace Engineering
Texas A&M University, 1994

SUBMITTED TO THE DEPARTMENT OF MATERIALS SCIENCE AND
ENGINEERING IN PARTIAL FULFILLMENT OF THE REQUIREMENTS FOR THE
DEGREE OF

MASTER OF SCIENCE IN MATERIALS SCIENCE AND ENGINEERING
AT THE
MASSACHUSETTS INSTITUTE OF TECHNOLOGY

JUNE 1998

©1998 Massachusetts Institute of Technology
All rights reserved.



Signature of Author: _____

Department of Materials Science and Engineering
May 8, 1998

Certified by: _____

Sumitomo Electric Industries Professor of Materials Science Engineering
Thesis Supervisor
Michael J. Cima

Accepted by: _____

Linn W. Hobbs
John F. Elliott Professor of Materials
Chairman, Departmental Committee on Graduate Students

Ceramic Microforming Process

by

Matthew E. Rosenthal

Submitted to the Department of Materials Science and Engineering
on May 8, 1998 in the Partial Fulfillment of the
Requirements for the Degree of Master of Science in
Materials Science and Engineering

ABSTRACT

A forming process for creating MEMS and mesoscale ceramic parts with micron scale features has been developed. This micromolding process takes advantage of clean room compatible techniques to create silicon etchings, which are used to create a silicone transfer mold. The silicone molds are used to make numerous sacrificial mold into which ceramic slurry is cast. The wax molds are sacrificed leaving green ceramic parts which are fired to produce the final component.

The process was found to reproduce features as small as 2 μm with a tolerance of $\pm 0.8 \mu\text{m}$ over about a 100 μm length scale. The production of several parts are examined, demonstrating the ability to make stand alone MEMS and mesoscale parts with complex geometries. A non-ceramic application involving precise particle arrangement is also discussed. Observations regarding part quality, defect formation, yield issues, and process enhancement are made, along with a characterization of the dimensional stability of the process. The costs associated with processing silicon molds are also compared to competing processing techniques.

This technique has generated excellent results and has potential to become a major forming tool to fill the materials selection gap in MEMS and mesoscale component design.

Thesis Supervisor: Michael J. Cima

Title: Sumitomo Electric Industries Professor of Materials Science Engineering

TABLE OF CONTENTS

LIST OF ILLUSTRATIONS AND FIGURES	5
LIST OF TABLES	9
ACKNOWLEDGMENTS	10
CHAPTER 1	11
1.1 INTRODUCTION	11
1.2 MEMS AND MESOSCALE DEVICE OVERVIEW	12
1.3 LIMITATIONS	18
1.4 ROLE OF CERAMICS	19
1.5 COMPETING TECHNOLOGIES	23
1.5.1 Non-ceramic Processes	23
1.5.2 Ceramic Processes	26
CHAPTER 2	32
2.1 MICROFORMING PROCESS	32
2.2 PROCESS GOALS	32
2.3 PROCESS DESCRIPTION	33
2.3.1 Initial Approach	33
2.3.2 Evolution of Design	33
2.3.3 Current Method	34
2.3.3.1 Photolithography and Etching	34
2.3.3.1.1 Hot KOH Etching	34
2.3.3.1.2 Deep RIE Etching	35
2.3.3.2 Silicone Master Mold	39
2.3.3.3 Wax Sacrificial Mold	40
2.3.3.4 Slurry Application	40
2.3.3.5 Wax Removal and Sintering	41
2.4 SPECIFIC PARTS	41

2.4.1 PZT Fibers	42
2.4.2 Zirconia	55
2.4.3 Micro Turbine.....	58
2.4.4 Micro Reactor.....	63
2.4.5 HIDE Tooling.....	65
2.5 CONCLUSION	70
CHAPTER 3	71
3.1 PROCESS PERFORMANCE	71
3.1.1 Minimum Feature Size	71
3.1.2 Part Quality.....	83
3.1.3 Yield	91
3.1.4 Dimensional Stability.....	93
3.2 CONCLUSION	101
CHAPTER 4	102
4.1 COST ANALYSIS	102
4.1.1 LIGA Processing	102
4.1.2 Deep RIE Processing.....	103
4.2 COST COMPARISON	103
CHAPTER 5	105
5.1 FUTURE WORK.....	105
5.2 PROCESS IMPROVEMENT.....	105
5.2.1 Quality Control.....	105
5.2.2 Yield Improvement.....	106
5.2.3 Scale Up	106
5.3 CONCLUSION	107
APPENDIX A MICROMOLD TOOLING.....	108
APPENDIX B FIBER TESTING APPARATUS	109
BIBLIOGRAPHY	110

LIST OF ILLUSTRATIONS AND FIGURES

FIGURE 1-1 SCHEMATIC OF SURFACE MICROMACHINED ACCELEROMETER A) AT REST AND B) DURING ACCELERATION	13
FIGURE 1-2 TEXAS INSTRUMENTS DIGITAL LIGHT PROCESSING CHIP.....	14
FIGURE 1-3 CLOSE UP OF 16 μm^2 MICRO MIRRORS	14
FIGURE 1-4 DETAILED VIEW OF A DLP MIRROR ASSEMBLY	15
FIGURE 1-5 MICRO GAS TURBINE ENGINE	16
FIGURE 1-6 PROTOTYPE MICRO UAV	17
FIGURE 1-7 PROTOTYPE SILICON MICRO REACTOR.....	17
FIGURE 1-8 SILICON STRENGTH VS. TEMPERATURE	21
FIGURE 1-9 WEIBULL DISTRIBUTION PLOT OF FAILURE PROBABILITY VS. VOLUME.....	23
FIGURE 1-10 LIGA PROCESS FLOW	25
FIGURE 1-11 LIGA PRODUCED NICKEL MICRO GEARS.....	25
FIGURE 1-12 PYROLIZED POLY(VINYLSILAZANE) PART PRODUCED FROM LIGA MOLDING	26
FIGURE 1-13 FIRED ZrO_2 PART STAMPED WITH LIGA PMMA STRUCTURE.....	27
FIGURE 1-14 FIRED ZrO_2 STAMPED AT A) 12 N/MM^2 AND B) 20 N/MM^2 WITH C) MACHINED METALIC DIE.....	28
FIGURE 1-15 CO-EXTRUSION PROCESS DIAGRAM	29
FIGURE 1-16 CO-EXTRUDED ALUMINA MICRO-PART A) AFTER ONE REDUCTION AND B) AFTER FOUR REDUCTIONS (FIRED)	30
FIGURE 1-17 A) POLYIMIDE STAMPING MOLD AND B) GREEN STAMPED CERIA ZIRCONIA	31
FIGURE 1-18 FIRED CERAMIC FEATURES CREATED BY STAMPING	31
FIGURE 2-1 PHOTOLITHOGRAPHY PATTERNING.....	35
FIGURE 2-2 KOH SILICON ETCHING.....	35
FIGURE 2-3 DEEP RIE PASSIVATION STEP ²⁶	37
FIGURE 2-4 DEEP RIE ETCHING STEP ²⁶	37
FIGURE 2-5 A) STS DRIE TRENCH AND B) SIDEWALL SCALLOPING.....	38

FIGURE 2-6 HIGH ASPECT RATIO PARTS PRODUCED BY DEEP RIE ETCHING	38
FIGURE 2-7 SILICONE MOLDING OF ETCHED SUBSTRATE	40
FIGURE 2-8 WAX MOLDING OF SILICONE MOLD	40
FIGURE 2-9 APPLICATION OF CERAMIC TO WAX MOLD.....	41
FIGURE 2-10 WAX REMOVAL AND SINTERING	41
FIGURE 2-11 WAX MOLD FOR 200 μM A) TRIANGULAR FIBER AND B) SQUARE FIBER	43
FIGURE 2-12 CASTING HEAD, WAX MOLD, AND HOLDER PLATE.....	45
FIGURE 2-13 PZT MOLD FILLING AFTER A) ONE CASTING AND B) FOUR CASTINGS	45
FIGURE 2-14 GREEN FIBERS ON HONEYCOMB DURING WAX MELTING.....	47
FIGURE 2-15 GREEN FIBERS ON PZT POWDER BED	47
FIGURE 2-16 CRUCIBLE SETUP FOR FIBER FIRING	48
FIGURE 2-17 PZT SINTERING SCHEDULE	48
FIGURE 2-18 FIRED TRIANGULAR PZT FIBER.....	49
FIGURE 2-19 FIRED SQUARE PZT FIBER	49
FIGURE 2-20 DISTORTED FIRED FIBERS ON CRACKED PZT BED	50
FIGURE 2-21 FIRED FIBERS WITH SINTERED PZT POWDERS	50
FIGURE 2-22 FIRED COMMERCIAL PZT FIBERS A) EXTRUDED AND B) DICED.....	51
FIGURE 2-23 FIRED MICROMOLDED PZT FIBER CROSS SECTION AND MICROSTRUCTURE .	52
FIGURE 2-24 FIRED PZT FIBER WITH FEATURE	53
FIGURE 2-25 INTERCONNECTED MICROMOLDED FIBER ARRAY.....	54
FIGURE 2-26 SELECTIVELY ELECTRODED FEATURED FIBERS IN A MATRIX	54
FIGURE 2-27 SILICON ETCHING FOR ZIRCONIA PART.....	56
FIGURE 2-28 FIRED ZIRCONIA PART WITH SILICON ETCH PLANES	56
FIGURE 2-29 FILLING DEFECTS IN FIRED ZIRCONIA PART.....	57
FIGURE 2-30 FIRED ALUMINA MICRO TURBINES PRODUCED FROM NON-AQUEOUS SLURRY	61
FIGURE 2-31 FIRED ALUMINA MICRO TURBINES PRODUCED FROM AQUEOUS SLURRY.....	62
FIGURE 2-32 FIRED ALUMINA MICRO REACTOR	64
FIGURE 2-33 DETAIL OF CHANNEL IN ALUMINA MICRO REACTOR.....	65

FIGURE 2-34 CCL ₄ HIDE SILICON ETCHING OF 2 μM HOLES	66
FIGURE 2-35 COPPER PARTICLES (1 μM DIST.) IN SILICON AFTER THREE APPLICATIONS ..	67
FIGURE 2-36 1.58 μM SILICA SPHERES IN SILICON SUBSTRATE	68
FIGURE 2-37 A) WAX MOLD OF HIDE ETCHING AND B) COPPER PARTICLES IN DAMAGED WAX MOLD.....	68
FIGURE 2-38 HIDE EMBOSSING TOOL IN FIRED ALUMINA.....	69
FIGURE 3-1 GEOMETRIC TEST FEATURES IN A) SILICON AND B) FIRED CERAMIC.....	72
FIGURE 3-2 MINIMUM NEGATIVE TEST FEATURE (1,4) IN A) WAX AND B) FIRED ALUMINA	73
FIGURE 3-3 UNSUCCESSFUL MINIMUM NEGATIVE TEST FEATURE (1,4) IN FIRED ALUMINA	73
FIGURE 3-4 MINIMUM POSITIVE TEST FEATURE (5,4) IN A)WAX AND B) FIRED ALUMINA	74
FIGURE 3-5 CIRCULAR FEATURE (3,1) IN FIRED ALUMINA	74
FIGURE 3-6 SQUARE FEATURE (3,2) IN FIRED ALUMINA	74
FIGURE 3-7 SMALLEST RESOLVABLE SQUARE FEATURE (4,2) IN FIRED ALUMINA	75
FIGURE 3-8 SMALLEST RESOLVABLE CIRCULAR FEATURE (4,1) IN FIRED ALUMINA.....	75
FIGURE 3-9 HIGH AR (6) STATOR TRAILING EDGE IN FIRED ALUMINA.....	76
FIGURE 3-10 HIGH AR (6) STATOR TRAILING EDGE WITH TAPER IN FIRED ALUMINA	76
FIGURE 3-11 HIGH AR (7.5) TURBINE ROTOR BLADE TRAILING EDGE.....	77
FIGURE 3-12 HIGH AR (7.5) TURBINE STATOR BLADES	77
FIGURE 3-13 CROSS SECTION OF TOP EDGE OF HIGH AR (7.5) TURBINE BLADE IN FIRED ALUMINA	78
FIGURE 3-14 HIGH AR (6.5) FIRED ALUMINA A) OUTSIDE AND B) INSIDE CORNER DETAIL	78
FIGURE 3-15 SCALLOPED SIDEWALLS OF SILICON ETCHING	79
FIGURE 3-16 HIGH AR (6.5) TURBINE BLADE WITH REPRODUCED ETCH RELICS.....	80
FIGURE 3-17 HIGH AR (7.5) TURBINE BLADE WITHOUT ETCHING RELICS IN FIRED ALUMINA	80

FIGURE 3-18 CLOSELY PACKED $<2\mu\text{m}$ PATTERN FROM HIDE ETCHING IN FIRED ALUMINA	81
FIGURE 3-19 FIRED ALUMINA DIMENSIONAL TEST SQUARES	82
FIGURE 3-20 FIRED ALUMINA LINES FORMING TEXTURED CERAMIC	82
FIGURE 3-21 VOID FORMATION DUE TO SHRINKAGE DURING DRYING	86
FIGURE 3-22 SQUARE PZT FIBERS WITH SHRINKAGE VOIDS.....	86
FIGURE 3-23 PZT FIBERS AND ALUMINA MICRO TURBINES CREATED FROM FLOCCULATED AND DISPERSED SLURRIES.....	87
FIGURE 3-24 MICROMOLDED PZT SETTER.....	88
FIGURE 3-25 PZT FIBERS A)FIRED ON MICROMOLDED SETTER (TOP) AND B) PZT POWDER BED (BOTTOM)	88
FIGURE 3-26 EFFECT OF CONTACT ANGLE ON MOLD FILLING	90
FIGURE 3-27 FIBER HANDLING WITH FORKLIFT TWEEZERS	92
FIGURE 3-28 SILICON ARRAY OF $12\ \mu\text{m}$ SQUARES.....	94
FIGURE 3-29 ACTUAL AND EXPECTED CHANGE ACROSS SEVERAL WAX MOLDS OVER 93 μm	98
FIGURE 3-30 ACTUAL AND EXPECTED CHANGE ACROSS SEVERAL FIRED PARTS OVER 93 μm	99
FIGURE 5-1 PROPOSED CONTINUOUS CASTING SETUP FOR PZT FIBERS.....	107

LIST OF TABLES

TABLE 1-1 MECHANICAL AND THERMAL PROPERTIES OF MATERIALS ⁴	20
TABLE 1-2 FRACTURE TOUGHNESS OF VARIOUS MATERIALS.....	22
TABLE 2-1 PZT RECIPE.....	43
TABLE 2-2 MICROMOLDED FIBER TESTING RESULTS	52
TABLE 2-3 SAMPLE AQUEOUS ALUMINA SLURRY RECIPE.....	59
TABLE 2-4 SAMPLE SOLVENT BASED ALUMINA SLURRY RECIPE	59
TABLE 3-1 DIMENSIONAL CHANGES ACROSS PROCESS STEPS (12 μm LENGTH SCALE)	95
TABLE 3-2 DIMENSIONAL CHANGES ACROSS PROCESS STEPS (93 μm LENGTH SCALE)	95
TABLE 3-3 DIMENSIONAL CHANGES ACROSS MULTIPLE MOLDS OVER 93 μm	98
TABLE 3-4 DIMENSIONAL CHANGE ACROSS FIRED PARTS OVER 93 μm	99
TABLE 4-1 CLEAN ROOM COSTS FOR A TYPICAL DRIE PROCESS RUN	103

ACKNOWLEDGMENTS

This work would not be possible without the support and motivation of several individuals:

- Professor Michael Cima. Professor Cima allowed me to explore the field of MEMS in a way that I had not previously imagined. He gave me the opportunity to participate on the ground floor of an exciting process, and provided me the latitude to chart my own course during its development. Thanks for your guidance and an incredible learning experience!
- Barbara Layne, John Centorino, and Lenny Rigione. Without these people's support and resourcefulness, nothing would ever get done in the lab. Thanks for keeping everything running smoothly!
- The CPRL Graduate Students. I could not have asked for a better group of people to be colleagues with. Thanks to everyone for answering my many questions, and for being a wonderful group of friends!
- Mindy Tupper, Tae Hwan Yu, Aaron Prazan, and Michael Liberatore. My partners on the micromolding team. Thanks for all the ideas and for helping make the process what it is today!
- Hillary Faye. My fiancée who has waited a long time for our big day. Her love and support keeps me going. Thank you for being so patient and for putting up with me!
- The Faye Family. Being only a stones throw away, the Faye Family was always there. Thanks for everything you have done for us!
- The Rosenthal Family. My parents and sister who have always believed in my goals and dreams. Thank you for supporting everything I do and for being the best family I could ever hope for!

Chapter 1

1.1 Introduction

Micro-electromechanical Systems (MEMS) are a class of machines which have rapidly evolved over the last decade. They are devices which sense, actuate, and pump, much in the same way as their macroscopic counterparts, only these machines reside on microchips, and are characterized by their micron sized dimensions. The most common MEMS device is found in almost every automobile in production; an accelerometer on a chip senses the impact of a collision and instantaneously triggers the airbag to cushion the blow.

Mesoscale devices are machines slightly larger than MEMS with millimeter sized parts and features. One such example, a miniature pacemaker implant, contains several parts which can be as small as 4 mm, yet must be machined to very tight tolerances.¹ Creating parts this small can be a challenge, requiring expensive specialized equipment. Fabrication of these devices is commonplace, however, as more specialized applications are developed, the materials base must be expanded.

Most MEMS devices are made of silicon, the same material used to create microprocessors. These devices can be easily mass produced using machinery and techniques common to the semiconductor industry. Silicon has proven to be a viable material from which to make MEMS devices, as silicon processing methods have been established for many years. However, silicon is not robust in harsh environments, such as elevated temperatures and corrosive atmospheres. Designers are turning to other materials to fill the needs of advanced designs requiring resistance to heat, oxidation, and damage.

There are several conventional techniques used to fabricate very small metal, plastic, and ceramic parts. Some of these processes are reviewed to examine their suitability for forming components for MEMS and mesoscale devices. Alternate methods

of production are being explored to expand the manufacturing avenue for ceramic MEMS parts. One such method, developed at the Ceramics Processing Research Lab, is the focus of this work.

1.2 MEMS and Mesoscale Device Overview

MEMS are machines with parts on the micron scale. These parts are integrated together with a computer controller to form the "system", which is then employed for its specific application. MEMS devices are not only small but inexpensive to produce thanks to the established infrastructure and techniques of the integrated circuit industry. Common MEMS devices include accelerometers, pressure sensors, mirror arrays, and fluidic devices.

MEMS devices have been in use for several years. The micro-accelerometer described in the introduction is a simple surface micromachined device on a chip capable of detecting accelerations less than ± 10 milli-g and as high as $\pm 50g$. The device consists of a silicon micromachined proof mass connected to anchors by flexible silicon tethers (Figure 1-1). A center plate rests between two fixed capacitor plates. The plate moves during accelerations creating a change in capacitance. The resulting voltage change is sensed and converted to an acceleration. The ADXL50 chip, introduced by Analog Devices in 1991, is one example of this type of device. This \$5 component has greatly reduced the costs associated with the electronics package in automotive air bags. New models are capable of sensing acceleration in two axis and contain all necessary electronics on one single chip to form a low cost, high performance sensor. Micro-accelerometers are available for use in consumer products such as car alarms and computer peripherals, as well as in industrial settings for vibration sensing and shock detection.^{2,3}

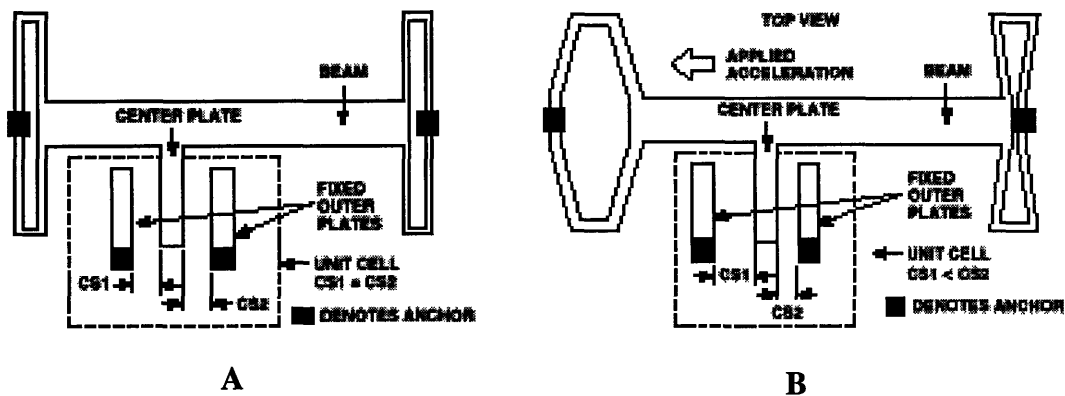


Figure 1-1 Schematic of Surface Micromachined Accelerometer A) at Rest and B) During Acceleration²

The HP Ink Jet Print Head is probably the largest volume MEMS device on the market today. The heart of the device consists of several micromachined orifices, behind which reside tiny heaters. A drop of ink is expelled each time one of the heaters is activated. This technology has brought about cheap color printing and resolutions approaching laser quality. The widespread popularity of ink jet printers is a testimony to the success caused by these little devices.⁴

Even more complex devices are now becoming available in the marketplace. The Digital Light Processing chip developed by Texas Instruments is one such example. The chip consists of an array of over half a million adjustable micro mirrors used to digitally project an image onto a large screen (Figure 1-2). The DLP provides a noise free image with precise reproduction of gray scale and colors. It is more efficient than liquid crystal displays as it depends on reflected rather than polarized light, and provides a sharper picture through its 1 μm spaced 16 μm^2 mirrors, providing a 90% reflective surface (Figure 1-3 and Figure 1-4).^{5,6}

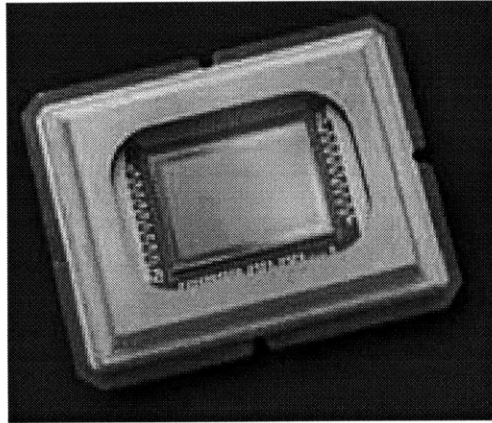
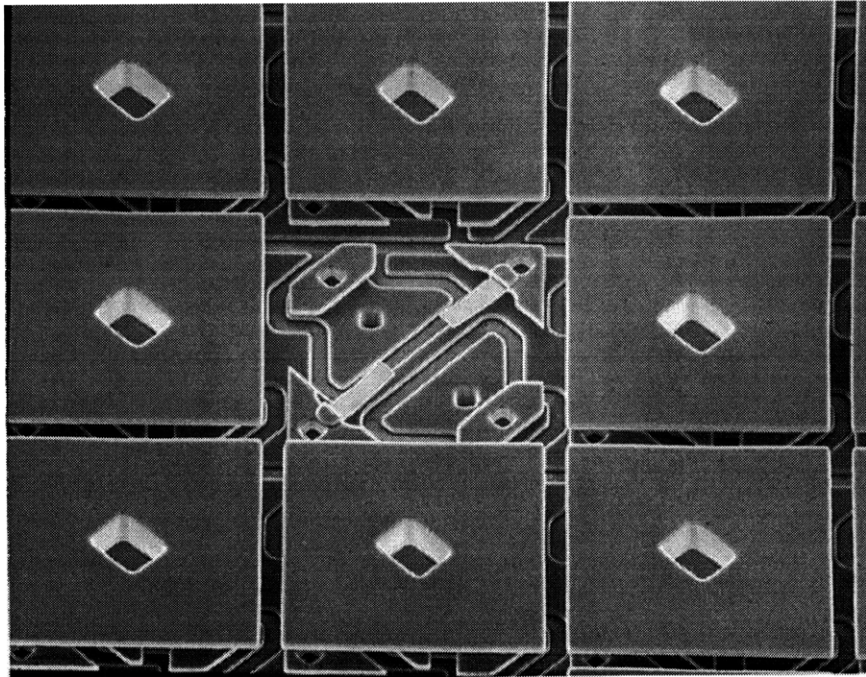


Figure 1-2 Texas Instruments Digital Light Processing Chip⁵



**Figure 1-3 Close Up of 16 μm^2 Micro mirrors
(One Mirror Removed to Show Detail Below)⁵**

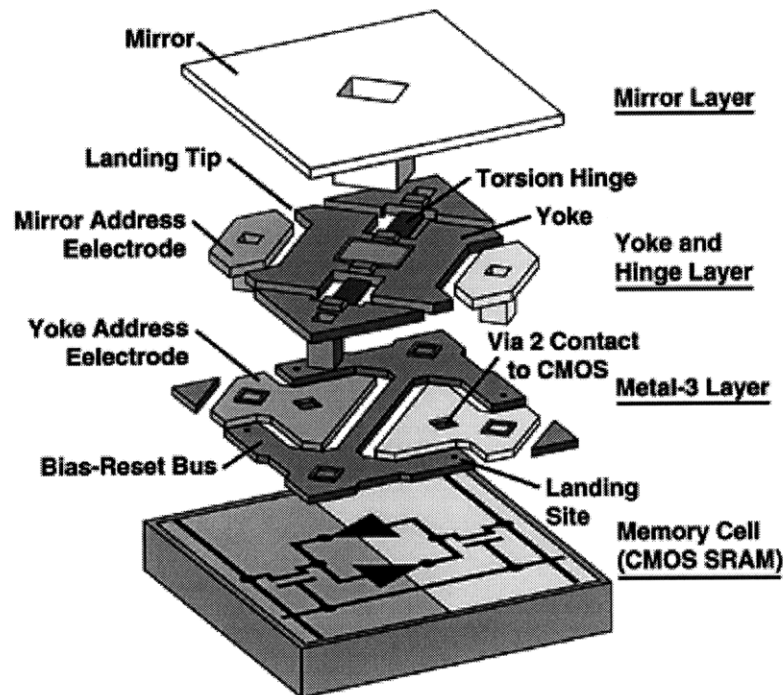


Figure 1-4 Detailed View of a DLP Mirror Assembly⁵

Applications more elaborate than the commercial products mentioned above are the subject of intense research. The micro turbine engine project at MIT is an example of one such application (Figure 1-5).⁷ The goal of the microturbine project is to produce a device that can deliver power at high density with a turbine disk approximately the size of a shirt button. These devices are currently fabricated out of silicon, however, in order to achieve elevated power efficiencies, a higher operating temperature (1700 K) is necessary. The final version of the turbine will require materials capable of handling the hot, corrosive environments encountered in the combustion sections of the device, as the mechanical properties of silicon degrade with increasing temperature. Designers are considering ceramics such as silicon carbide (SiC) as a possible solution. The microforming process described here has successfully produced turbine disks from alumina (Al₂O₃) as a proof of concept.

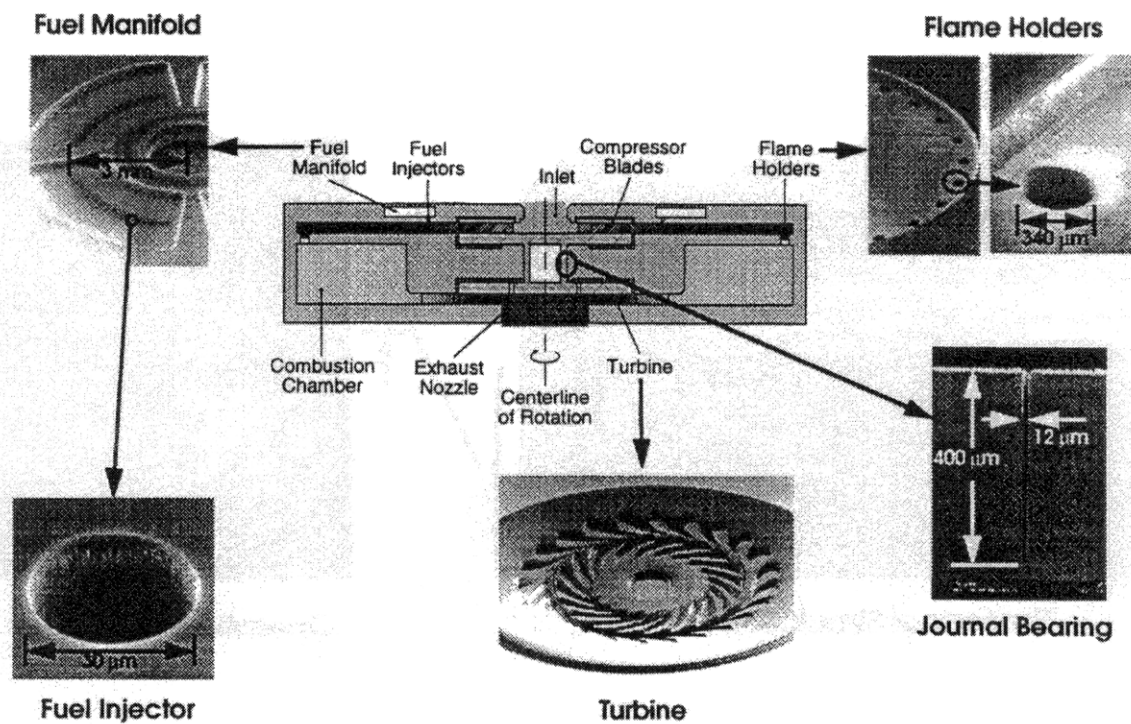


Figure 1-5 Micro Gas Turbine Engine⁷

Mesoscale devices are a class of machines that bridge the gap between MEMS devices and conventional machines.⁸ Devices on the mesoscale have been in production for several years. Miniature pacemakers, containing several small high precision parts, can be implanted into cardiac patients with minimally invasive surgery. Production of these devices relies on high precision machining and injection molding techniques. Other devices such as a micro un-piloted autonomous vehicle (UAV), fluidic release devices, and chemical reactors are subjects of current research.

There are several potential applications for devices of this scale. Troops could deploy low cost micro UAV's (Figure 1-6) on the battlefield to transmit back real time surveillance.⁹ Small fluidic release devices could administer tiny amounts of chemicals for drug delivery or analysis.¹⁰ Finally, micro reactors could produce small amounts of volatile chemicals on demand, or act as field deployable sensing devices for hazardous materials (Figure 1-7).¹¹ These applications are only examples of the potential mesoscale

devices have in several industries. However, manufacturing technologies must be developed to produce these tiny devices out of materials suitable for the task.

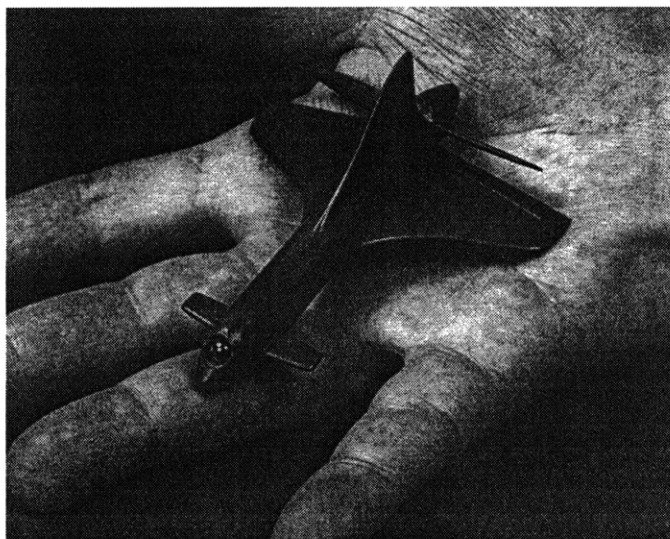


Figure 1-6 Prototype Micro UAV⁹

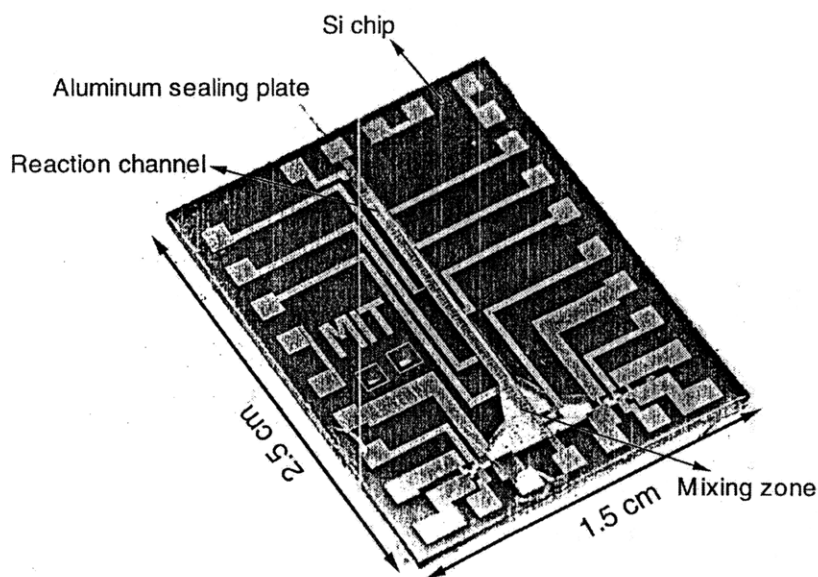


Figure 1-7 Prototype Silicon Micro Reactor¹¹

1.3 Limitations

MEMS and mesoscale devices have a number of limitations. They are susceptible to vibration, temperature, shock, fatigue, and corrosion. The delicate parts found in small machines must be able to withstand the very same forces machines on a macro scale experience. Mass production of MEMS devices can make them relatively inexpensive to replace, however, mesoscale devices often consist of many tiny, inaccessible parts, and individual component replacement can be difficult. Finally, device designs are entering an era where traditional materials such as silicon are not suitable for the desired operating conditions.

The materials out of which devices are constructed must change to meet the specific needs of more complex and exotic designs. Silicon processing techniques adopted from the IC industry have been the mainstay of MEMS production, however, there is a growing need for materials with properties superior to silicon. Advanced concepts, such as the micro reactor, require materials that can withstand the unique operating conditions of the device. Plastic, metal, and silicon are not suitable for use in many of these specialized environments.

There are several advantages to expanding the materials selection base for MEMS and mesoscale devices. The micro UAV could take advantage of high strength low density materials, as well as employ piezoelectric actuators to manipulate its flight surfaces. Applications such as the micro reactor or micro turbine would greatly benefit from the higher operating temperatures and oxidation resistance offered by ceramic materials. While these devices are currently made out of silicon, limitations imposed by the material properties of silicon prevent operation at optimal performance levels. The potential benefits of utilizing ceramics in these devices to overcome the deficiencies of silicon warrant the expansion of the materials selection base for mesoscale and MEMS parts.

1.4 Role of Ceramics

Only in the last 40 years have a class of materials known as technical ceramics been developed. Technical ceramics are a unique class of materials which exhibit properties suitable for high temperature corrosive environments. They also offer increased strength at low densities, making them a viable structural material. Special classes of ceramics, such as lead zirconate titanate (PZT), exhibit piezoelectric properties making them suitable for actuation and sensing applications. Insertion of technical ceramics into systems as both structural and non-structural components has been the subject of intense research. Turbine manufacturers are considering ceramics and ceramic composites as hot section components for aircraft and power generating engines. The high temperature durability of ceramics offers the ability to increase turbine temperatures, resulting in improved efficiency, increased power output and reduced emissions.¹² Oxide-oxide ceramic composites are of particular interest because of their inherent oxidation resistance and non-catastrophic failure modes.¹³ Expanding the materials selection tool box for designers is important as more innovative designs are considered. In light of recent advances in ceramic materials, it is only logical that they be considered for mesoscale and MEMS devices.

Understanding the properties of ceramics in comparison to other materials is necessary before they can take their place as a viable material for microforming. Table 1-1 lists properties of several materials used in mesoscale and MEMS production.⁴

Material	Yield (GPa)	Modulus (GPa)	Density (g/cm ³)	Thermal Conductivity (W/cm°C)	Thermal Expansion (xE-6/°C)
Diamond	53	1035	3.5	20	1.0
SiC	21	700	3.2	3.5	3.3
Al ₂ O ₃	15.4	530	4.0	0.5	5.4
Si ₃ N ₄	14	385	3.1	0.19	0.8
SiO ₂	8.4	73	2.5	0.014	0.55
AlN	N/A	260	3.3	0.301	4.03
Si	7.0	190	2.3	1.57	2.33
Steel	4.2	210	7.9	0.97	12
W	4.0	410	19.3	1.78	4.5
Mo	2.1	343	10.3	1.38	5.0
Al	0.17	70	2.7	2.36	22
Au	0.13	57	19.3	2.97	14.2

Table 1-1 Mechanical and Thermal Properties of Materials⁴

Silicon has elastic properties similar to that of steel, but is less dense and has a higher thermal conductivity. Unfortunately, silicon is a brittle material, and is therefore subject to fracture from mechanical shock. Ceramic materials such as Al₂O₃ also experience brittle failure, however, they can have more than twice the yield stress and half the thermal conductivity of silicon. Mechanical properties of silicon also begin to degrade as temperature increases (Figure 1-8), thus silicon is less than ideal for high temperature applications.¹⁴

Other mechanical properties of ceramics, such as fracture toughness, are also superior to silicon (Table 1-2), although metals still have almost an order of magnitude higher K_{IC}.¹⁵ Nevertheless, higher strength and lower thermal conductivity ceramics can be used to take the place of metals and plastics in several applications. Successfully microformed ceramics can become a viable material alternative in environments where shock and brittle fracture are not a concern. Applications requiring piezoelectric properties, such as ultrasonic imaging devices or active composites, must use ceramic materials to achieve the desired electromechanical responses.

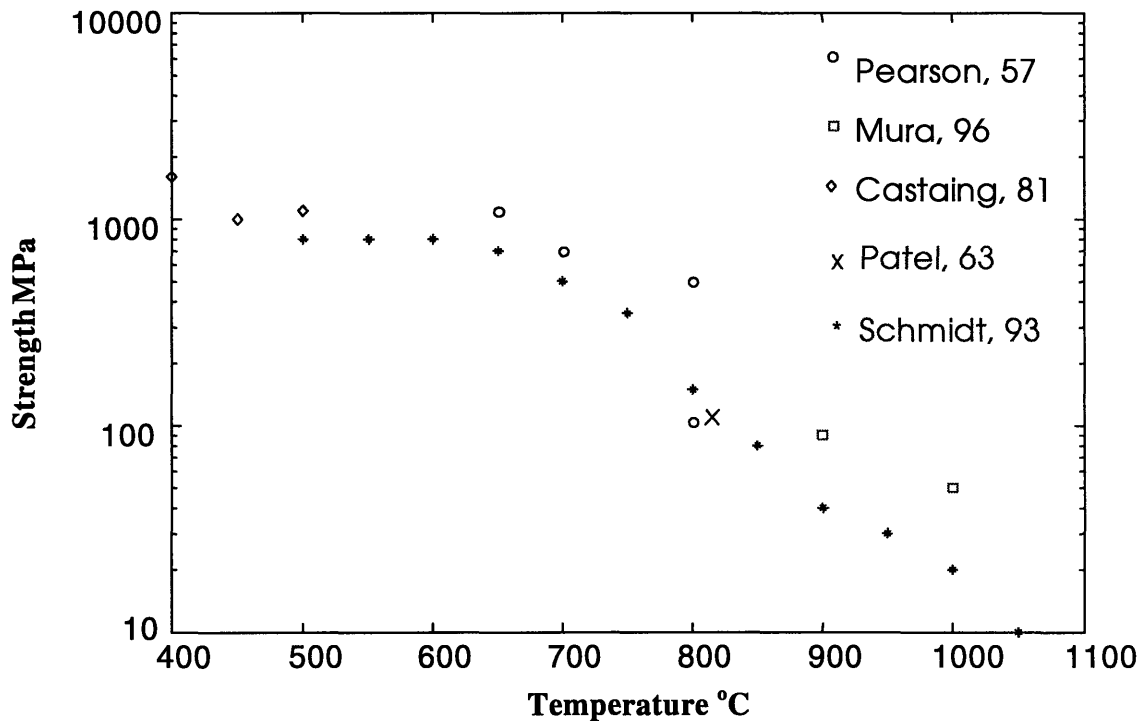


Figure 1-8 Silicon Strength vs. Temperature¹⁴

Incorporation of ceramics in structural applications has historically been a challenge for designers. Insertion of ceramic parts in mechanical systems is limited by brittle failure due to growth of cracks exceeding critical size. Ceramic materials fail catastrophically at a flaw of critical size, as demonstrated by Griffith crack theory. The following equation relates fracture stress σ_f to the flaw size (c), elastic modulus (E), fracture energy (γ), and a geometric constant (A):

$$\sigma_f = A \left(\frac{E\gamma}{c} \right)^{1/2}$$

Weibull flaw distribution theory states that as part volume decreases, the probability of it containing a flaw of critical size also decreases. This assumes that any failure at any flaw will result in complete part failure (weakest link), and that flaws are evenly distributed

throughout a part. The smaller the part, the less chance of there being a flaw that will lead to failure. A Weibull distribution for the probability of survival (P_s) is given by:

$$P_s = 1 - P_f = \exp\left[-\frac{V}{V_o}\left(\frac{\sigma - \sigma_u}{\sigma_o}\right)^m\right] \text{ for } \sigma > \sigma_u$$

where $\sigma_u=0$ for ceramics. A plot of probability of failure versus part volume can be obtained by normalizing the volume, and applying experimentally derived, material specific constants to the above equation. Figure 1-9 demonstrates that as part volume decreases, so does the probability of failure due to flaws. Therefore, the small volume of MEMS parts inherently reduces the probability of failure due to the part containing a crack of critical length.

One of the major challenges of bringing ceramics into the MEMS design community is the forming of raw materials into usable components. Achieving such a goal with the required degree of accuracy and cost effectiveness will allow production of advanced designs mentioned earlier. This work centers on attempts to form components for these devices using a newly developed microforming technique.

Material	K_{IC} (MPa•m ^{1/2})
Si	0.6
Al ₂ O ₃ (Single Crystal)	2
Al ₂ O ₃ (Polycrystalline)	3.5-4.0
SiC (Polycrystalline)	3.0-3.5
ZrO ₂ (Polycrystalline)	2
Si ₃ N ₄ (Sintered)	4-6
Al alloys	33-44
Steel	44-66

Table 1-2 Fracture Toughness of Various Materials

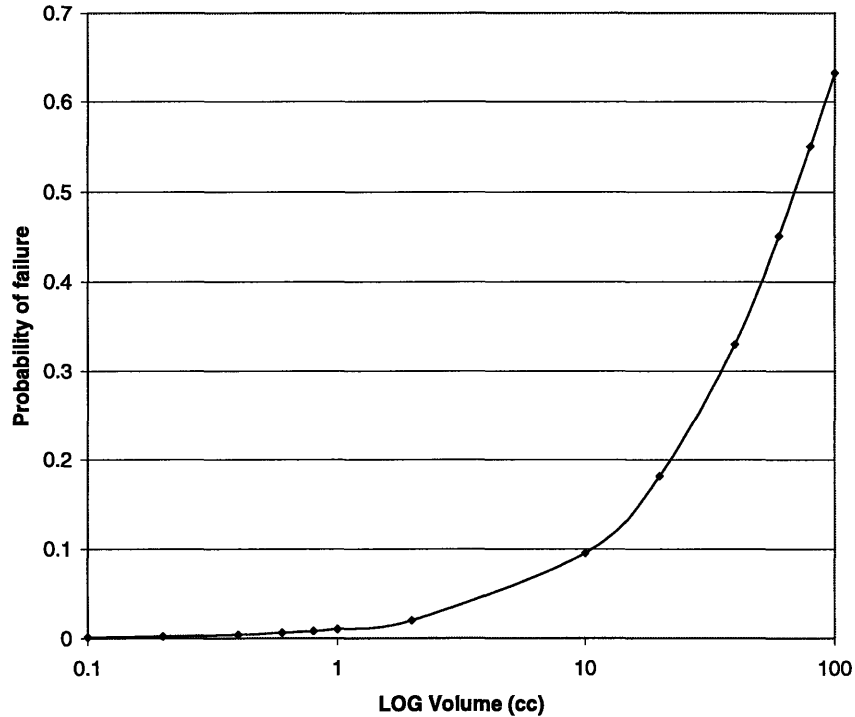


Figure 1-9 Weibull Distribution Plot of Failure Probability vs. Volume
 ($\sigma=400\text{MPa}$, $\sigma_0=400\text{MPa}$, $m=10$; $V_0=100$)

1.5 Competing Technologies

There are several methods used to create MEMS and mesoscale parts, many of which are simply refinements in traditional machining techniques, although most are limited to non-ceramics. Several forming methods are based on LIGA derived micro molds, a costly forming process designed to create high aspect ratio structures. Techniques such as slurry casting and tape embossing utilize these micro molds to form the ceramic structures.

1.5.1 Non-ceramic Processes

Refinements in conventional forming techniques, such as lathe milling, end milling, and injection molding, have made possible the production of small precision

components. Mold inserts, used for injection molding and compression molding, can be made with laser ablation techniques, micro milling, and electro-discharge machining. These techniques have the ability to form metals and plastics to within millimeter and micron accuracy.¹⁶ Other methods such as milling are capable of a positioning accuracy of 0.0025 mm and resolutions of 0.001mm.¹⁷ Unfortunately, machining of ceramics results in a large occurrence of surface flaws that can act as crack initiation sites.

Injection molding of plastics is employed in the manufacture of compact disks (low aspect ratio), and higher aspect ratio parts can be produced with LIGA derived mold inserts. These inserts can produce parts with very high aspect ratios (up to 600) out of amorphous (PMMA, PC) and semi-crystalline (POM, PVDF) thermoplastics.¹⁸ One limitation of injection molding is that evacuation holes must be provided to prevent the trapping of air during material infusion. Placement of these holes becomes difficult as feature size decreases.

A process that is capable of creating high aspect ratio micromolds is the LIGA method. LIGA is an acronym for the German Lithographie (lithography), Galvanoformung (electroforming), and Abformung (molding) process, which was developed in late 1970's for slotted nozzles used in uranium isotope separation. The process (Figure 1-10) used X-rays from a synchrotron source to pattern a thick PMMA resist. The PMMA was developed to produce a high aspect ratio polymer structure. The inverse microstructure pattern was then formed through electroplating of a metal such as copper or nickel (Figure 1-11). Other polymer molds could be made from this metal mold. LIGA has proven to be a good tool for creating high aspect ratio metallic parts and micromolds, with applications in injection molding, embossing, and micromolding.⁴ The cost and accessibility of synchrotron X-ray radiation necessary to produce LIGA molds, however, can be prohibitive, as there are only a handful of sources available throughout the country. Consequently, the processing of LIGA forms is not compatible with the existing microfabrication infrastructure, and new technologies such as deep reactive ion etching are coming online which are capable of obtaining similar results.

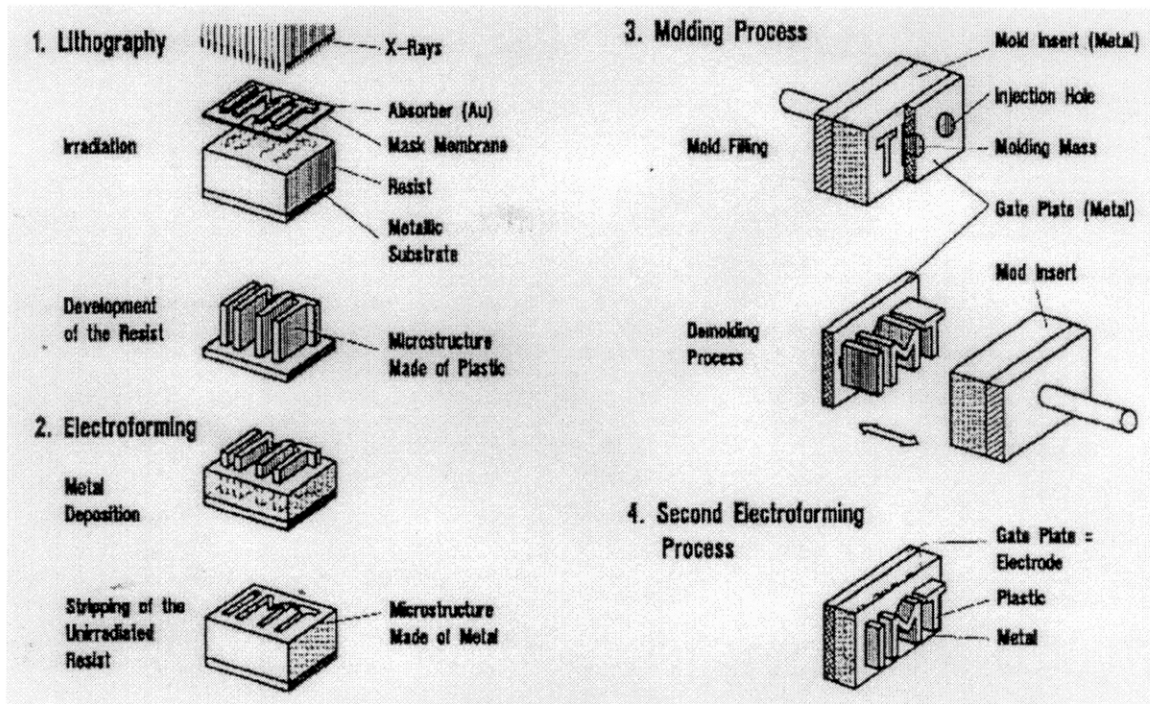


Figure 1-10 LIGA Process Flow⁴

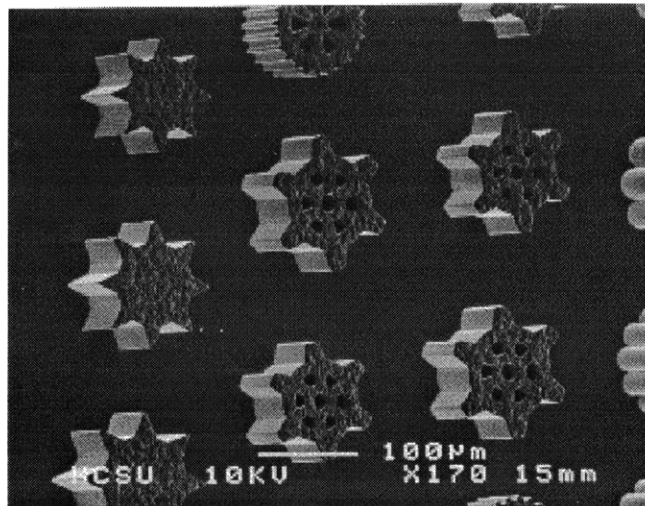


Figure 1-11 LIGA Produced Nickel Micro Gears⁴

1.5.2 Ceramic Processes

Several adaptations of conventional machining techniques have been used to form micro ceramics. Modifications of thermoplastic injection molding processes, ultrasonic machining, mold casting, and embossing are some examples of forming processes which have been used to create small ceramic parts. Tools created through the LIGA process have also been frequently used in micro ceramic forming processes. This section describes several methods used to create ceramic micro forms.

Many processes utilize LIGA derived molds as embossing tools for ceramic tapes, or as sacrificial molds into which ceramic material was cast. Figure 1-12 shows a complex part created by casting a preceramic polymer, poly(vinylsilazane), into a LIGA produced PMMA mold. The polymer was pyrolyzed to form a silicon nitride ceramic with good feature resolution. The walls of the channels were very smooth, although the top surface roughness was a result of the molding used.¹⁹ Limitations of pyrolysis included large shrinkage during the reaction, and the limited types of ceramic that can be created through polymer pyrolysis reactions.

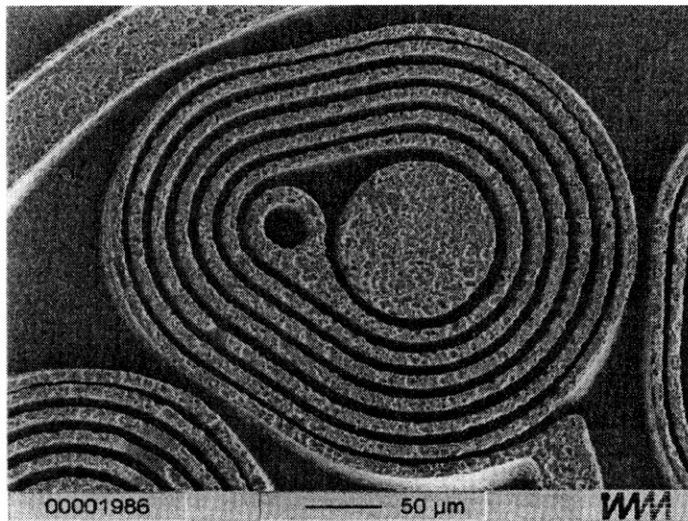


Figure 1-12 Pyrolyzed Poly(vinylsilazane) Part Produced from LIGA Molding¹⁹

Ceramic structures have also been formed by stamping LIGA produced molds onto green ceramic tapes. Figure 1-13 shows a ZrO_2 part that was created with a PMMA mold produced by the LIGA technique. The mold was 200 μm high with 50 μm hexagonal columns (for an aspect ratio of 4), and was stamped onto a green ZrO_2 tape. The low mechanical strength of PMMA required that low stamping pressures be used (6 N/mm^2), resulting in forms that were not as deep as the original mold. Other stamping attempts using machined and LIGA produced metallic dies were performed at higher pressures (12-20 N/mm^2) to achieve better pattern transfers (Figure 1-14). However, the large mechanical forces necessary to achieve complete mold transfer illustrate one of the difficulties of stamping: separation from the die resulting in distortion and cracking of the green tape.²⁰

Both of these processes used LIGA molding. Unfortunately, the high intensity X-ray radiation required to make these molds is very costly and not readily accessible, making LIGA incompatible with current processing technology. The economic feasibility of LIGA is questionable, and therefore other processing options were explored. These included adaptations of conventional processing techniques, and examination of developing processes utilizing alternate technology.

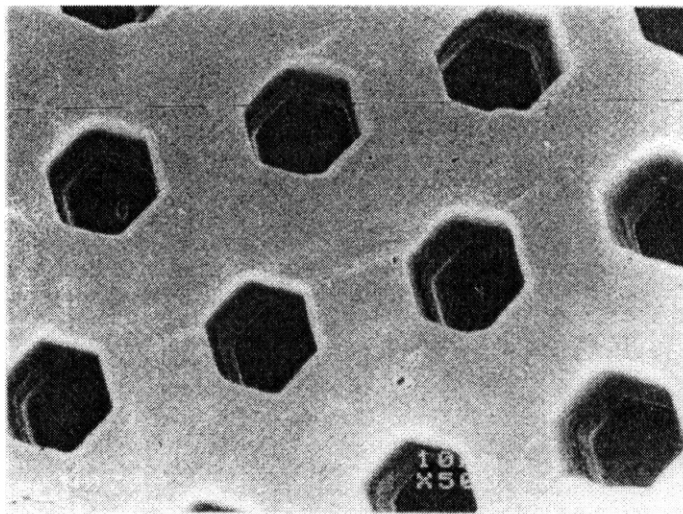


Figure 1-13 Fired ZrO_2 Part Stamped with LIGA PMMA Structure²⁰

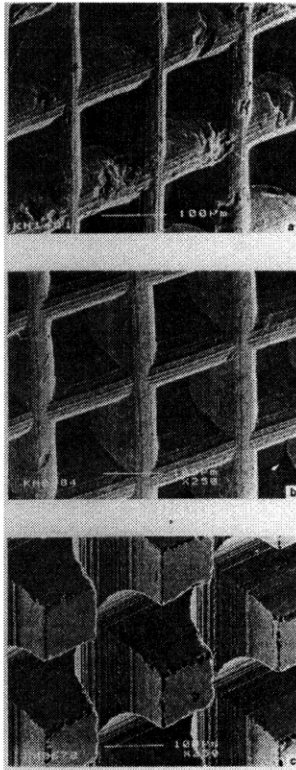


Figure 1-14 Fired ZrO₂ Stamped at a) 12 N/mm² and b) 20 N/mm² with c) Machined Metallic Die²⁰

There are several conventional machining techniques available to create ceramic parts with mesoscale features. Ultrasonic machining uses a steel tool and ultrasonic vibration to cut into a ceramic material. This method has proven the ability to create features as small as 0.76 mm.²¹ Laser drilling is capable of creating blind vias and through holes in ceramic substrates with feature resolution down to 1-2 μm, although complex raised patterns can become very expensive to produce.²² Other techniques, such as micro endmilling have shown promise as new forming tools in silicon and polymers.⁴ However, as pointed out earlier, machining of ceramics can lead to unwanted surface flaws and only certain types can be successfully machined.

Micro extrusion has been examined as a novel method for forming ceramic parts. A co-extrusion process has been developed to create axisymmetric ceramic forms with two dimensional micron sized features. This co-extrusion process progressively

compressed the shape through a series of reduction dies. The initial ceramic form was embedded in a matrix of carbon black and forced through progressively smaller dies (Figure 1-15). The form was compressed until the desired dimensions were achieved. Initial and final extruded shapes are shown in Figure 1-16. This method had limitations in that the smallest feature size appeared to be around 10 μ m, and the final sintered part appeared to lose some of its initial resolution through the reduction steps. Additionally, instabilities in extrusion material interfaces, varying slurry viscosity, and distortions in flow fields destroyed shape fidelity. Finally, discrete stand-alone parts must be cut from the extrusion, a challenging prospect.²³

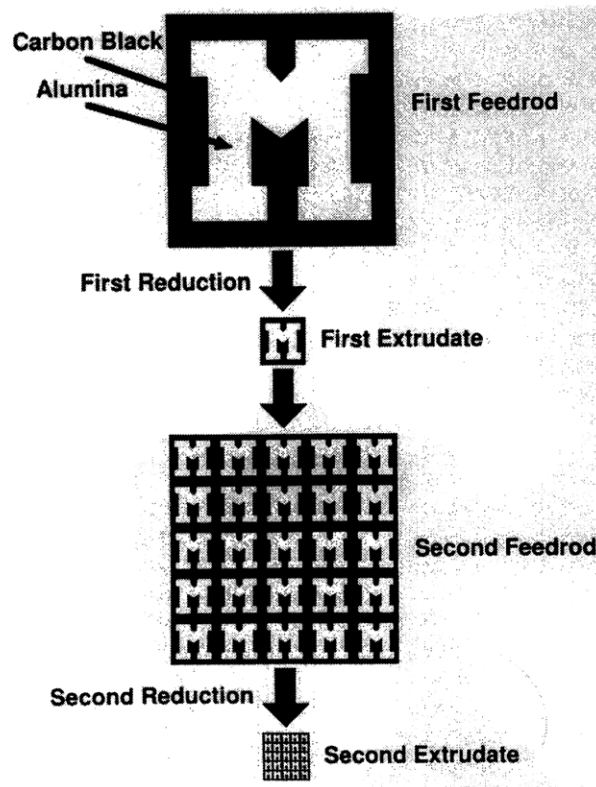


Figure 1-15 Co-Extrusion Process Diagram²³

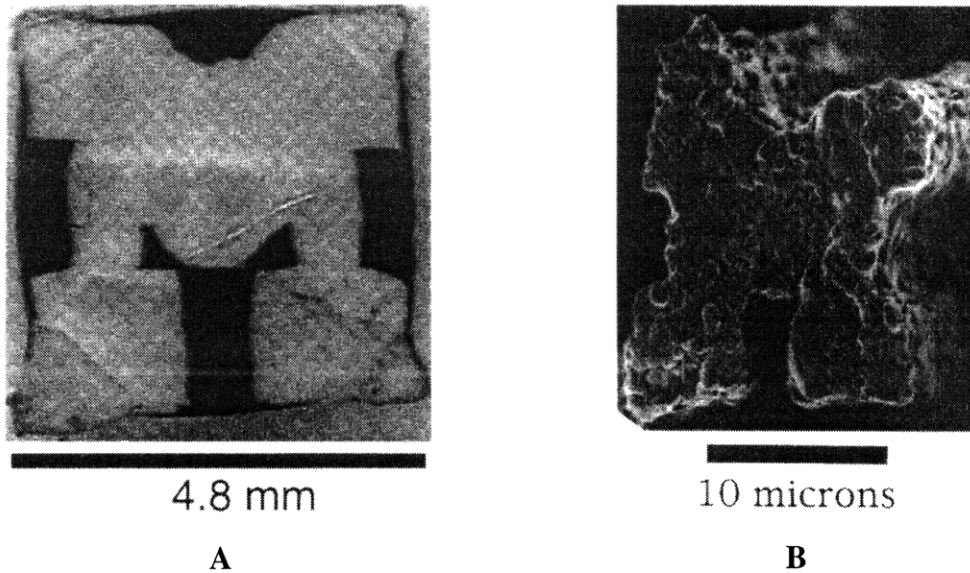


Figure 1-16 Co-Extruded Alumina Micro-Part A) After One Reduction and B) After Four Reductions (Fired)²³

A ceramic forming process that did not rely on LIGA molding was a plasma etched polyimide stamping process. The process utilized an oxygen plasma etch using a titanium mask over polyimide. The resulting polyimide micromold pattern was pressed onto a green ceramic tape with 20 – 30 MPa of pressure, and was then separated from the mold resulting in a pattern transfer to the ceramic. Features below 9 μm were destroyed during the separation step. Figure 1-17 shows the polyimide mold and the resulting ceria-zirconia structure. This process was successful in producing positive features as small as 4 μm wide and 9 μm tall (AR=2.25) (Figure 1-18).²⁴

A non-LIGA processing methodology and a direct casting technique characterize the new micromolding process described in this work. Several etching techniques were used to create micromolds into which ceramic materials were cast. The most revolutionary etching method, deep reactive ion etching (DRIE), was used to form molds similar to those produced through LIGA. Deep RIE was less expensive than LIGA, compatible with current processing techniques, and was easy to control and perform. The process described in this work was used to produce low and moderate aspect ratio

ceramic parts using reusable tooling, simple processing techniques, and equipment readily available in industry.

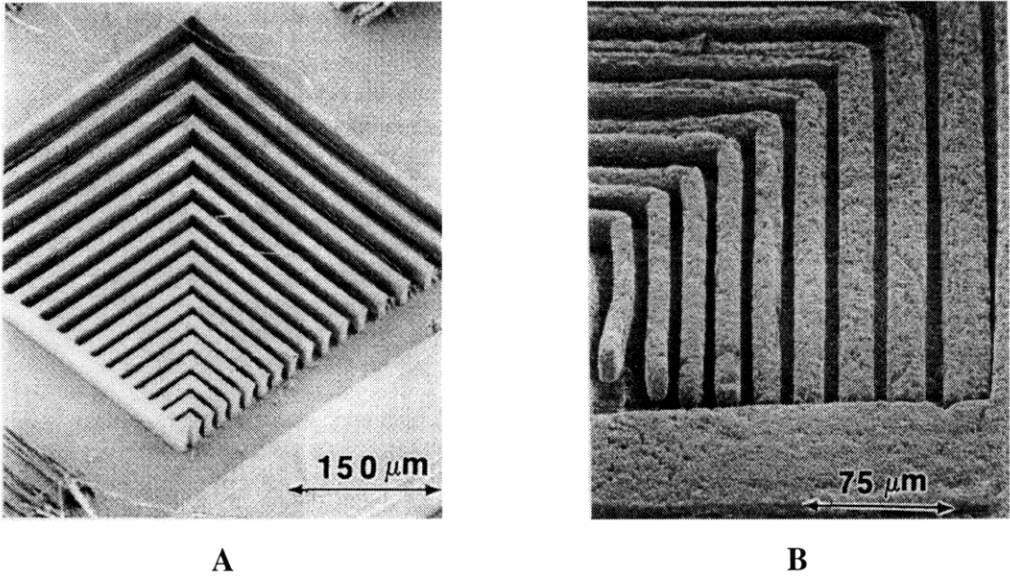


Figure 1-17 A) Polyimide Stamping Mold and B) Green Stamped Ceria Zirconia²⁴

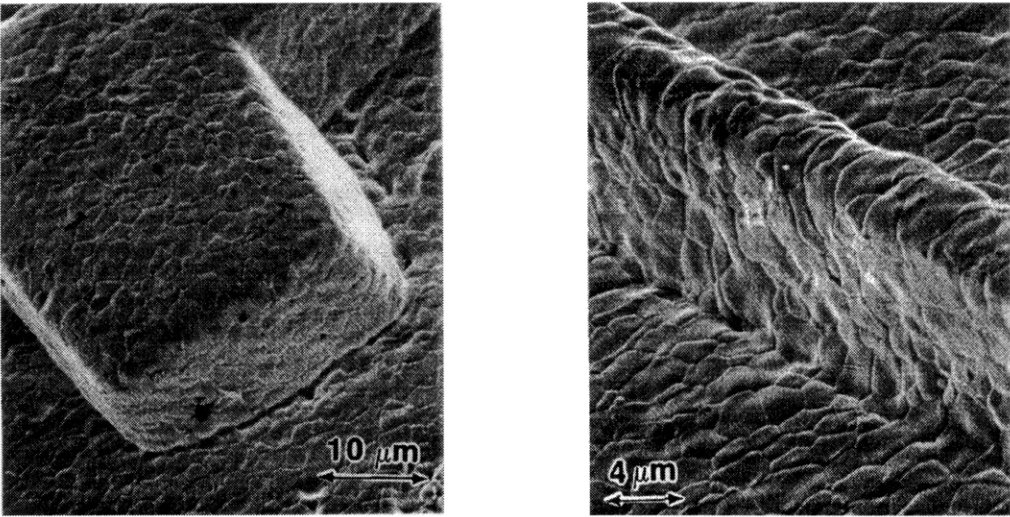


Figure 1-18 Fired Ceramic Features Created by Stamping²⁴

Chapter 2

2.1 Microforming Process

A process was developed to create ceramic parts using standard photolithography techniques and new etching methods. This process had an advantage over previous methods in that it did not employ costly LIGA processing, was easily scaleable, and could be performed using the most basic of microelectronic processing equipment. Factors such as ease of processing, reproducibility of features, and reusability of tooling were all considered while developing the process.

2.2 Process Goals

The goal of the process was to create ceramic parts with micron scale features for practical use in MEMS and mesoscale devices. Not only did the process have to be one which utilized readily available materials and techniques, but also had to be simple to perform consistently and reliably.

The process should be able to produce identical parts every time. This is important, especially in MEMS manufacturing environments, as devices can have very tight tolerances. Applications such as the micro turbine engine require components with tolerances on the order of one micron. Out of tolerance parts can lead to excessive part wear and friction. Since friction can be a major problem in MEMS devices, any source of wear can lead to catastrophic failure. Understanding the dimensional changes throughout the process is critical in designing precision parts.

It must be inexpensive and easy to produce tooling and parts. Manufacturing costs are a large driver in the market cost of the product. MEMS with multiple moving parts will be considerably more expensive to produce than simple monolithic devices. Extra

cost is incurred in forming of three-dimensional structures, in assembling small parts, and in the systems level integration of the various components.

2.3 Process Description

2.3.1 Initial Approach

The initial design philosophy was based on casting ceramic slurry into a microfabricated mold. The part would be removed from the mold, fired, and placed in service. While slurry tape casting processes have been available for years, it was unclear how a slurry would perform with a micromold. Additionally, a process that embodied reusable tooling, scaled to a large manufacturing environment, and utilized existing processing infrastructures was desired. Several challenges were encountered during process development, resulting in a gradual evolution of the process over time.

2.3.2 Evolution of Design

Initial attempts centered on the manufacture of PZT fibers, and consisted of making a mold by cutting lines in an aluminum block. A PZT slurry was cast into the grooves, however, there was no way to remove the green fibers intact. Additionally, the dimensions of the cutting blade limited the size of the fibers. A more robust procedure was developed using photolithography and silicon. This method allowed a silicon mold to be produced with any pattern, yet fibers cast into these molds still could not be removed. The next step was to investigate transfer molding, using silicone rubber to make a transfer mold of the silicon etching. A second silicone mold was made from the transfer mold, into which fibers were cast. It was hoped that the flexibility of the silicone mold would allow the fibers to be removed intact. This method met with limited success as only very short lengths of fibers (a few mm) were successfully removed. A mold was required that could be removed with little mechanical disturbance to the green fibers, as

they were very fragile. Utilization of a lost mold procedure was the key to evolving the process into its current form.

2.3.3 Current Method

The micromolding technique used several different photolithography methods to achieve the initial silicon mold. The method by which the silicon was etched determined the geometry of the final silicon master mold. Several different methods, each of which produced a different geometry, were used to etch silicon. While several wet and dry silicon etching techniques were available, the primary methods used in this process were KOH and deep reactive ion etching (DRIE). Unlike LIGA, both methods required only the use of standard UV photo alignment equipment.

2.3.3.1 Photolithography and Etching

2.3.3.1.1 Hot KOH Etching

The hot potassium hydroxide (KOH) method of etching used a nitride layer as an etching mask. Approximately 1000 Å of silicon nitride was deposited onto a silicon wafer in a PlasmaQuest CVD reactor. A one micron layer of positive photoresist (OCG 825-20) was spun coat onto the wafer at 3000 RPM. The wafer was placed in a standard photolithography alligner (KarlSuss) and exposed to UV light through a photomask containing the desired features. The UV light de-polymerized the exposed areas of the photoresist which was removed with a developer (1:1 OCG 934), leaving a photoresist mask over the nitride. The wafer was immersed in a buffered hydrofluoric acid bath (BOE) which etched away the nitride not protected by photoresist (Figure 2-1). The resist was stripped with ethanol, leaving a nitride mask on silicon. The wafer was placed in a hot KOH bath (85° C, 10.4 M), where areas not covered by silicon nitride were etched.

KOH etched silicon preferentially in the $\langle 100 \rangle$ direction, resulting in a final etching with walls at 54.7 degrees. Alignment of features with respect to the silicon flat was important, as their orientation to the $\langle 100 \rangle$ plane would determine the final geometry of the etching. This mold was used to create triangular PZT fibers. The KOH method was limited by the geometries available with the preferential etch.

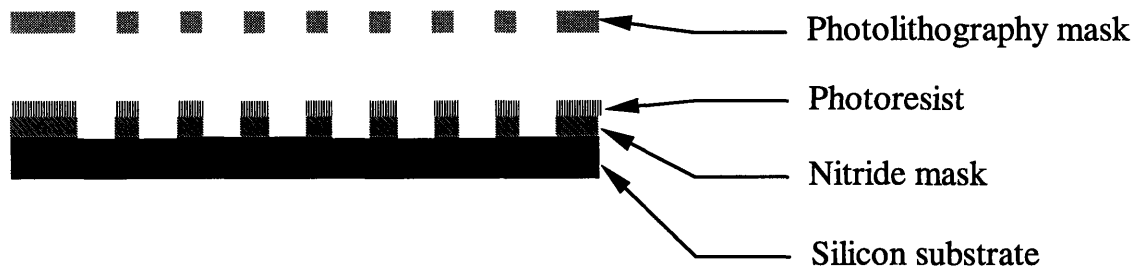


Figure 2-1 Photolithography Patterning

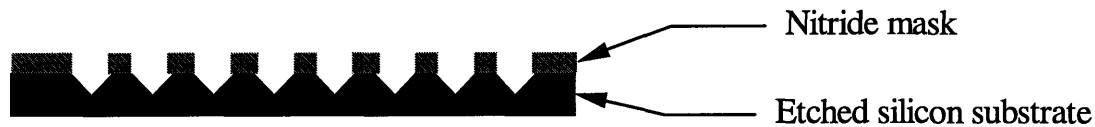
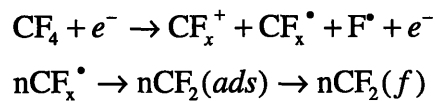


Figure 2-2 KOH Silicon Etching

2.3.3.1.2 Deep RIE Etching

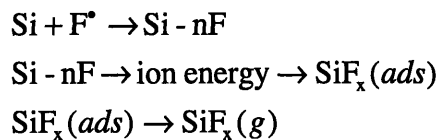
The second method employed in making silicon molds was deep reactive ion etching (DRIE), utilizing the STS Multiplexing Deep RIE system. This new method was an anisotropic dry etching process capable of creating 90 degree sidewall, high aspect ratio molds. The STS Etcher was capable of etching randomly shaped and aligned features in $\langle 100 \rangle$ silicon, and was even capable of etching straight through a standard sized wafer.²⁵ Alternating etching and passivation steps made up this two cycle process. The cycle began with the deposition and dissociation of a fluorocarbon gas (C_4F_8), which polymerized to form a passivating layer (Figure 2-3).



The gasses were then switched to SF₆ which was dissociated in a plasma. Fluorine ions selectively removed the surface passivation at the bottom of the trench, due to the direct ion bombardment. The passivation layer on the sidewalls remained intact, protecting the silicon from the etching step.



Further ion bombardment on the bottom of the trench caused absorption of F ions to form a SiF_x product, which was then desorbed as a gas (Figure 2-4).



The cycle repeated until the desired depth was reached. A scalloping effect could be produced through this alternating process, although sidewall surface roughness of less than 0.15 μm could be achieved.²⁶ Examples of surface scalloping are presented in Figure 2-5. Complex structures produced through deep RIE are shown in Figure 2-6.

The STS Etcher only required a thick layer of photoresist as a mask, eliminating the need to deposit nitride and work with HF. A 10-15 μm layer of AZ4620 was spun onto a silicon wafer (1500 RPM for 30 seconds) and exposed in a photoaligner (KarlSus) for 400 seconds through a photomask. The amount of photoresist required was a function of etch depth, as the etcher had a selectivity to photoresist of 75:1. Alignment was not an issue, as there were no crystallographic implications during STS etching. The pattern was

developed using AZ422 developer and placed in the STS Etcher. Etching took place at the rate of 2.5 $\mu\text{m}/\text{minute}$. A 1 μm Teflon-like layer of C_4F_8 was applied in the machine to serve as a release layer during subsequent processing.

Deep RIE etching was capable of creating high aspect ratio structures very similar to those produced through LIGA. The STS Etcher was compatible with the current clean room infrastructure, was easy to perform, and achieved excellent results. Deep RIE etching was used to create all of the vertical sidewall molds used in this process.

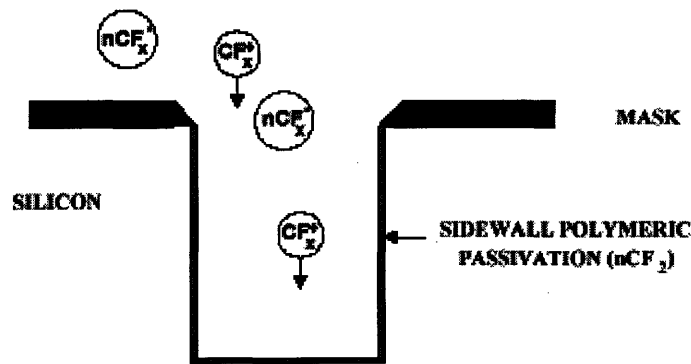


Figure 2-3 Deep RIE Passivation Step²⁶

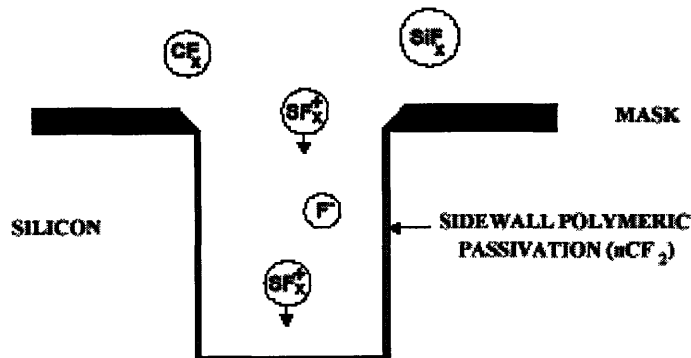
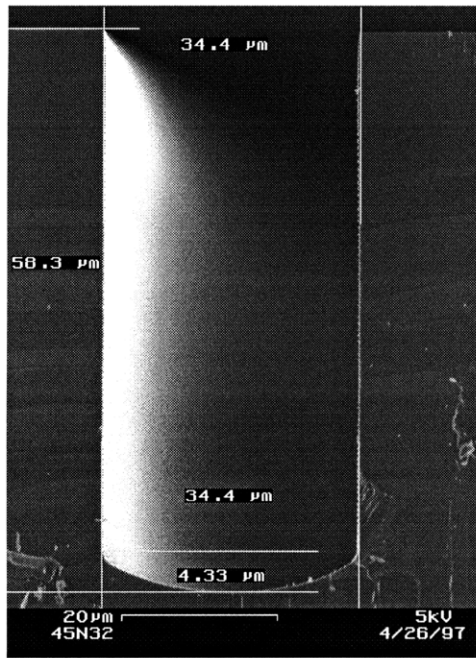
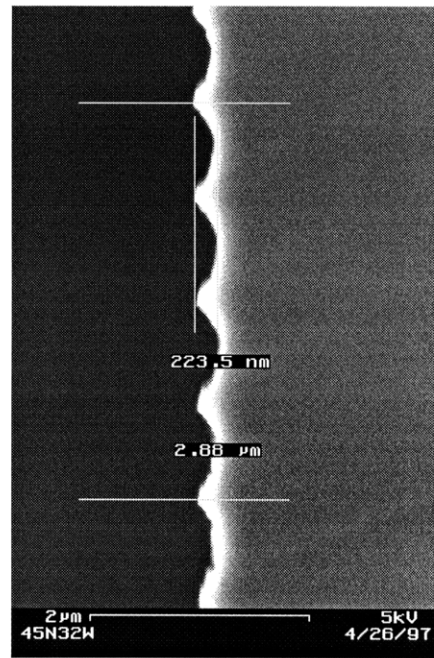


Figure 2-4 Deep RIE Etching Step²⁶



A



B

Figure 2-5 A) STS DRIE Trench and B) Sidewall Scalloping²⁷

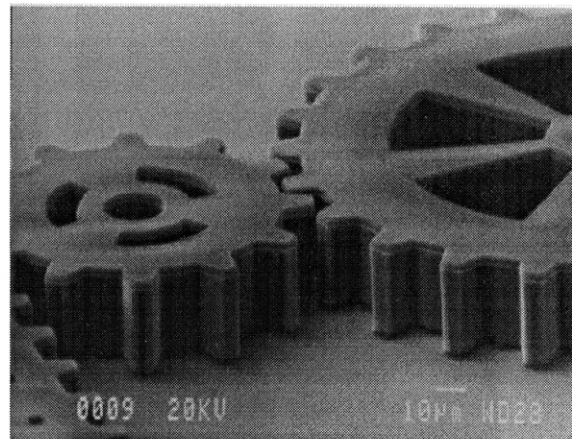
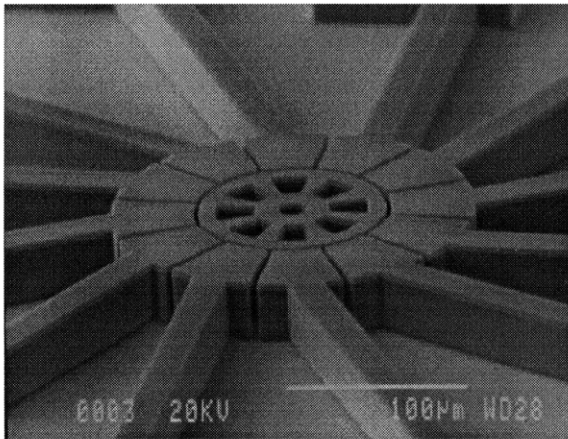


Figure 2-6 High Aspect Ratio Parts Produced by Deep RIE Etching²⁸

2.3.3.2 Silicone Master Mold

The silicon mold was the first of several reusable tools produced for this process. The silicon tool was now used to create the next mold in the transfer operation. A master mold was created from the etched silicon substrate using silicone rubber, however, before applying the silicone, a release layer had to be deposited onto the silicon wafer.

The silicone rubber was nearly impossible to separate from the silicon without a release layer, resulting in the destruction of both the silicon and silicone molds. Silicon etchings from the STS Etcher could have a release layer (C_4F_8) deposited during processing; however, silicon etched by other means required a separate deposition. Several release layers were experimented with, including spray on lubricant (Contour Release Agent and Dry Lubricant). The spray lubricant left a very faint film pattern on the silicon, which transferred to the silicone. This introduced an undesirable surface roughness into the process stream. Instead, a thin layer of Teflon-like material was deposited in a CVD reactor. This material was a plasma enhanced CVD hexafluoropropylene oxide (HFPO), which was similar in composition to Teflon.²⁹ About 500 Å was sufficient facilitate smooth mold separation.

The silicon etching was ready to be transferred to silicone after application of the release layer. The wafer was diced and placed in a small enclosure to contain the uncured silicone. For a 3" by 3" mold, 64 grams of RTV31 (GE Silicones) was thoroughly mixed with its curing agent (DBT 1 drop/4 grams) and poured onto the silicon etching (Figure 2-7). The mold was cured for 24 hours after deairing in a vacuum bell jar. Curing times varied inexplicably, so verification of complete curing was necessary before attempting separation. The molds were separated by gently pulling them apart, creating a positive silicone master mold. The silicon could be used to make another silicone mold, although experiments indicated that best results occurred after re-depositing another release layer.

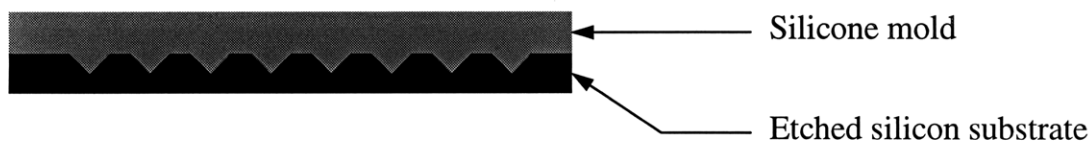


Figure 2-7 Silicone Molding of Etched Substrate

2.3.3.3 Wax Sacrificial Mold

The silicone master mold was used to produce multiple sacrificial molds. Liquid paraffin (100° C) was poured onto the silicone mold and allowed to solidify (Figure 2-8). The wax had to be hot enough so that solidification did not occur immediately upon contact with the silicone mold, or a poor reproduction would result. A glass slide was placed on top of the wax after it was poured if a rigid backing was desired. The wax was removed from the silicone mold, creating a negative mold. No release layer was necessary, as the wax naturally debonded from the silicone. Numerous wax molds were produced from one silicone mold. Photographs of silicon, silicone, and wax molds can be found in Appendix A.

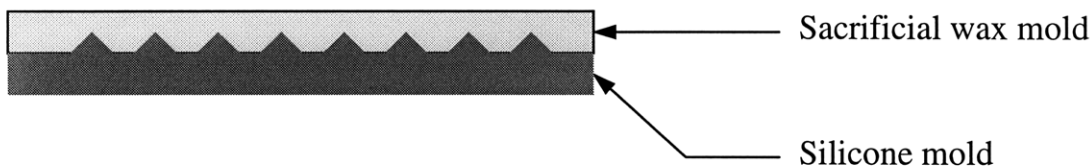


Figure 2-8 Wax Molding of Silicone Mold

2.3.3.4 Slurry Application

A slurry of the desired material was cast or applied with a pipette onto the sacrificial wax mold (Figure 2-9). In the case of cast parts, up to three castings were performed to insure complete mold filing. Pipetted parts only required one application of slurry. Parts were allowed to dry thoroughly before the wax removal step. Drying

conditions depended on the type of slurry used, and were specified for each part produced.

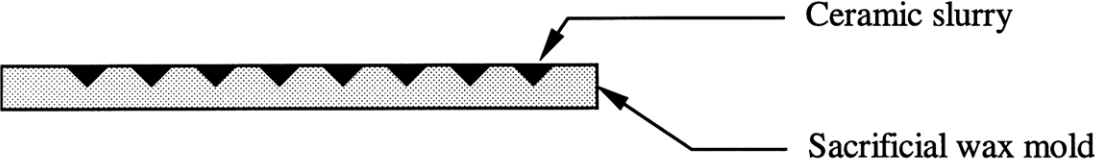


Figure 2-9 Application of Ceramic to Wax Mold

2.3.3.5 Wax Removal and Sintering

The mold was placed in an oven (100° C) on a porous substrate for wax removal (Figure 2-10). Porous alumina was used for larger scale parts, while an extruded alumina honeycomb structure was used for delicate standalone parts. The parts were placed in a furnace for binder burnout and sintering after the wax was completely removed. Several firing procedures and process variations were established for different parts and materials, and are detailed in Section 2.4.



Figure 2-10 Wax Removal and Sintering

2.4 Specific Parts

Several different parts were fabricated during process development. This was done to test the capabilities of the process, and to generate a variety of test structures.

Each part had specific processing issues which are explained in this section. PZT fibers were produced to demonstrate the ability to create very small stand alone parts. Zirconia parts and alumina micro turbines were used to explore complex shapes, while alumina micro reactors were fabricated to demonstrate mesoscale forming capability. Finally, a non-ceramic use of the molding process was examined.

2.4.1 PZT Fibers

PZT fibers are currently being investigated as an actuating material for active composites. The electromechanical response produced by piezoelectric fibers in a matrix can be used for controlling vibration, manipulating airfoil shapes, and suppressing sound.³⁰ Due to the immature nature of this technology, there are only a few commercial sources of PZT fibers. CeraNova (Hopedale, MA) currently produces 120-140 μm diameter circular fibers in 6" lengths through a proprietary extrusion process.³¹ Square PZT fibers as small as 100 μm on a side and 3" long are produced by Staveley Sensors (East Hartford, CT), using a fine diamond saw to dice fibers from fired PZT ceramic.³² Both processes have several limitations: extrusion requires large amounts of binder which can result in porous fired structures, and dicing can result in undesired surface flaws and residue. Additionally, the geometry of the fibers are limited by the tooling and methods used during production.

The microforming process provided an alternate method for making PZT fibers. Fibers created through this method could have varying morphologies (fibers with features), a concept not available through conventional fiber processing means. The process was also capable of producing small lot sizes, making it ideal for compositional studies. Finally, the micromolding process had the potential to produce fibers in mass quantities using easily produced, reusable tooling, giving it the potential to be a competitive alternative to other commercial sources.

Wax molds for triangular and square fibers (Figure 2-11) were created by the etching methods described above using a photomask containing 200 μm line widths.

Several PZT 5H slurry formulations were investigated, the most successful of which is listed in Table 2-1.

Material	Weight %	Volume %
PZT 5H	85.93	40
Methyl Ethyl Ketone (MEK)	10.69	46.04
Ethanol	2.62	11.51
Plasticizer (BBP)	0.087	0.275
Dispersant (Phosphate Ester)	0.24	0.80
Binder (PVB)	0.43	1.375

Table 2-1 PZT Recipe

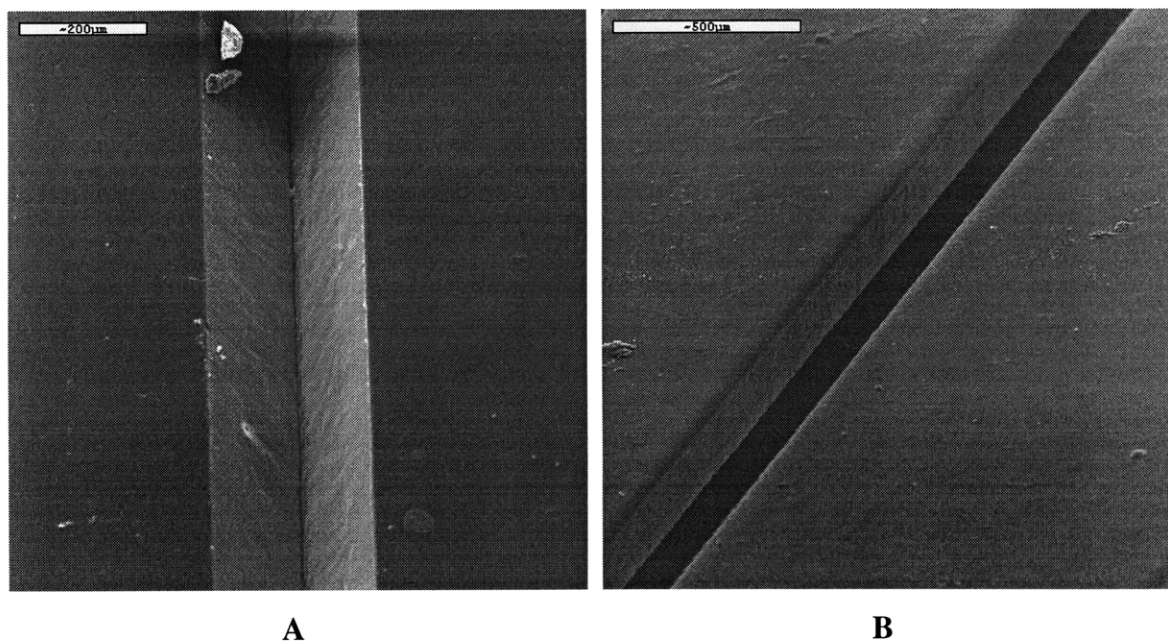


Figure 2-11 Wax Mold for 200 µm A) Triangular Fiber and B) Square Fiber

Ethanol, methyl ethyl ketone (MEK), and poly vinyl butyrate (PVB) (Butvar 76, Monstato Corp.) were placed in a 250 ml Nalgene bottle and stirred with a magnetic stir bar to thoroughly dissolve the PVB binder. A dual solvent system was used to prevent binder segregation during drying. Benzyl butyl phthalate (BBP) and phosphate ester (Emphos C) were then added along with ¼" zirconia milling media (100 beads). PZT 5H powder (PZT EC-76, EDO Corp.) was added slowly: half the powder was initially put in, and the slurry placed on a rolling mill for one hour. The rest of the powder was added in 10 g increments, with an hour of milling between additions. The slurry was allowed to mill for 12 hours after the final powder addition before use.

Slurry was cast into the wax mold using a silicone squeegee, either manually or with an automated tape casting device. A template was designed to hold a 3" X 3" mold to prevent movement during casting. Figure 2-12 shows the template with a wax mold, along with the automated casting head. The casting head consisted of a modified tape casting device with a squeegee attached.³³ A 40 durometer squeegee was mounted with two micrometers for adjustment. An automated casting arm, enclosed in a glove box to slow solvent evaporation rate, was used to push the casting head. Micrometer adjustments were necessary to level the blade for each mold since there were dimensional differences in the thickness of the wax molds. Slurry was manually applied in a line across the mold, and the casting head squeegeed the material across. The casting head produced fairly consistent results when properly adjusted; however, a film of material could remain if there were variations in thickness across the mold. Multiple castings (4) were performed to completely fill the mold, as typical slurries only contained about 40% solids. Figure 2-13 illustrates the necessity of casting multiple times. The material was allowed to dry between castings to ensure complete settling of the material into the mold. The squeegee effectively removed material between individual fibers, although a light wiping with ethanol could be used to remove excess.

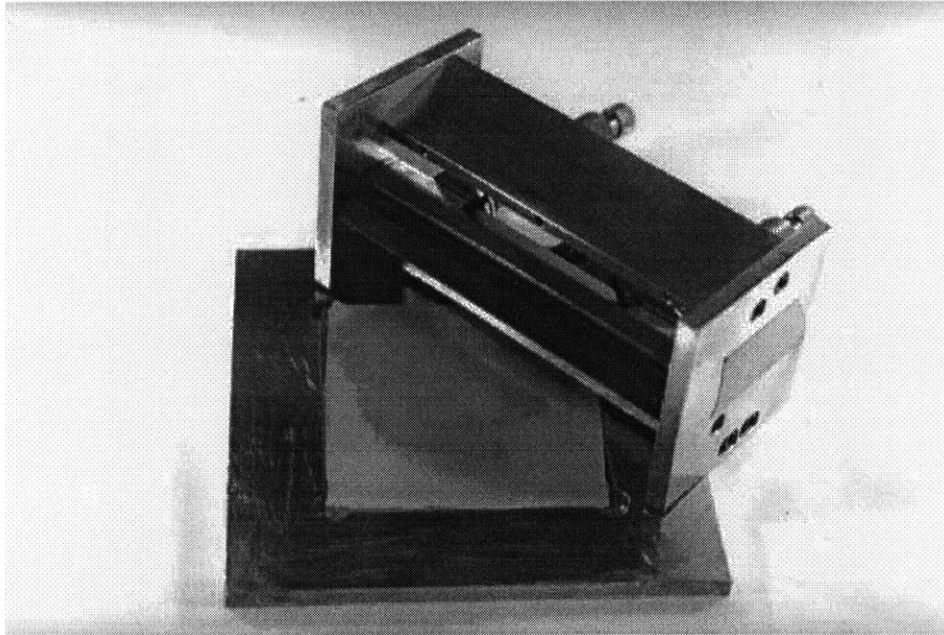
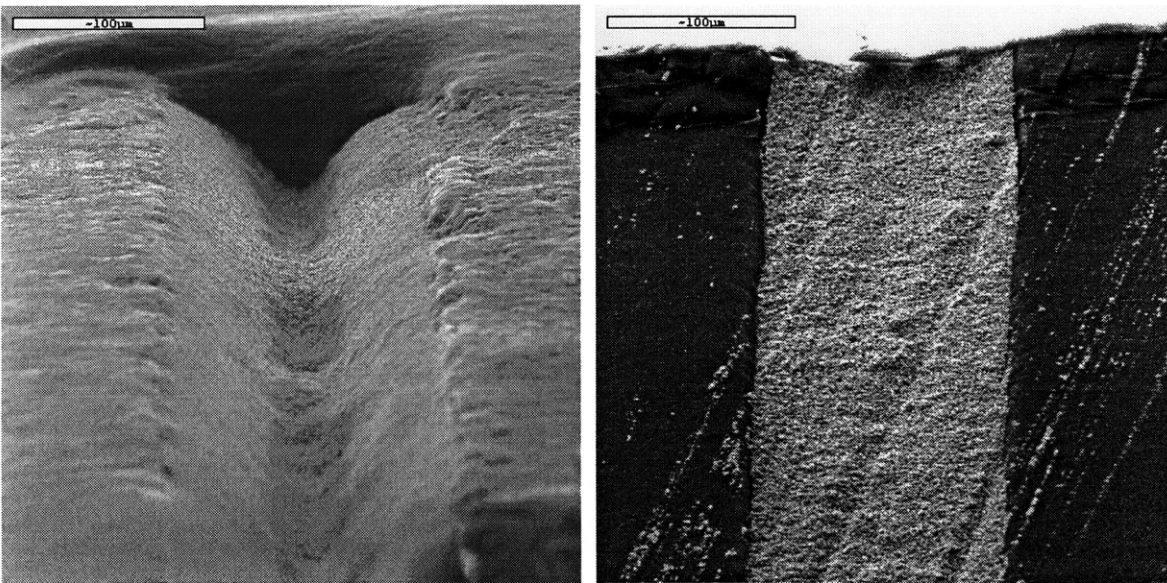


Figure 2-12 Casting Head, Wax Mold, and Holder Plate



A

B

Figure 2-13 PZT Mold Filling after A) One Casting and B) Four Castings

Casting operations were performed in a nitrogen glove box for best results. The volatile nature of the solvents caused them to evaporate very quickly; therefore, casting in the enclosure was necessary. Manual casting in the glove box was very cumbersome. It could be done in a fume hood, however, it had to be done quickly before solvent loss made the slurry uncastable.

The wax molds containing the cast PZT fibers were placed in an oven face down on an alumina honeycomb surface to remove the mold (Figure 2-14). The honeycomb was preferred to porous alumina due to the smaller area of contact between the green fiber and the substrate. Removal of fibers from a porous alumina substrate was possible, but since the fibers tended to stick, yield was relatively low. Green fibers the entire length of the mold (3") were successfully produced.

The green fibers were placed on a bed of loose PZT powder (Figure 2-15) and sealed in a crucible for firing (Figure 2-16). A crucible within a crucible arrangement was used to seal the cavity to prevent lead loss. The fibers were arranged on a loosely packed powder bed, covered with another crucible, and the surrounding space filled with PZT powder to form a seal. The entire setup was covered with an alumina plate and placed in a furnace (Teresco) for binder burnout and firing.

A binder burnout step at 500 °C for eight hours was followed by four hours of sintering at 1200 °C. An annealing step down was performed to avoid formation of a second phase PbO, which had poor piezoelectric properties and introduced large flaws that were undesirable in the final fiber. The entire firing schedule is illustrated in Figure 2-17. Cross sections of fired triangular and square PZT fibers are presented in Figure 2-18 and Figure 2-19.

This sintering method met with limited success. The packing density of the powder bed was important, as tightly packed powders would sinter and crack resulting in broken fibers. The fibers also had a tendency to curve, a phenomenon that is currently under investigation (Figure 2-20). PZT granules sintered to the fibers as a result of using a bed of loose PZT powder as the setter (Figure 2-21). Alternate firing arrangements,

such as firing on a micromolded setter, are under consideration to straighten the fibers and avoid contact with loose PZT powder.

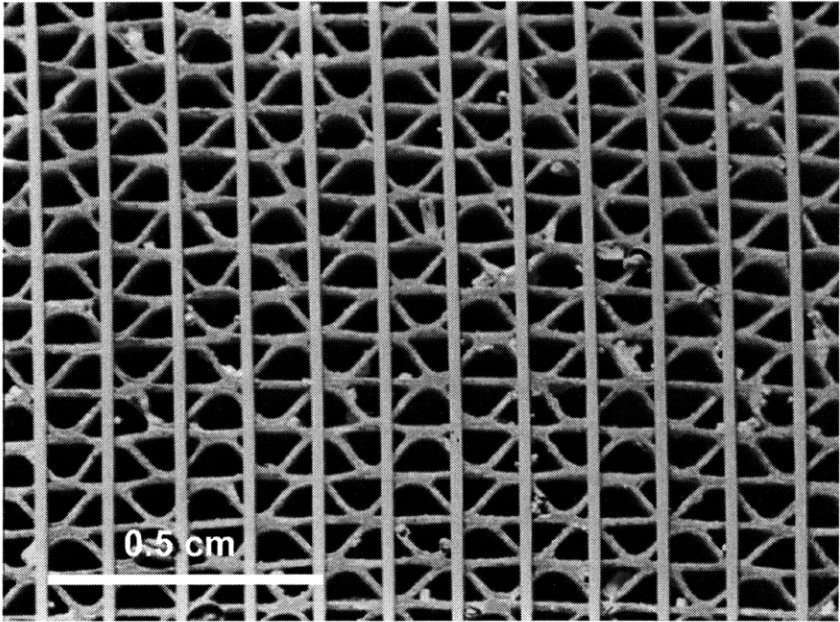


Figure 2-14 Green Fibers on Honeycomb During Wax Melting⁴⁰

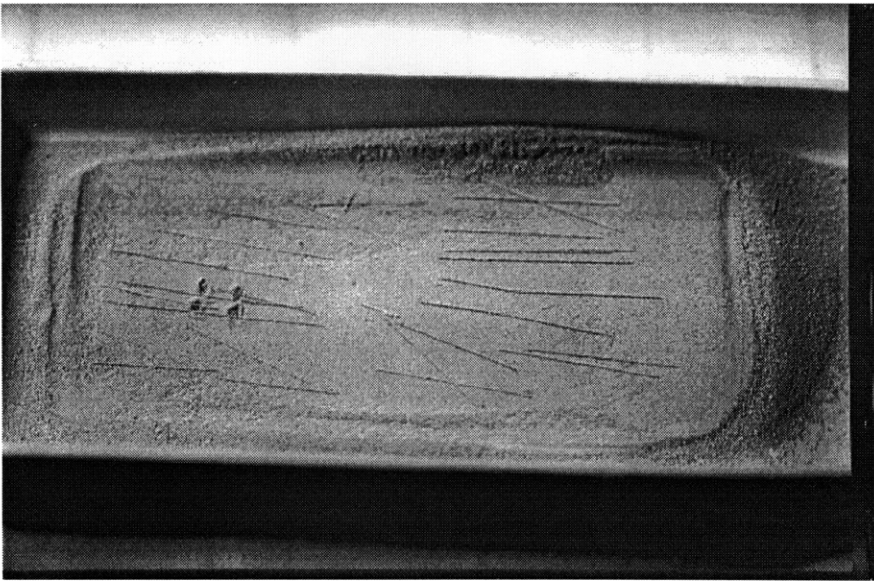


Figure 2-15 Green Fibers on PZT Powder Bed

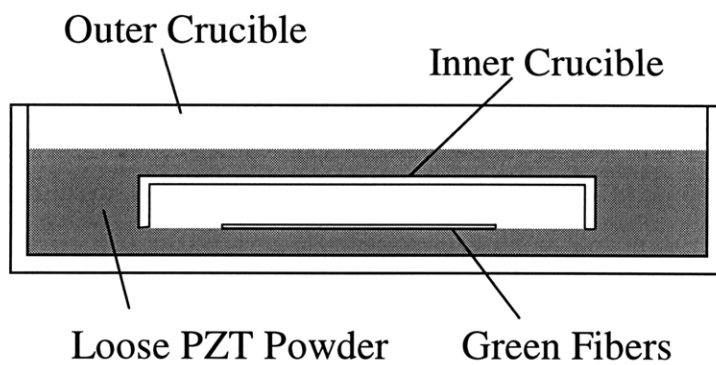


Figure 2-16 Crucible Setup for Fiber Firing

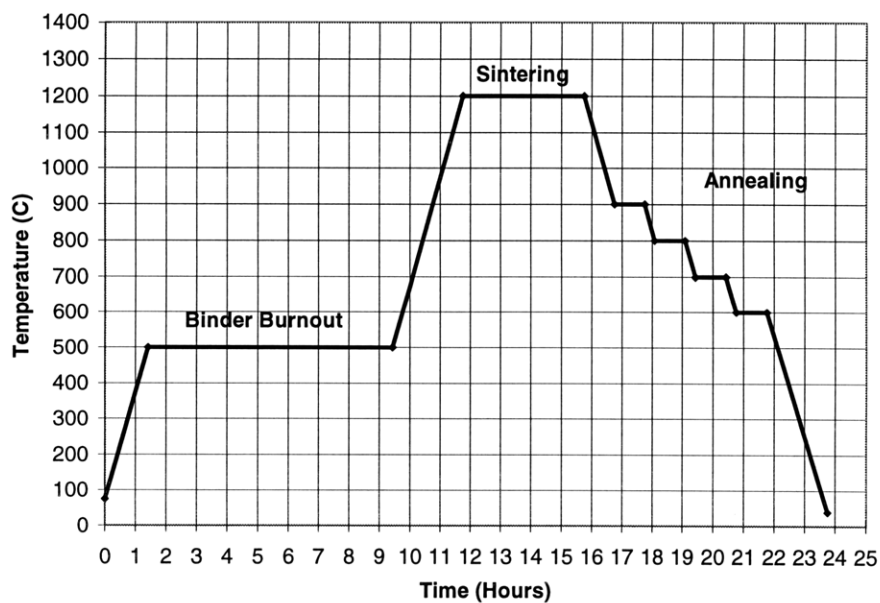


Figure 2-17 PZT Sintering Schedule

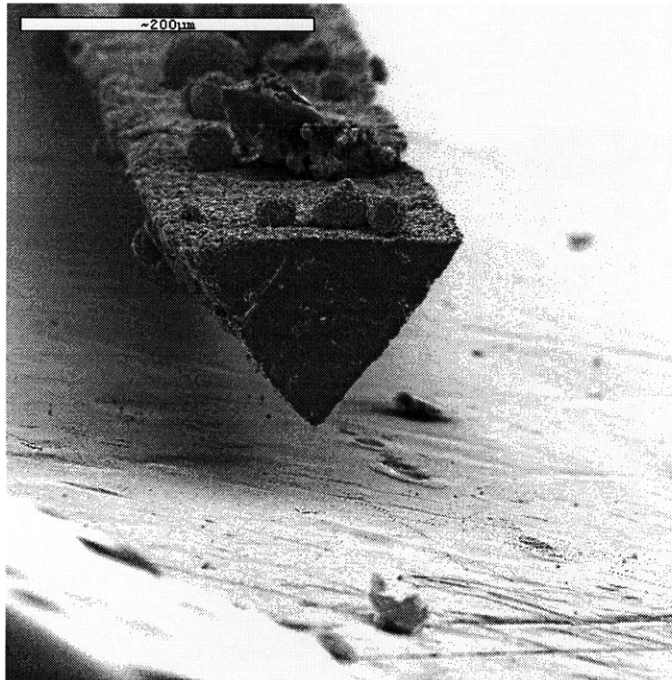


Figure 2-18 Fired Triangular PZT Fiber

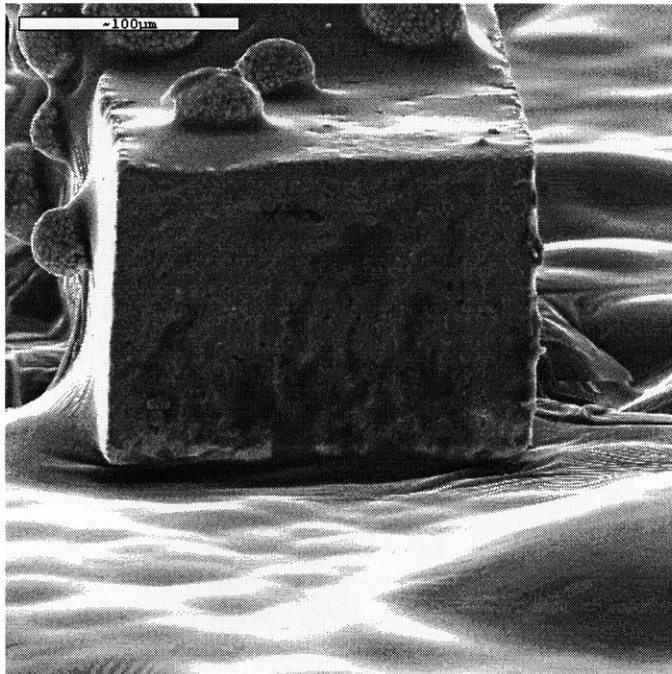


Figure 2-19 Fired Square PZT Fiber

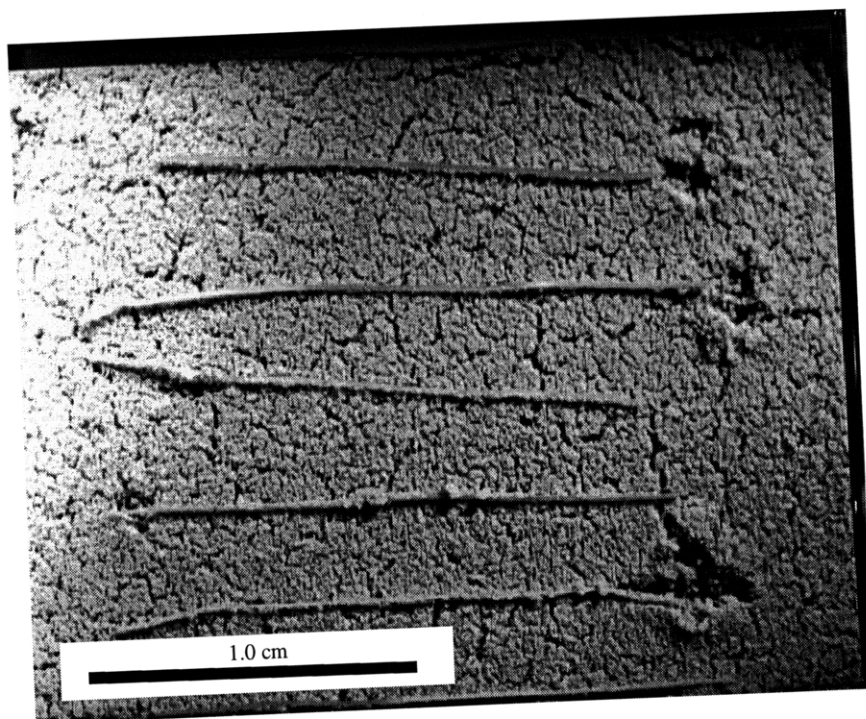


Figure 2-20 Distorted Fired Fibers on cracked PZT Bed

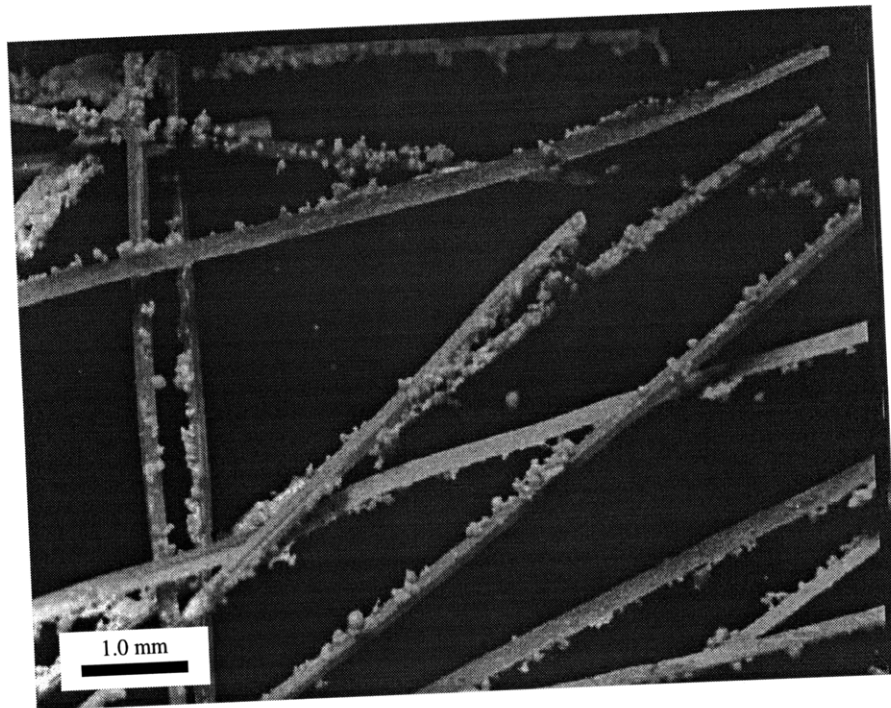


Figure 2-21 Fired Fibers with Sintered PZT Powders

Low pressure mercury porosimetry (Autopore II 9200) was used to determine fired fiber density. A small sample of material was placed in a calibrated volume penetrometer, which was filled under pressure with mercury. Knowing the sample weight, mercury weight, and penetrometer volume, density of the sample could be determined. Fibers were found to have a density of 97.3% of theoretical. A comparison of microstructure between commercially available fibers and micromolded fibers is presented in Figure 2-22 and Figure 2-23. Porosity of micromolded fibers was equal or superior to those commercially available.

A measurement of piezoelectric properties was performed on several micromolded fibers, and was found to be comparable to those of commercially produced fibers. See Appendix B for a diagram of the fiber testing apparatus. Studies have shown that fibers of similar composition exhibit a strain of 2167 ± 493 ppm, and that microstructure and porosity played a role in fiber performance. Values obtained for micromolded fibers were similar to those obtained from commercial PZT 5H fibers. Further study into the optimization of grain size and final porosity should result in better performance. Results of fiber testing are presented in Table 2-2.

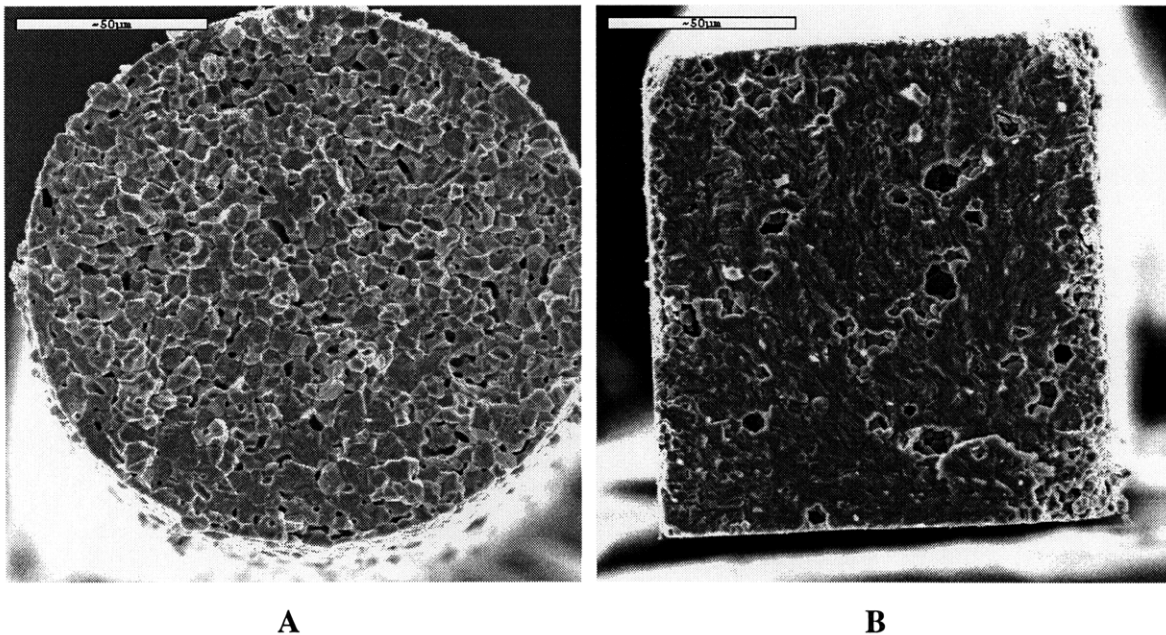


Figure 2-22 Fired Commercial PZT Fibers A) Extruded³¹ and B) Diced³²

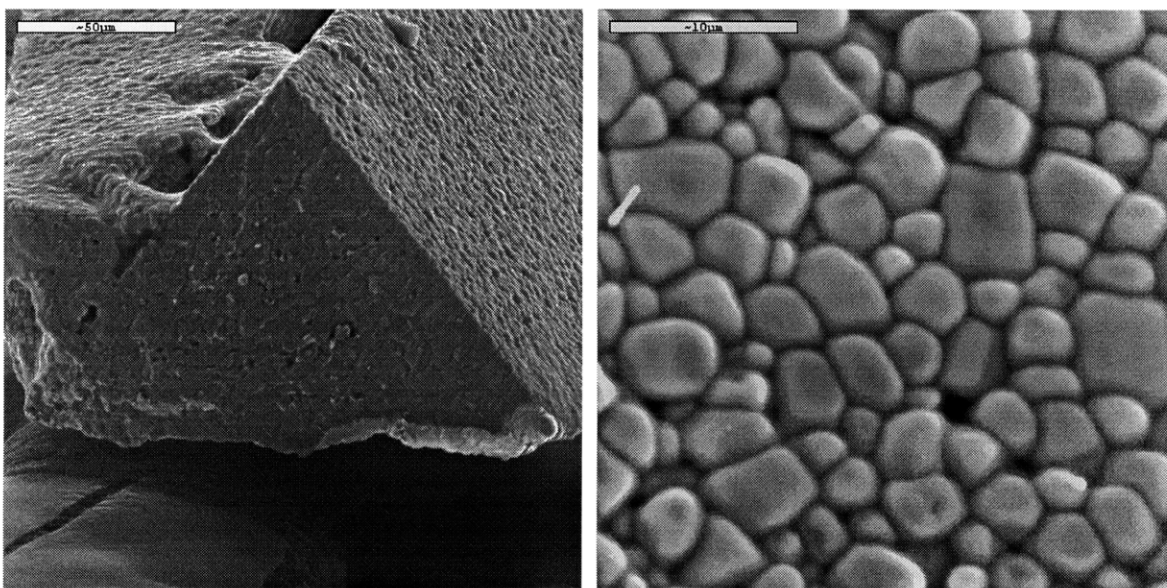


Figure 2-23 Fired Micromolded PZT Fiber Cross Section and Microstructure

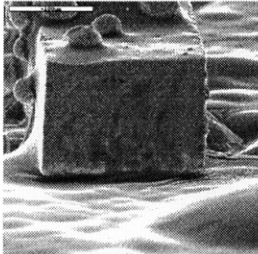
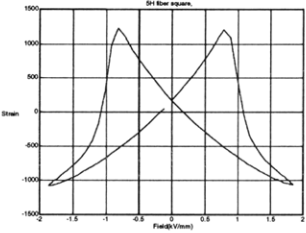
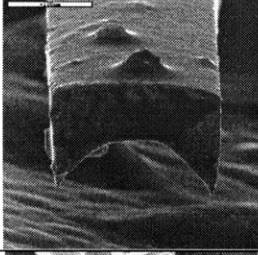
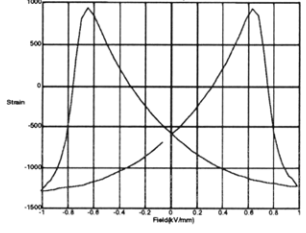
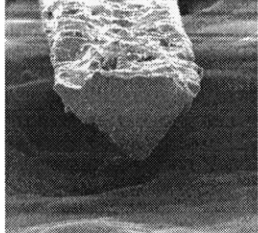
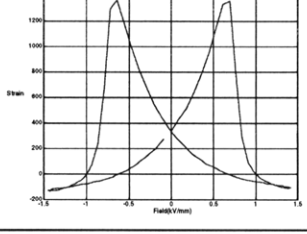
Shape	Hysteresis Loop	Strain (ppm)	Area (μm^2)
		2,275	27,245
		2,187	19,515
		1,493	8,349

Table 2-2 Micromolded Fiber Testing Results

The micromolding process demonstrated the ability to make PZT fibers, however, the ultimate goal was to be able to produce fibers with features. Featured fibers could contain a tab or other feature (Figure 2-24) that could be machine identifiable and placed precisely in a matrix. Other advanced concepts included creating sheets of interconnected fibers which could be easily placed into composites (Figure 2-25). Fibers with small tabs on the ends could also be electroded and connected directly to an electrical source, increasing E field penetration. Finally, variable geometry fibers could increase matrix coupling and fiber effectiveness (Figure 2-26).³⁴

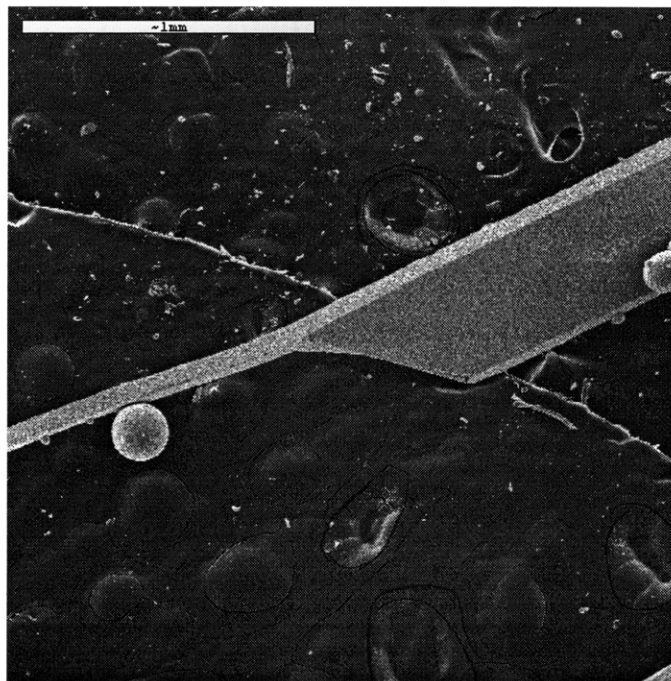


Figure 2-24 Fired PZT Fiber with Feature

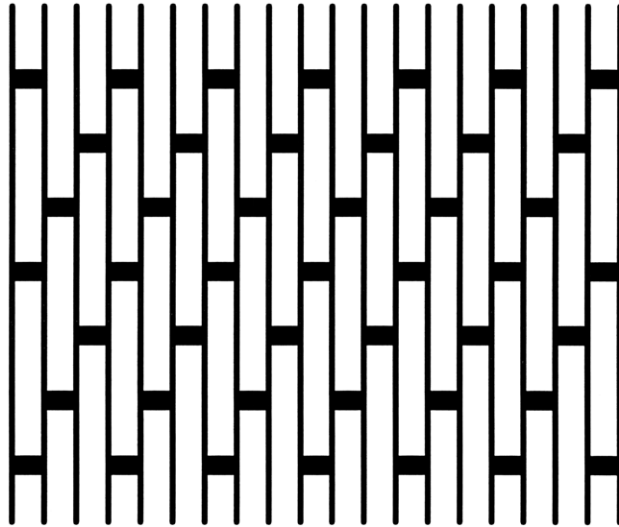


Figure 2-25 Interconnected Micromolded Fiber Array

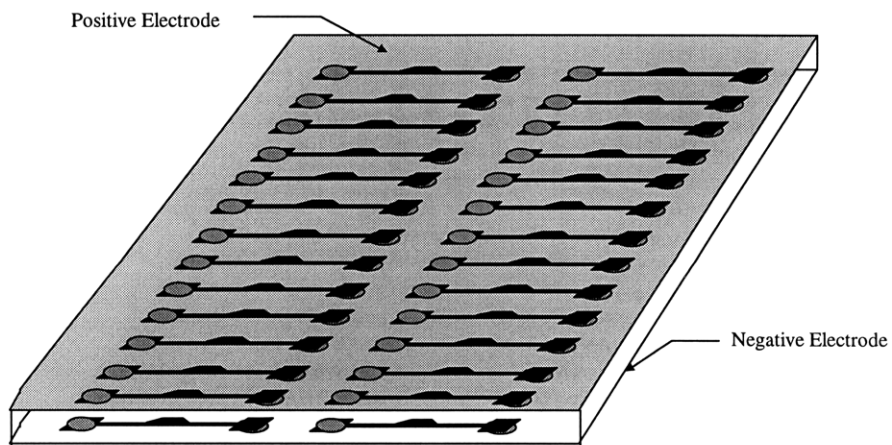


Figure 2-26 Selectively Electroded Featured Fibers in a Matrix

2.4.2 Zirconia

The first attempt at making other parts with features was done with a simple KOH etching of several closely spaced grooves (Figure 2-27). A 30% volume water and zirconia slurry was prepared and milled with zirconia media for 12 hours. A bead of slurry was applied with a pipette to the mold and allowed to dry. The part was melted from the wax mold on a porous alumina substrate and fired at 1500 °C for four hours. The sintered part is shown in Figure 2-28.

A comparison of Figure 2-27 and Figure 2-28 reveal excellent reproducibility from silicon to ceramic. Textures in the original silicon etching even reproduced well. The striation lines on the side walls of the V grooves were silicon planes present in the original etching, a result of a small misalignment during photolithography. These lines were also reproduced in the final zirconia part. Some parts did experience defects, as evident in Figure 2-29 where wetting bubbles formed in the part. A large drying void was also observed in the center of the bead. These filling and drying defects were experienced throughout all the parts produced, and will be examined in subsequent sections.

The results provided by the production of the zirconia part demonstrated the feasibility of creating a ceramic part through the micromolding process. Even the subtlest of textures were carried across the process steps to the final part. These encouraging results indicated that much more complex features were possible. Experiments with PZT fibers and zirconia parts indicated that KOH etched shapes were possible, however, this method of silicon etching was limited by the etch geometry. A part containing complex vertical sidewall features, the micro turbine, was the next challenge.

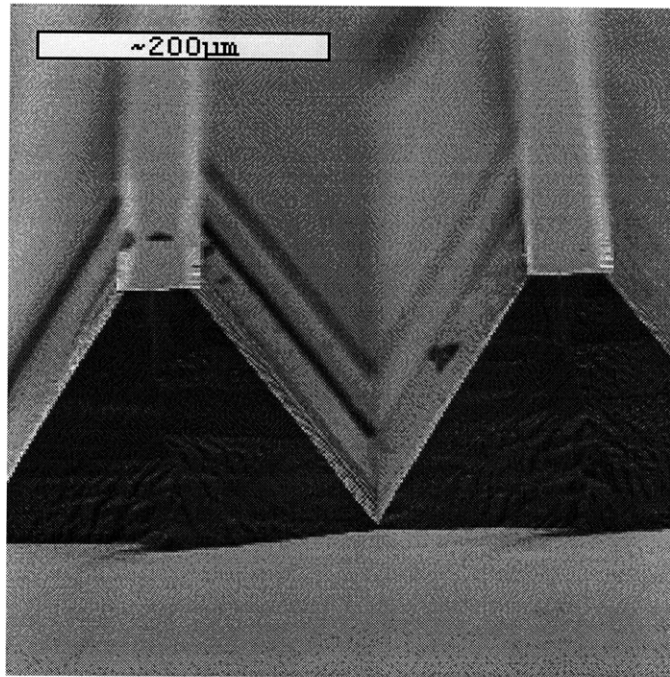


Figure 2-27 Silicon Etching for Zirconia Part

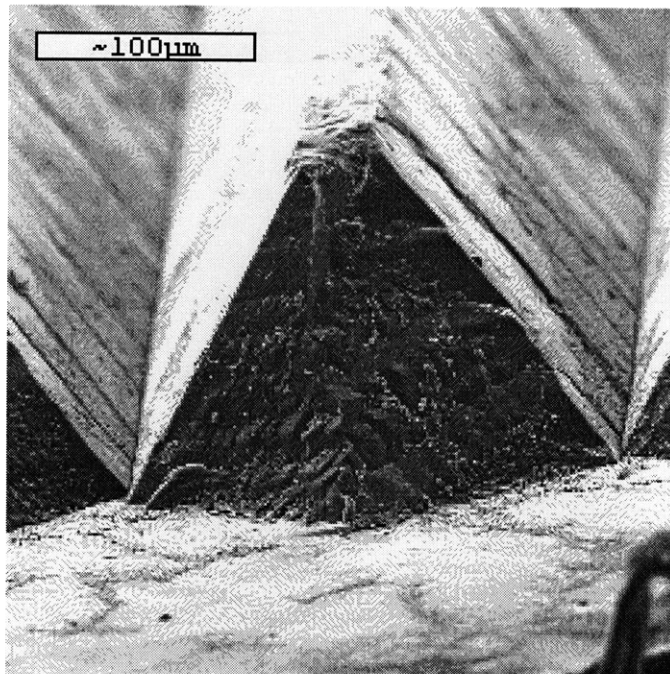


Figure 2-28 Fired Zirconia Part With Silicon Etch Planes

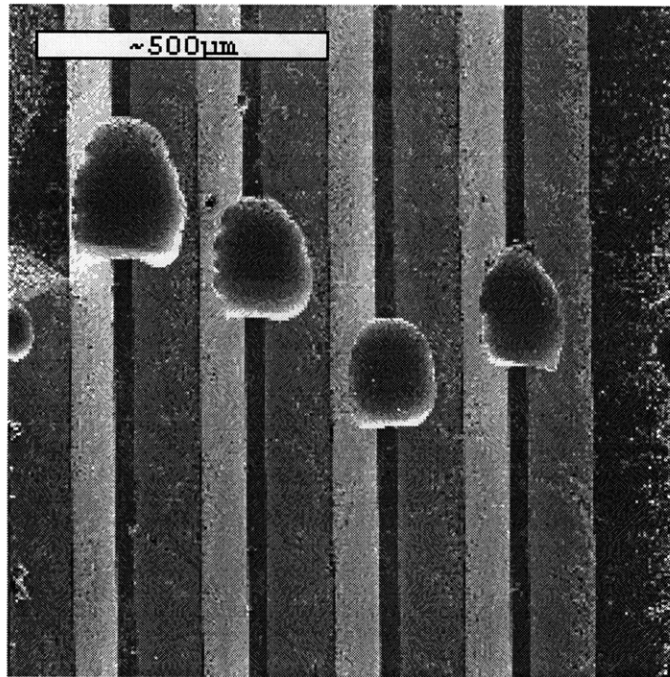
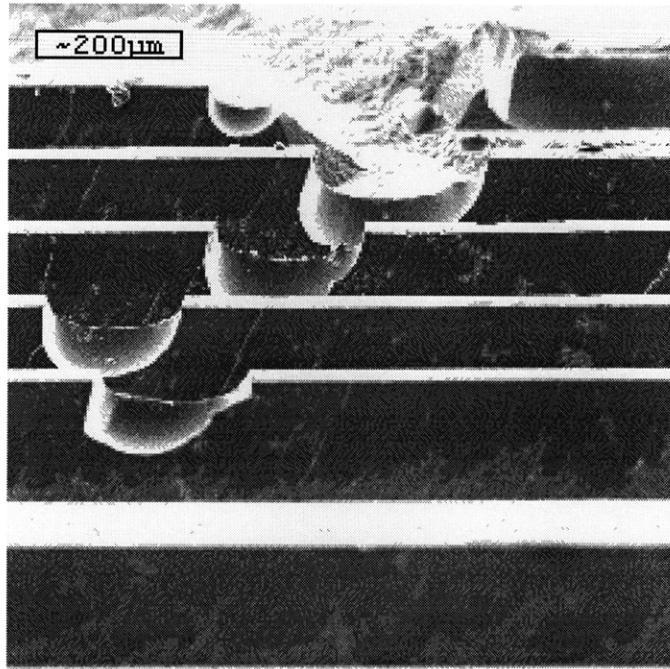


Figure 2-29 Filling Defects in Fired Zirconia Part

2.4.3 Micro Turbine

The micro turbine device is a high power density micromachine currently under development at MIT.⁷ The ideal material for this application would be one that has high strength, low density, good oxidation resistance, good creep resistance, and high toughness. Additionally, it requires parts with tolerances as small as one micron. Currently, the micro turbine is fabricated out of silicon, however other materials will be required to run the turbine at desired temperatures of up to 1700 K. The strength of silicon begins to decrease as temperature increases (Figure 1-8), and does not have good creep resistance or toughness.³⁵ It would be desirable to fabricate the hot section components out of a material that would be better suited for the high temperature corrosive environment of combustion. Ceramic materials such as silicon carbide or mullite are better suited for this application, and are good candidates for the microforming process.

A micro turbine was produced out of alumina to demonstrate the ability to create complex parts with vertical sidewalls. This proof-of-concept rotor/stator section of the turbine engine was selected for its curved airfoils and small high aspect ratio features. The turbine was 6 mm in diameter with blades 60 μm high, and had a minimum feature size of about 10 μm , for a maximum aspect ratio of 6. Another version of the turbine had blades 150 μm high with 20 μm minimum features, for a maximum aspect ratio of 7.5. Negative STS etchings of the turbines were obtained from the principal investigators and subjected to the micromolding process.

Several aqueous and non-aqueous alumina slurries were experimented with. Examples of aqueous and solvent based slurries are found in Table 2-3 and Table 2-4 respectively. Aqueous slurries were made by placing water, methanol, 1 M nitric acid, and 8000 molecular weight poly-ethylene glycol in a 500 ml Nalgene bottle and charging the mixture with alumina grinding media (1/2 liquid height). The mixture was placed on a roller mill for one hour to allow the PEG to dissolve. Half of the 0.5 μm alumina

powder (Ceralox with MgO sintering aid) was added and the mix placed back on the roller mill. After one hour, half of the remaining powder was added, and allowed to mill for another hour. The remaining powder was then added and allowed to mill for 24 hours. Post milling, three drops of surfactant (Surfaynol 104E) were added to improve mold wetting characteristics, and a 540 mM solution of CaCl₂ was added to flocculate the slurry. Slurry flocculation was necessary to avoid drying defects, a phenomenon described in subsequent sections. The solvent based slurry was prepared in a manner identical to the PZT slurries described earlier.

Material	Weight %	Volume %
Alumina	60.29	27.80
Water (deionized)	17.99	32.88
Methanol	11.99	21.92
Binder	3.01	5.13
Dispersant	2.64	4.82
Flocculant	4.07	7.44

Table 2-3 Sample Aqueous Alumina Slurry Recipe

Material	Weight %	Volume %
Alumina	61.67	25.0
MEK	27.70	55.28
Ethanol	6.93	14.10
Dispersant (Menhaden Fish Oil)	0.62	1.07
Plasticizer (DBT)	1.23	1.80
Binder (PVB)	1.85	2.75

Table 2-4 Sample Solvent Based Alumina Slurry Recipe

The alumina slurry was applied with a pipette as one bead, rather than through casting several times, as it was a stand alone part with significant thickness. This resulted in one solid piece which was easily handled. The parts were fired at 1650 °C for one hour after a four hour binder burnout step at 600 °C.

Fired micro turbines were successfully produced from both slurry formulations. A difference between turbines produced from aqueous and non-aqueous slurries was apparent. While the solvent based slurries filled the wax molds well, they frequently exhibited drying defects (Figure 2-30). However, reproduction of individual turbine blades was excellent. The flocculated aqueous based slurries did not experience the drying defects, but had problems with filling defects (Figure 2-31). This problem was more pronounced in the higher aspect ratio turbines. Part quality was largely a function of slurry dispersion state and mold wetting, as will be examined later.

Attempts making a complex, high aspect ratio part using the micromolding technique were very successful. While there were some issues regarding defects, initial results were encouraging, and improvement could be expected by adjusting slurry formulations. Production of micro turbines has demonstrated the versatility of the process and the capability to produce ceramic parts with micron scale features.

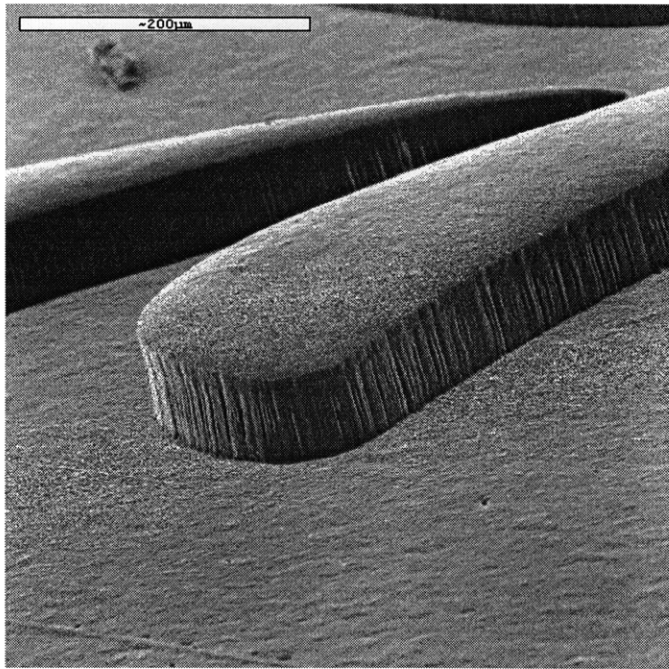
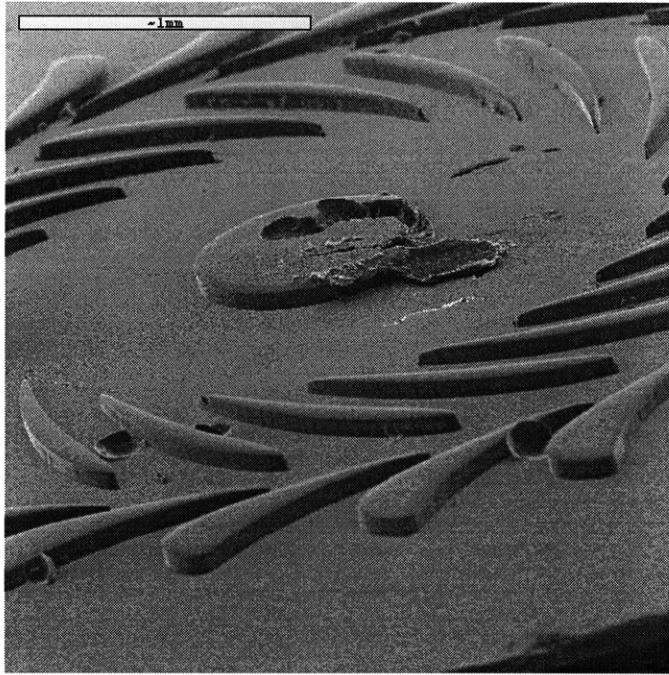


Figure 2-30 Fired Alumina Micro Turbines Produced from Non-Aqueous Slurry

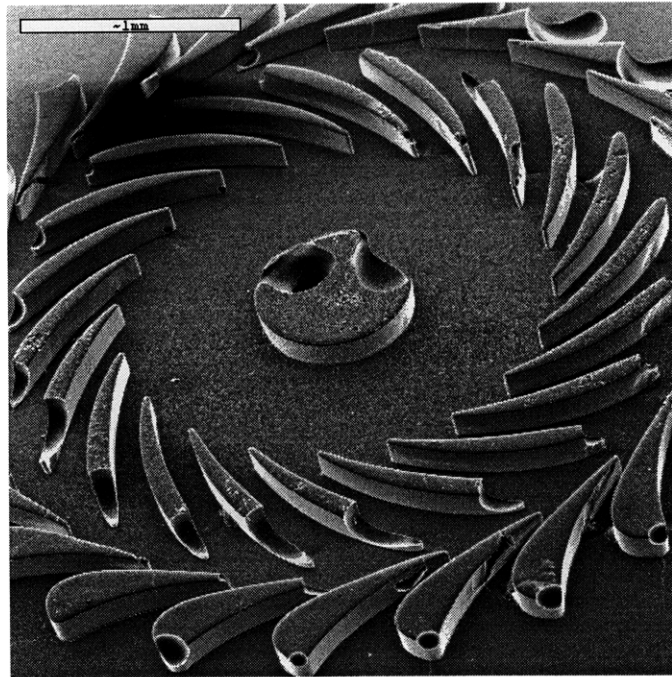
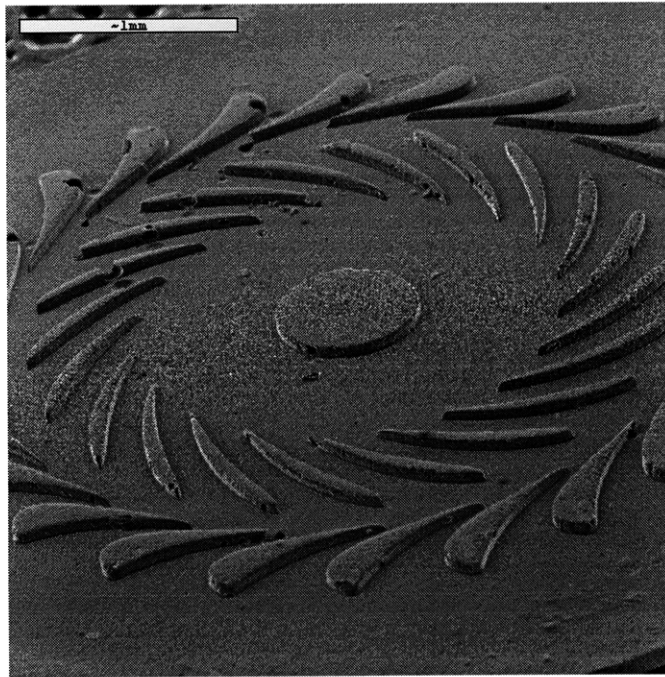


Figure 2-31 Fired Alumina Micro Turbines Produced from Aqueous Slurry

2.4.4 Micro Reactor

The ability of the process to reproduce mesoscale parts with larger features was also investigated. A micro reactor chip being developed at MIT was selected for this experiment due to its relatively large channel dimensions (1 mm). There are several potential uses for a micro reactor: it could be used as an on site production plant for small amounts of toxic chemicals, obviating the need for transportation. Many micro reactors could be arrayed together to produce mass quantities of chemicals, or to act as a pilot plant for new processes. Currently, the micro reactor is being designed out of silicon, with a silicon nitride membrane covering the reactor channel (see Figure 1-7). A desirable reaction temperature is 1100°C, making a ceramic micro reactor more desirable than a silicon one. The highly corrosive conditions produced by certain reactions also warrant the use of ceramics.³⁶

A mold was created from a silicon micro reactor produced through KOH etching. Deionized water and centrifugally classified 1 μm powder (30% weight) (Ceralox with MgO sintering aid) was placed in a 250 ml Nalgene bottle and charged with alumina media. The mixture was allowed to mill for 12 hours and then 1 % volume binder (Duramax B-1023) was slowly stirred in. The slurry was immediately applied and allowed to dry in a humidity oven at 40 °C and 90% relative humidity. Humidity oven drying was necessary to avoid cracking in the green part. A binder burnout step was performed at 600 °C for four hours in a Nytec furnace and sintering occurred at 1650 °C for one hour in a Teresco furnace.

Figure 2-32 shows a fired micro reactor part. The details of the channel were also reproduced well (Figure 2-33). The reactor exhibited some warpage, a phenomenon believed to be caused by particle size and density gradients through the part. Furthermore, some macro cracking was observed. It was believed that by adjusting the slurry properties and drying conditions, that the warpage and cracking could be mitigated. It was for this reason that a narrow 1μm particle size distribution powder was obtained

through a centrifugal classification system and used to create reactors in the hopes of reducing warpage due to particle size gradients. The effect of using narrow particle size distribution powders, however, has not been quantified.

Experiments with making micro reactors, while not extensive, demonstrated the ability to produce parts with mesoscale dimensions. The parts produced experienced some defects related to slurry composition and processing conditions, however these problems are expected to be overcome with refinement of slurry properties.

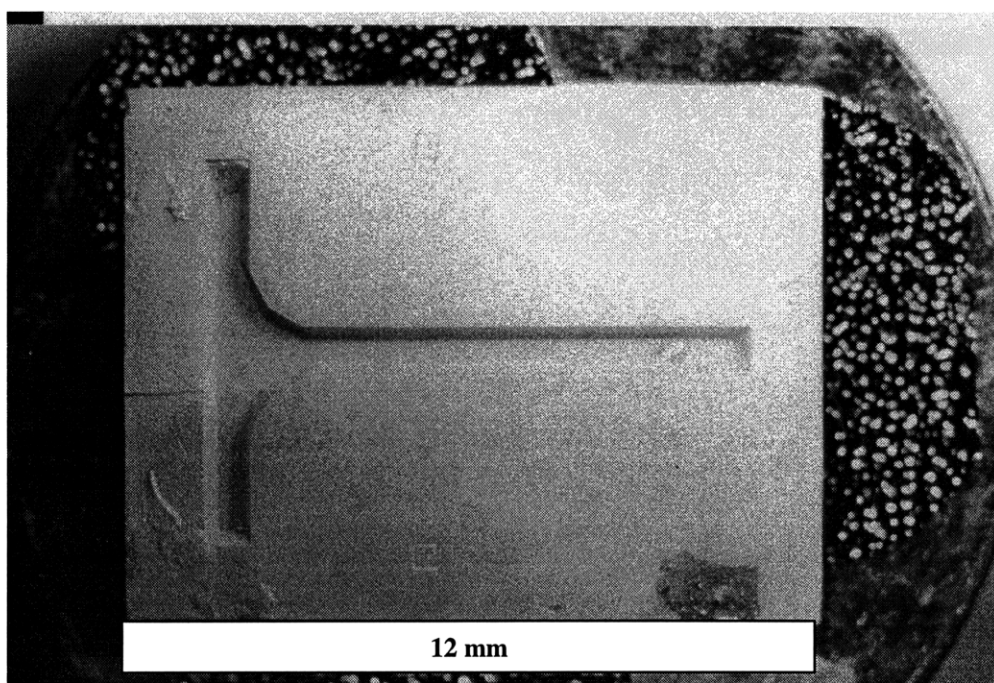


Figure 2-32 Fired Alumina Micro Reactor

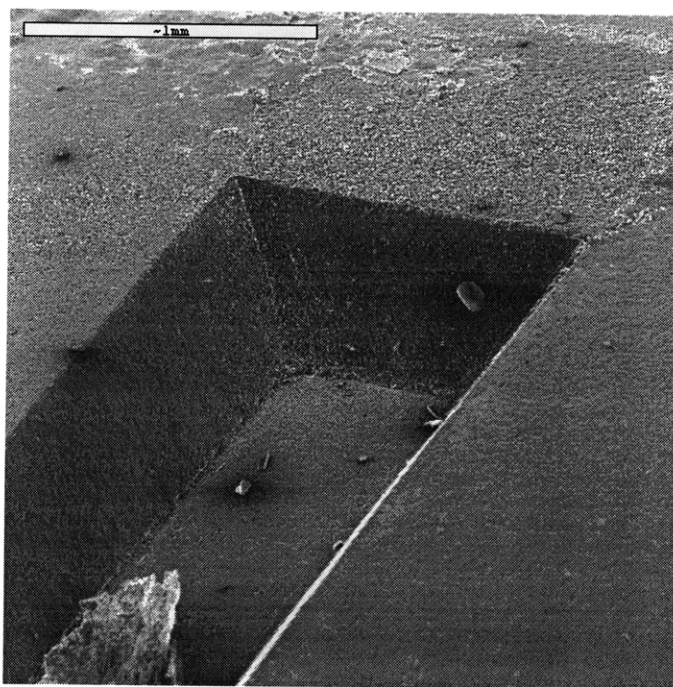


Figure 2-33 Detail of Channel in Alumina Micro Reactor

2.4.5 HIDE Tooling

The main focus of the process was on forming ceramic parts, however, other material forming applications were explored. The micromolding process was used to precisely arrange particles in a lattice arrangement in an effort to create a highly controlled infrared dielectric emissivity (HIDE) device. Theoretically, arranging metallic particles in a diamond lattice would produce a large omnidirectional photonic bandgap in the infrared regime.³⁷ If a fabric consisting of these arrays could be fabricated, it could be used to cloak infrared signatures.

A photolithography mask was created with a lattice of 2 μm squares and circles arrayed 3.5 μm apart. Approximately 2 μm of photoresist was coated (1500 RPM) on silicon and was patterned with the photolithography mask in a photo alligner (KarlSus). A CCl_4 plasma silicon etch was sufficient for this application as the depth of the holes was only 2 μm . The resulting silicon etching is shown in Figure 2-34.

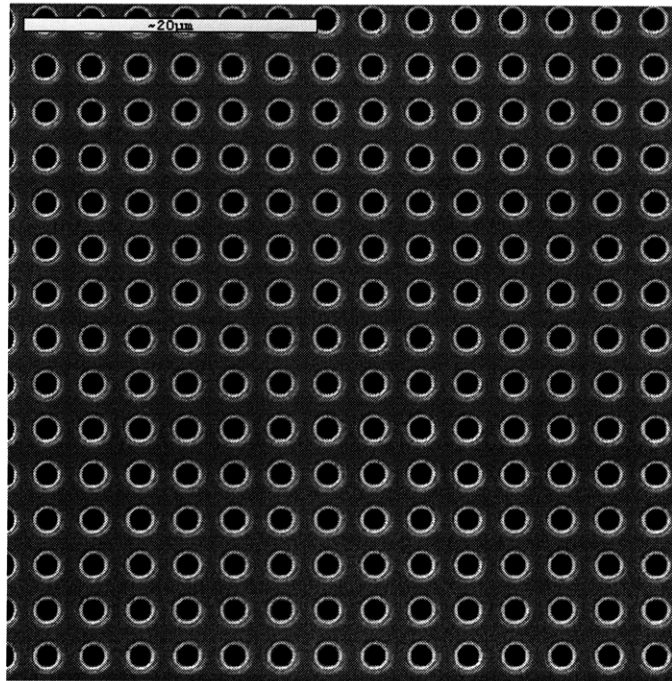


Figure 2-34 CCl₄ HIDE Silicon Etching of 2 µm Holes

A solution of ethanol and one micron air classified copper powder (UltraFine Powders, Woonsocket, RI) was made by adding 3.56 mg of powder to 10 ml of ethanol. The solution was placed in a sonicator for one hour to disperse the particles, and then applied to a 16 mm x 16 mm silicon substrate, which was also sitting on a plate in a sonic bath. A micro pipette was used to dispense 0.25 ml of the solution, which was held on the substrate by surface tension. Sonication was used to “shake” the particles into the holes. Copper particles were ballistic, meaning they rapidly fell when in a liquid. The copper settled into the holes, and the excess was wiped clean after the ethanol evaporated. Three applications resulted in near complete filing of the matrix (Figure 2-35). The powder used had a wide size distribution so many holes contained several particles while others only contained one.

Ideally, a metallic sphere would occupy each hole. This concept was demonstrated using precisely sized silica spheres. Ten drops of an aqueous 2.5% solids

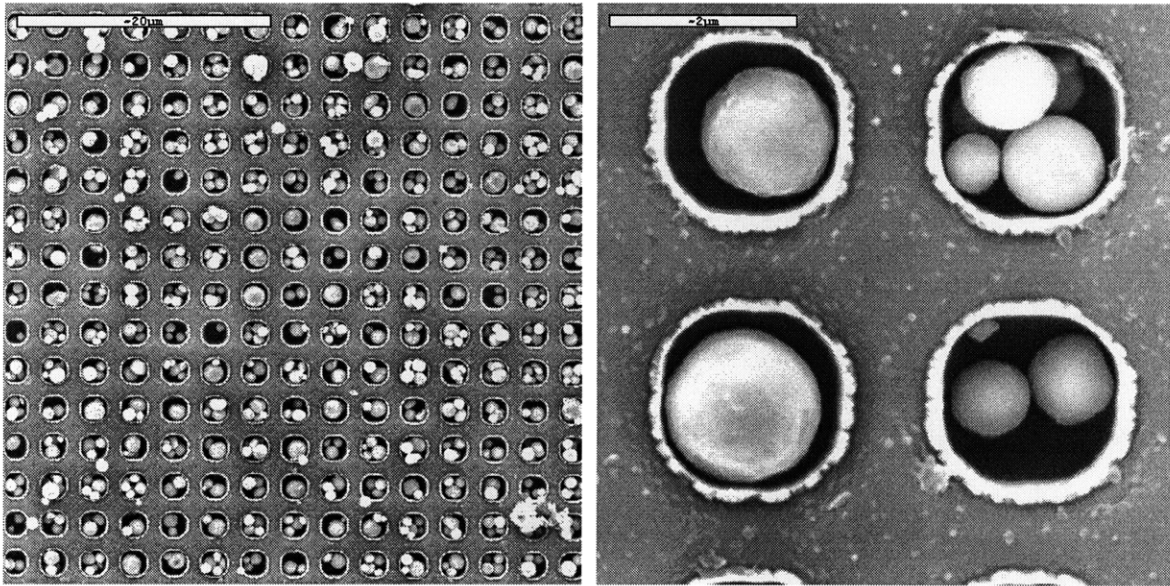


Figure 2-35 Copper Particles (1 μm Dist.) in Silicon After Three Applications

solution of $1.58 \pm 0.06 \mu\text{m}$ silica spheres (Duke Scientific, Palo Alto, CA) were placed in a small beaker, and the water allowed to evaporate. Ten milliliters of ethanol were added to the dried spheres and the solution placed in a sonic bath for one hour to disperse the particles. The solution was applied to the silicon in the same manner as the copper particles. The silicon array was almost completely filled after two applications, demonstrating that given the correct size distribution of particles, a precise arrangement of monosized spheres was possible. Figure 2-36 illustrates a perfectly filled array of particles. Improvements in powder processing should yield a more uniform particle size powder in order to perfectly fill the holes. Investigations into metallizing readily available silica spheres could also provide a source of monioside metallic particles.

Attempts were also made to fill a wax mold with particles. A wax transfer mold was produced replicating the $2 \mu\text{m}$ holes with only minimal distortions, however, application of copper particles using the described method resulted in damage to the mold (Figure 2-37). This indicated that paraffin was too soft a media to apply the particles too.

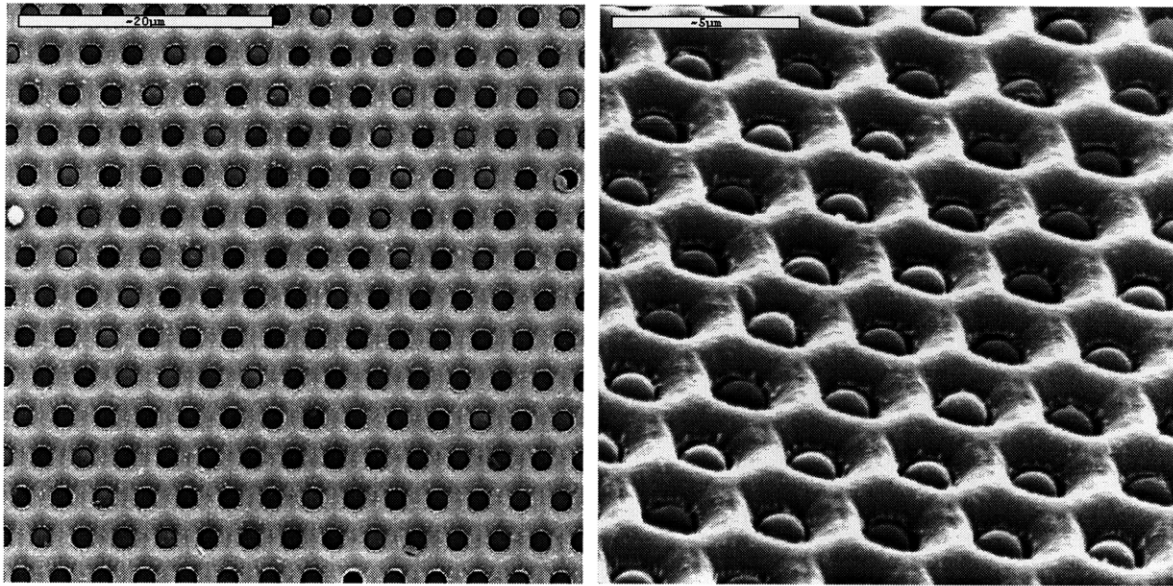
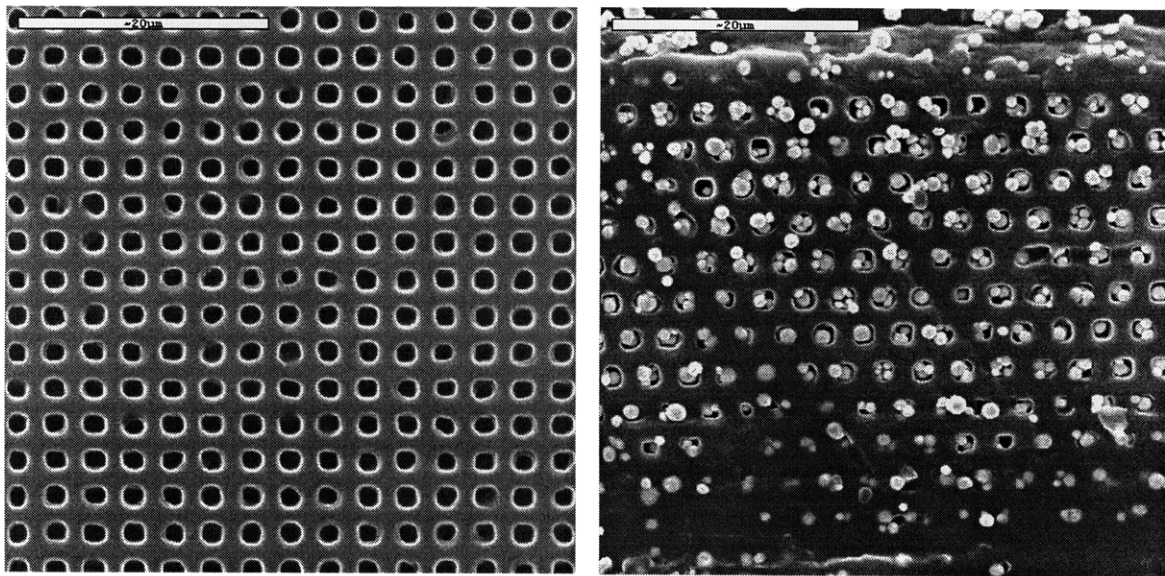


Figure 2-36 1.58 μm Silica Spheres in Silicon Substrate



A

B

Figure 2-37 A) Wax Mold of HIDE Etching and B) Copper Particles in Damaged Wax Mold

Other materials such as epoxies and polyimides should be investigated as suitable molding materials. The ultimate goal would be to create a thin structure with one layer of the lattice, and then to stack several layers together to form the final array. Producing a tool to stamp a more robust material could be one possible solution.

An aqueous alumina slurry identical to those used for the micro turbine was applied to a wax mold of the HIDE etching. Figure 2-38 shows the resulting structure in fired alumina. The molding process successfully produced a precisely arranged array of ceramic posts, which could be used as an embossing tool to pattern other substrates. This pattern was also a testament to the fine features possible with the micromolding process.

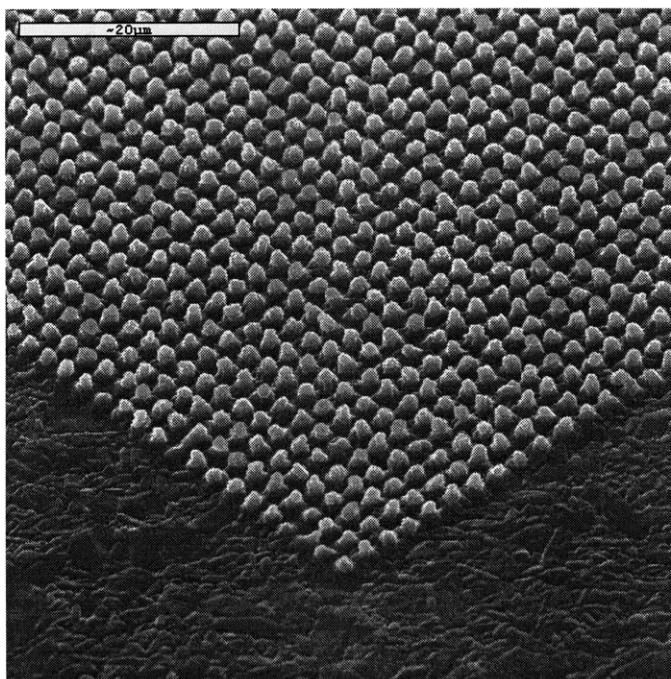


Figure 2-38 HIDE Embossing Tool in Fired Alumina

2.5 Conclusion

A micromolding process was developed which was capable of producing a variety of MEMS and mesoscale parts. The process utilized reusable tooling and was very easy to perform, however, the process will not be of much use until it has been properly characterized and optimized. Understanding the origin of defects will be crucial to the formation of components. Dimensional changes across process steps will make designing for final part measurements a challenge. While initial results were very encouraging, several issues regarding slurry composition and part quality remain to be solved. In the next section, the limitations of the process are explored, along with factors influencing these issues. A quantitative assessment of feature resolution and dimensional stability of the transfer steps is also presented.

Chapter 3

3.1 Process Performance

A quantitative assessment of process performance is required before it can progress from the laboratory into production. There are many aspects of this process which require characterization and analysis for development to continue. Understanding how the process works is key to developing improvements in processing methodology.

Several aspect of process performance are examined in this chapter. Minimum feature resolution is explored, factors influencing yield and part quality are explained, and an analysis of dimensional stability is presented. This initial inquiry into the performance and phenomena of the process represents the first step in refining the method into a viable production tool.

3.1.1 Minimum Feature Size

Experiments were conducted to determine how small a feature could be produced with the micromolding method. A test pattern of geometric shapes was etched in silicon and subjected to the micromolding process to produce the pattern in ceramic (Figure 3-1). (each feature was referred to by its position X,Y) The pattern demonstrated that positive and negative features smaller than two microns could be resolved, although significant feature degradation was observed below two microns. Figure 3-2A shows feature (1,4), two rectangles separated by a one micron line which was degraded in the wax. While this feature was successfully reproduced in fired ceramic (Figure 3-2B), the two rectangles were not resolved in other samples (Figure 3-3). This, along with observations of degradation in the wax mold, suggests that negative feature resolution was a function of wax mold quality. Feature (5,4), two lines approximately two microns wide, were used to gauge the minimum positive features possible. Figure 3-4 shows the feature in wax and in fired alumina. The negative features were on the order of two microns and appear to

have reproduced with only slight degradation. Note that the width of the lines were on the order of a sintered grain.

The resolution of the process was tested by comparing the diminishing sizes of circles and squared in rows 1 and 2 of the feature grid. Note that the smallest circle (5,1) and square (5,2) were not reproduced in silicon due to reaching the limit of the photolithography equipment. There was a discernable difference between the circle (Figure 3-5) and square (Figure 3-6) in features (3,1) and (3,2), which measured approximately six microns across. Resolution began to falter in features (4,1) and (4,2), which measured only about 2.5 microns across (Figure 3-8 and Figure 3-7). Therefore feature resolution below six microns was difficult, but not impossible, to maintain. Resolution again also appeared to be limited by the sintered grain size of the ceramic.

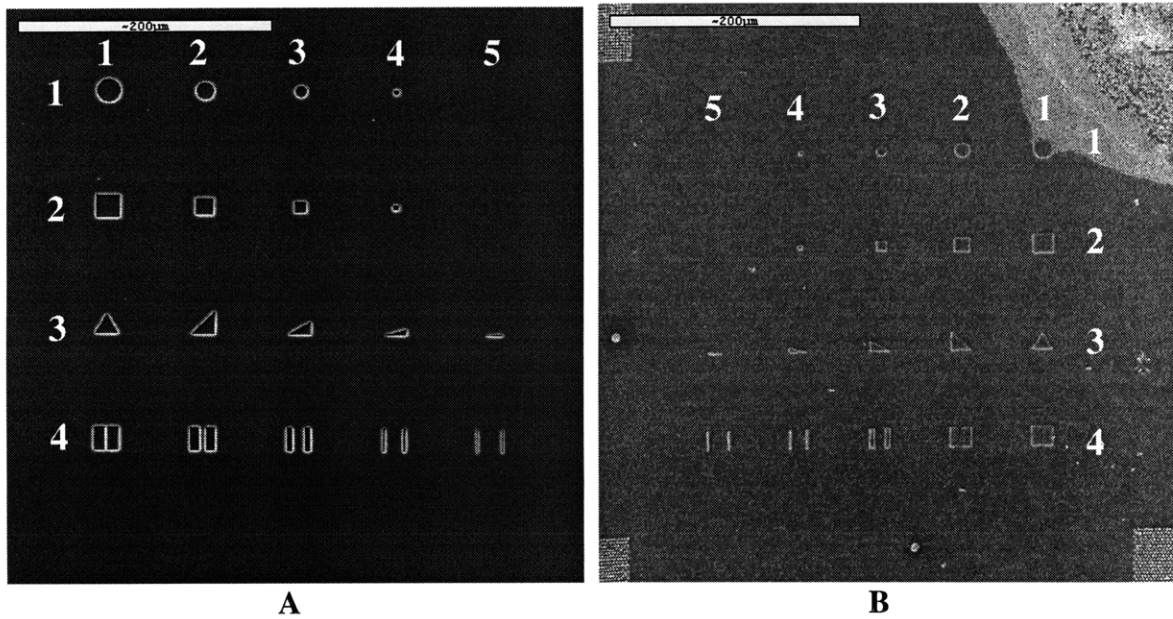


Figure 3-1 Geometric Test Features in A) Silicon and B) Fired Ceramic

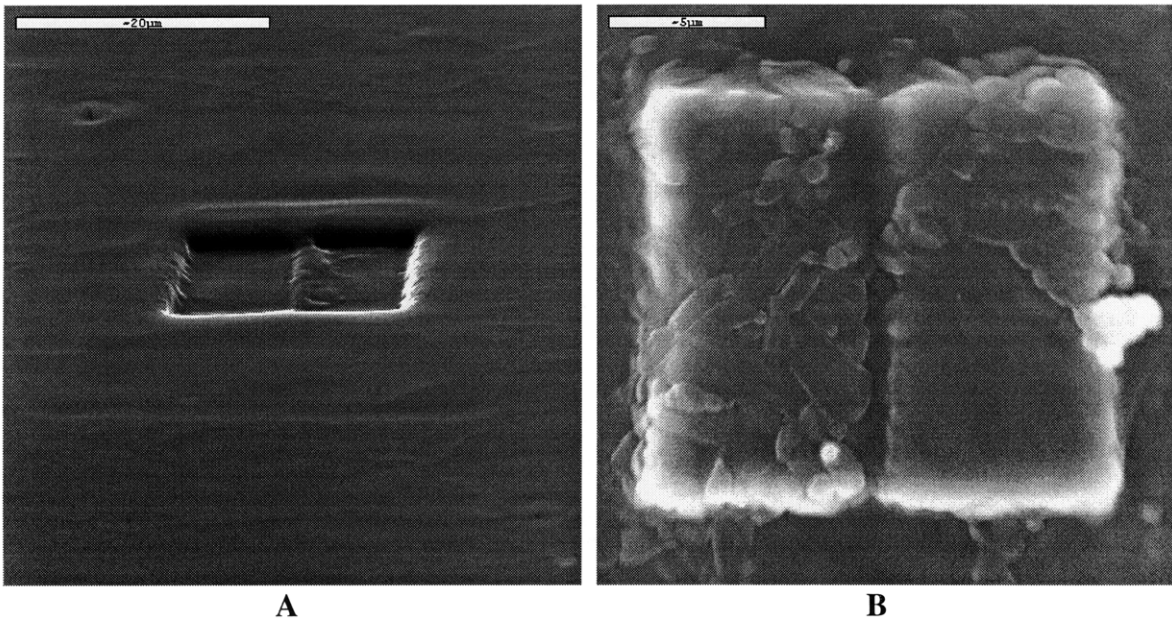


Figure 3-2 Minimum Negative Test Feature (1,4) in A) Wax and B) Fired Alumina

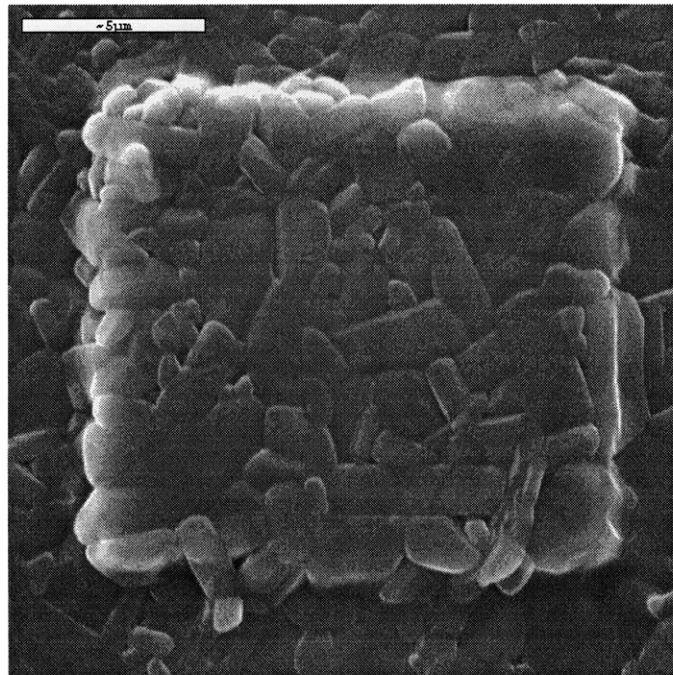


Figure 3-3 Unsuccessful Minimum Negative Test Feature (1,4) in Fired Alumina

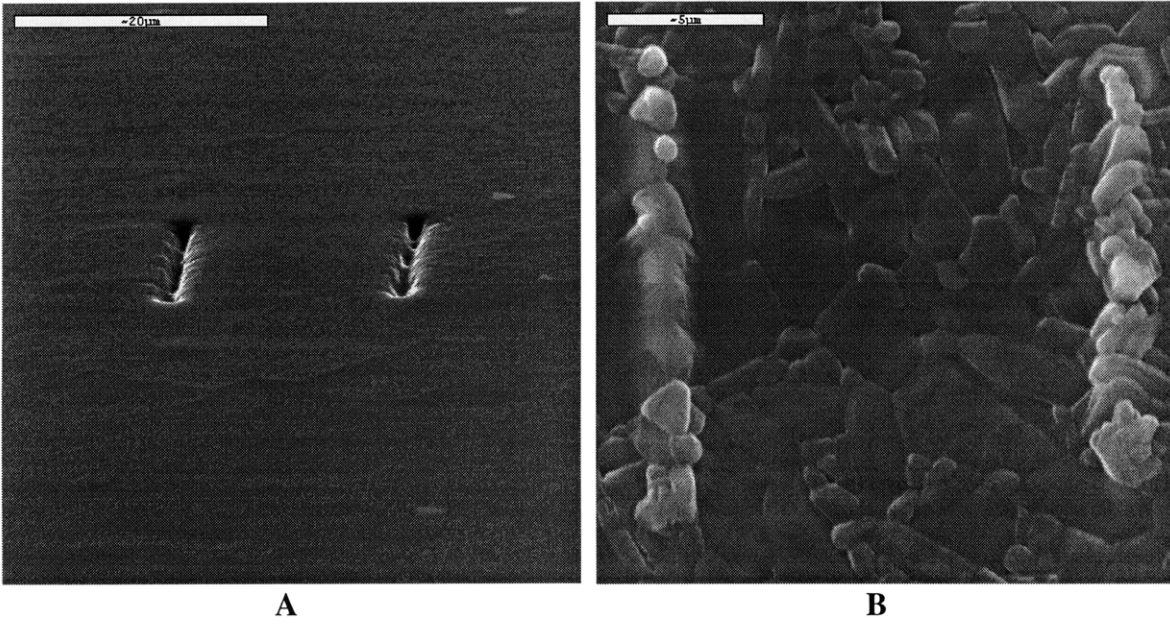


Figure 3-4 Minimum Positive Test Feature (5,4) in A)Wax and B) Fired Alumina

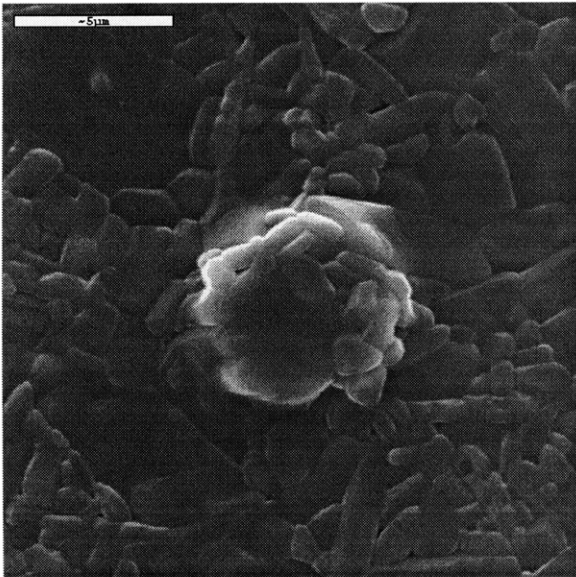


Figure 3-5 Circular Feature (3,1) in Fired Alumina

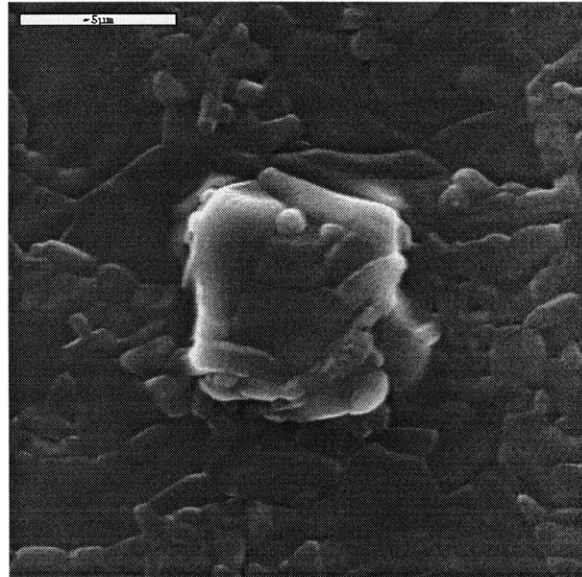


Figure 3-6 Square Feature (3,2) in Fired Alumina

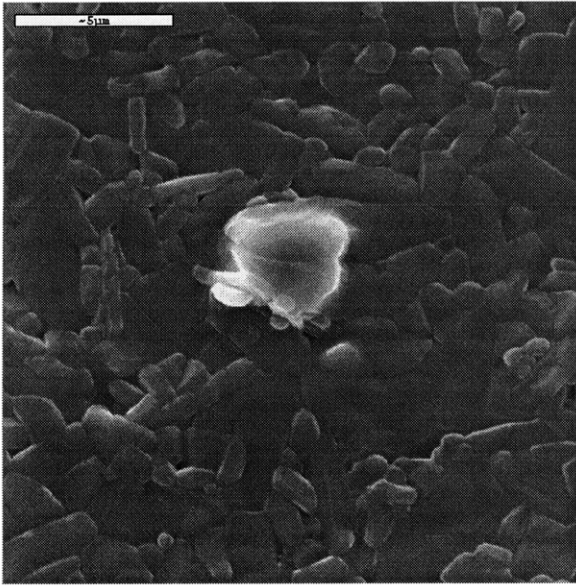


Figure 3-7 Smallest Resolvable Square Feature (4,2) in Fired Alumina

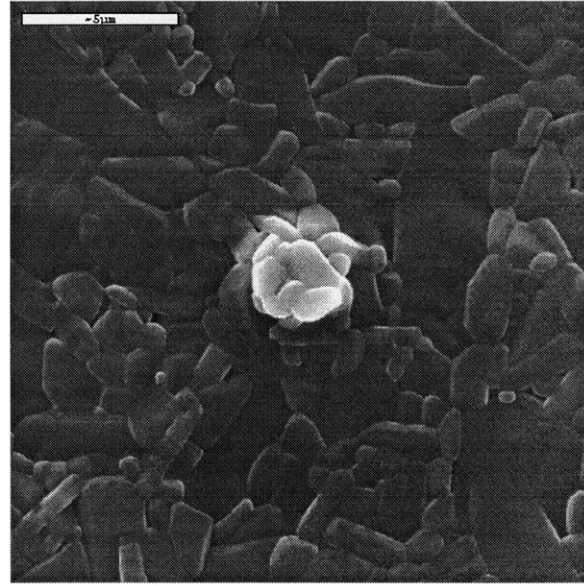


Figure 3-8 Smallest Resolvable Circular Feature (4,1) in Fired Alumina

The higher aspect ratio features found on the micro turbines also reproduced well. A detailed view of the smallest feature, an airfoil trailing edge, is presented in Figure 3-9. The blade tip was about 10 μm wide and 60 μm high, for an aspect ratio of 6. Some blades, however, exhibited significant tapering at the tips (Figure 3-10). This was most likely a result of the DRIE etch. Even higher aspect ratio turbine blades showed excellent minimum feature resolutions. Figure 3-11 shows the trailing edge of a blade tip 20 μm wide and 150 μm high (AR=7.5). Although these deep turbines experienced several filling defects, several blades were successfully produced (Figure 3-12). These defects allowed a cross sectional view of the corner of one of the blades (Figure 3-13). The curvature of the top surface of the blade was again a result of the DRIE etching process (see Figure 2-5), and demonstrated that curvature control of corners could be dominated by the etching process parameters. Detailed photos of the 6.5 aspect ratio turbine blades showed excellent resolution on both the outside and inside 90° corners, approaching that of the sintered grain size (Figure 3-14).

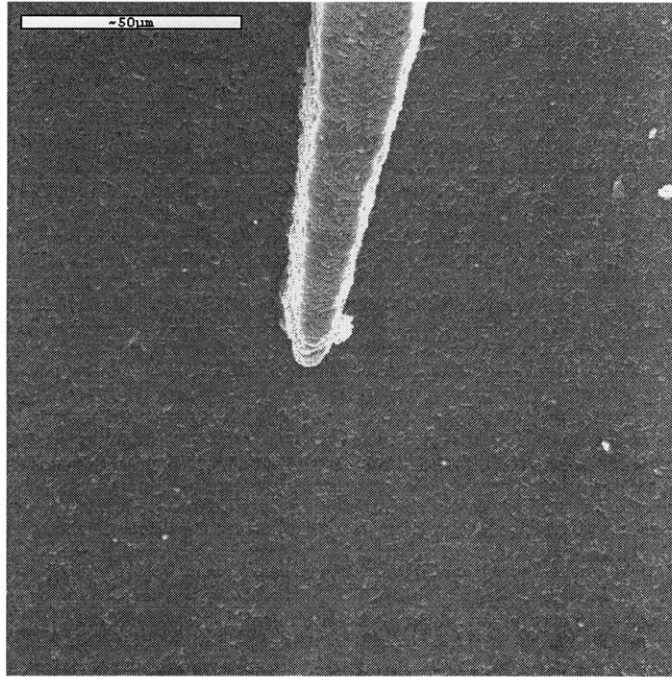


Figure 3-9 High AR (6) Stator Trailing Edge in Fired Alumina

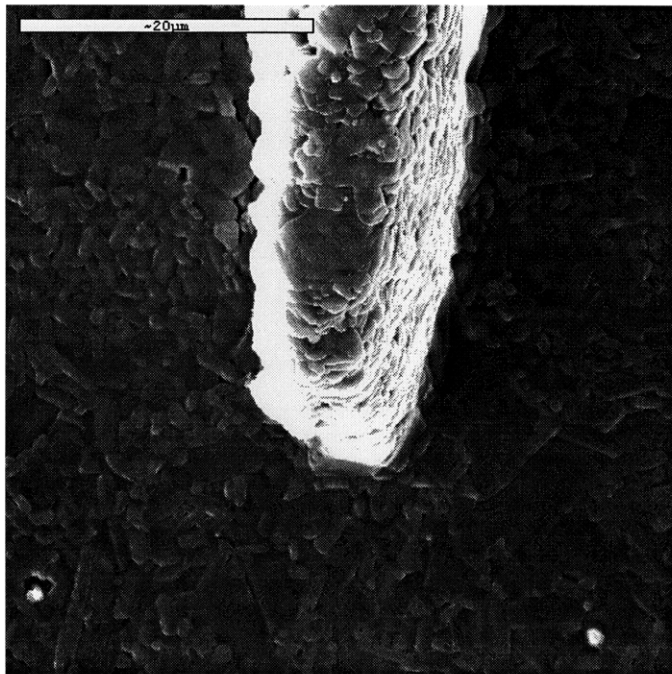


Figure 3-10 High AR (6) Stator Trailing Edge with Taper in Fired Alumina

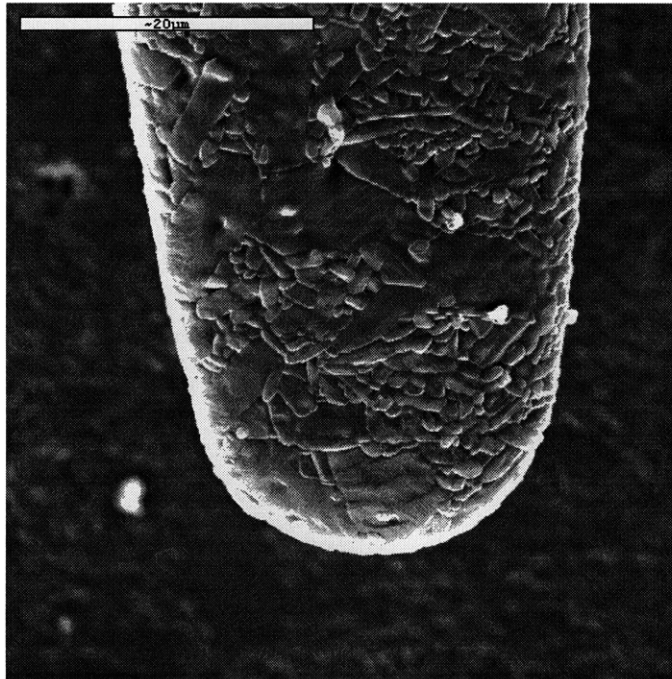


Figure 3-11 High AR (7.5) Turbine Rotor Blade Trailing Edge

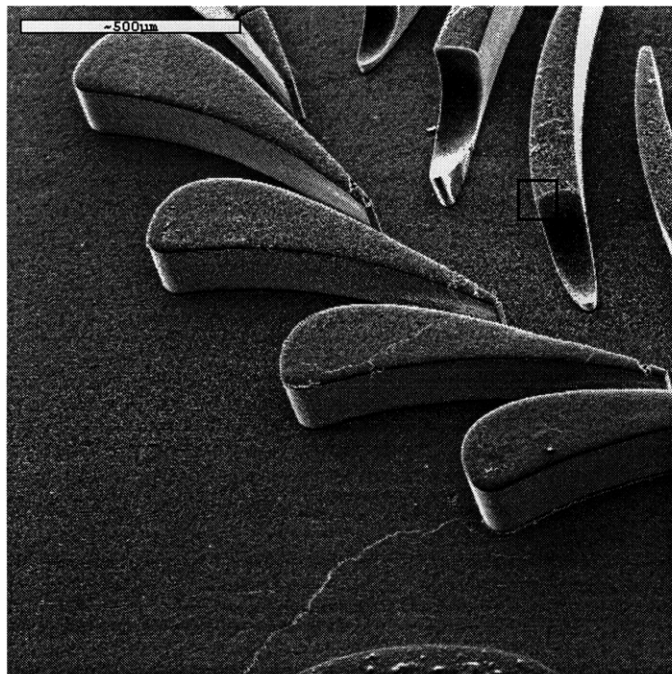


Figure 3-12 High AR (7.5) Turbine Stator Blades

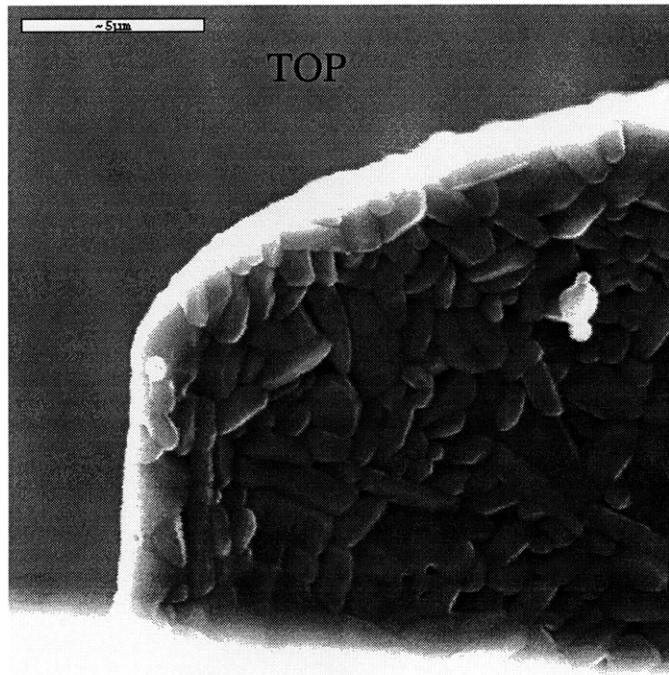


Figure 3-13 Cross Section of Top Edge of High AR (7.5) Turbine Blade in Fired Alumina

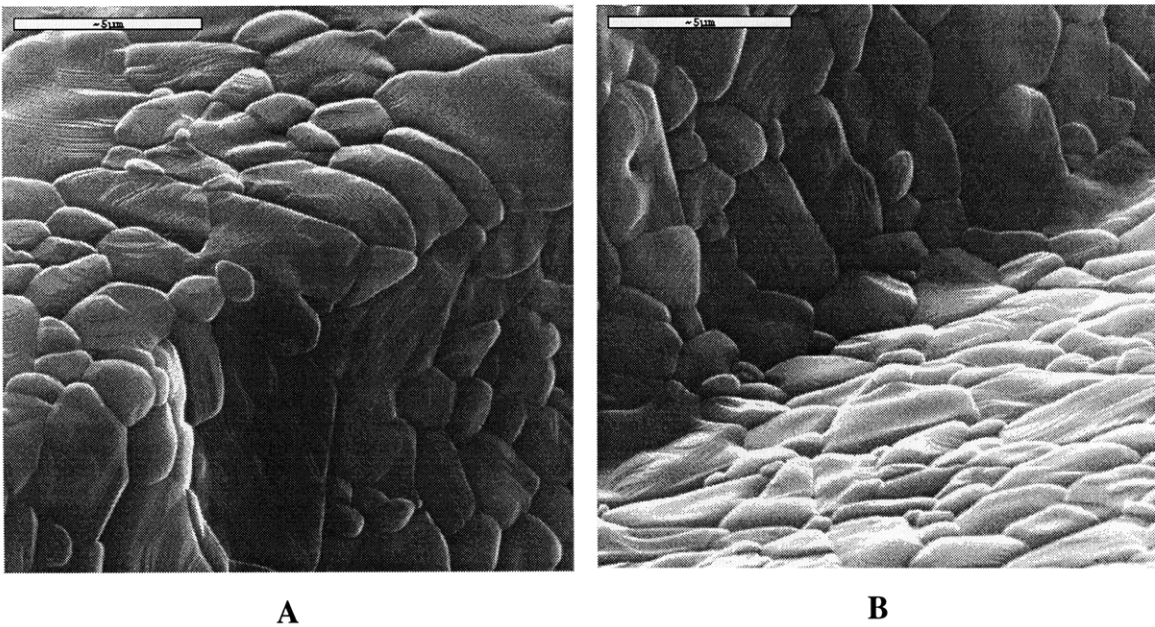


Figure 3-14 High AR (6.5) Fired Alumina A) Outside and B) Inside Corner Detail

The smallest features observed on turbine blades were the etching striations produced in some silicon molds (Figure 3-15). These striations appeared to be about three microns wide, and could be seen clearly in many of the turbines produced (Figure 3-16). This vertical scalloping was due to the uneven degradation of the photoresist during etching. The smooth sides of the blades in Figure 3-17 demonstrated that it was possible to eliminate these striations through proper DRIE processing techniques.

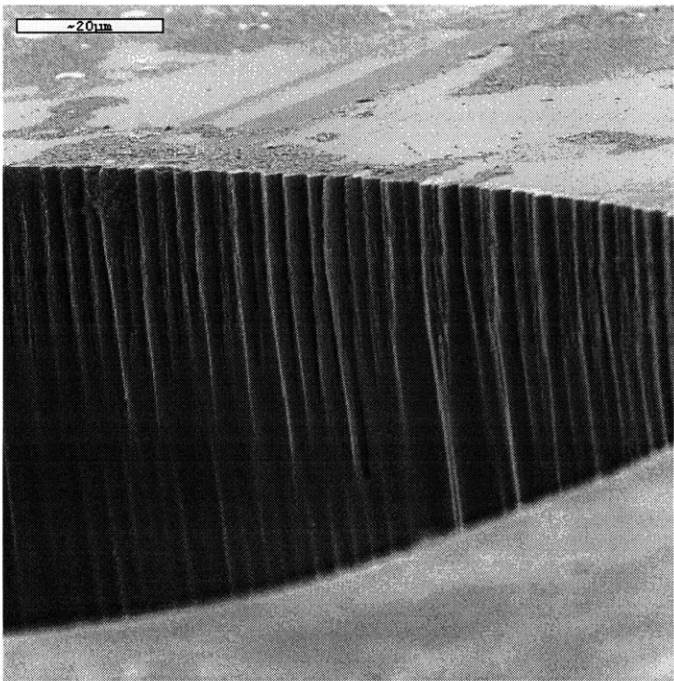


Figure 3-15 Scalloped Sidewalls of Silicon Etching

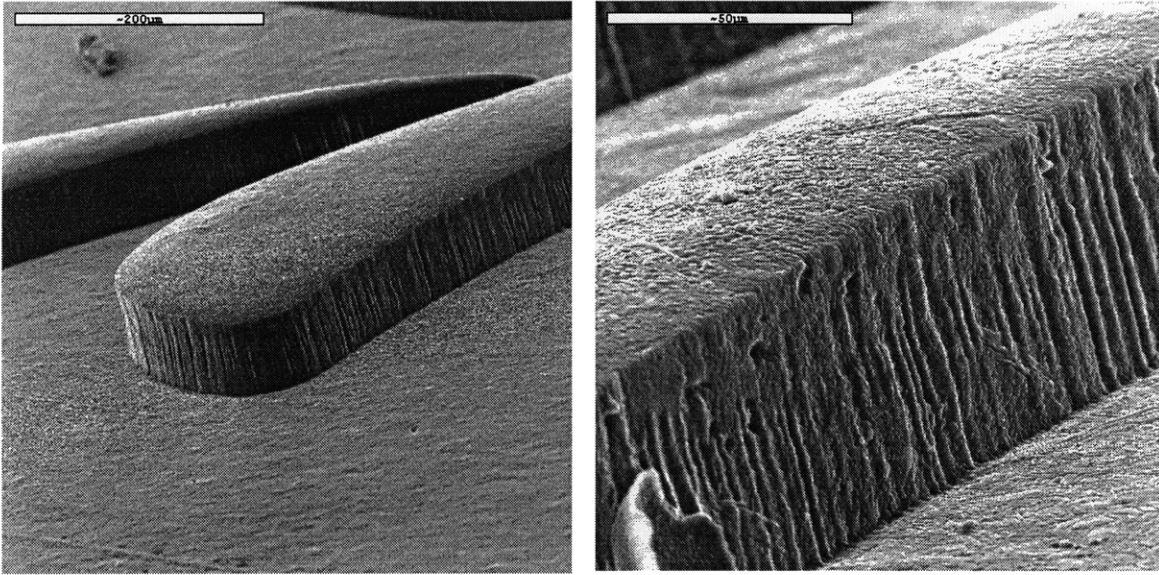


Figure 3-16 High AR (6.5) Turbine Blade With Reproduced Etch Relics

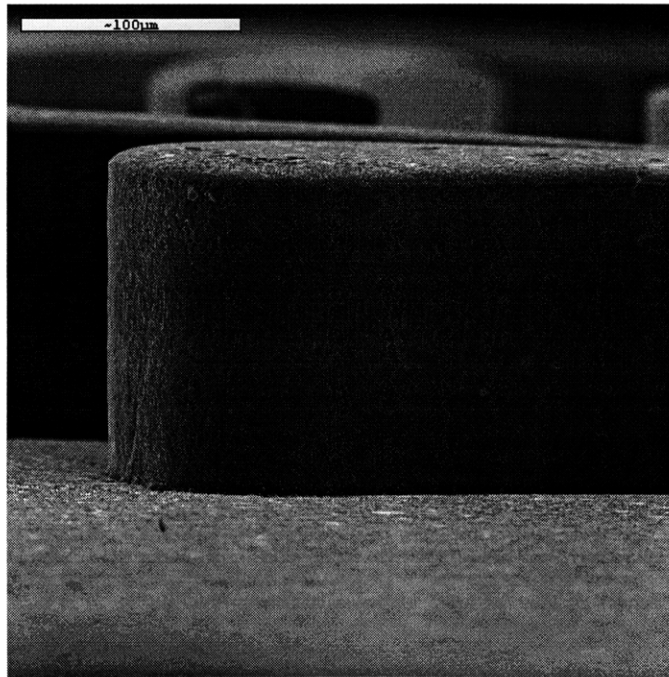


Figure 3-17 High AR (7.5) Turbine Blade Without Etching Relics in Fired Alumina

Several other small feature sets were created using the HIDE mold and a test pattern (used in section 3.1.4). Figure 3-18 shows the closely spaced structures formed in alumina from the HIDE etchings. Experiments with the HIDE patterns have demonstrated that low aspect ratio, closely packed features smaller than 2 μm can be successfully patterned. Additionally, a test pattern of squares (Figure 3-19) were successfully produced in ceramic and measured to determine dimensional stability of the process. Several other features resident on the same mask, such as closely spaced lines, were also produced, demonstrating the versatility of the process to make such “textured” ceramics. These lines were 5 μm wide with a spacing that diminishes to 5 μm (Figure 3-20).

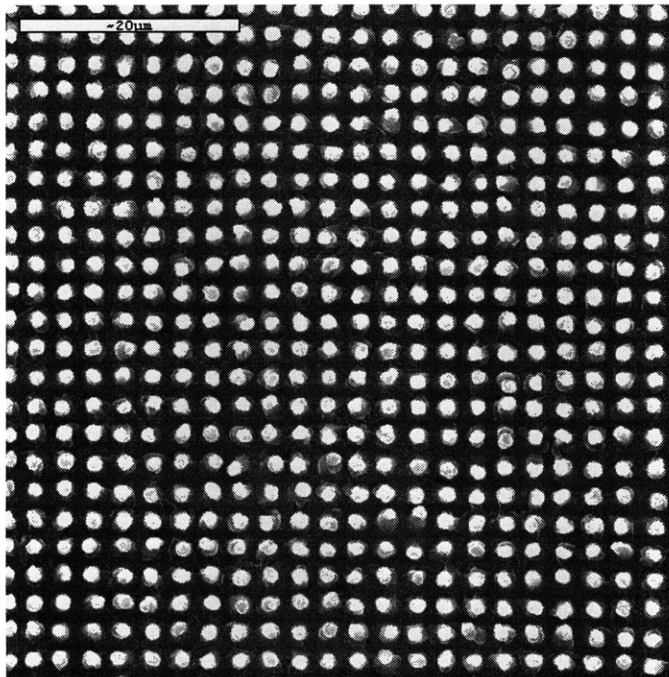


Figure 3-18 Closely Packed $<2\mu\text{m}$ Pattern from HIDE Etching in Fired Alumina

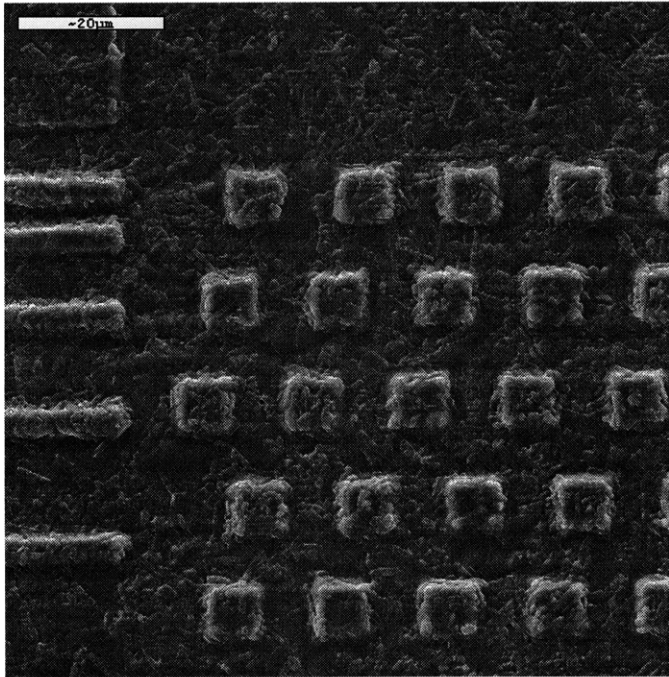


Figure 3-19 Fired Alumina Dimensional Test Squares

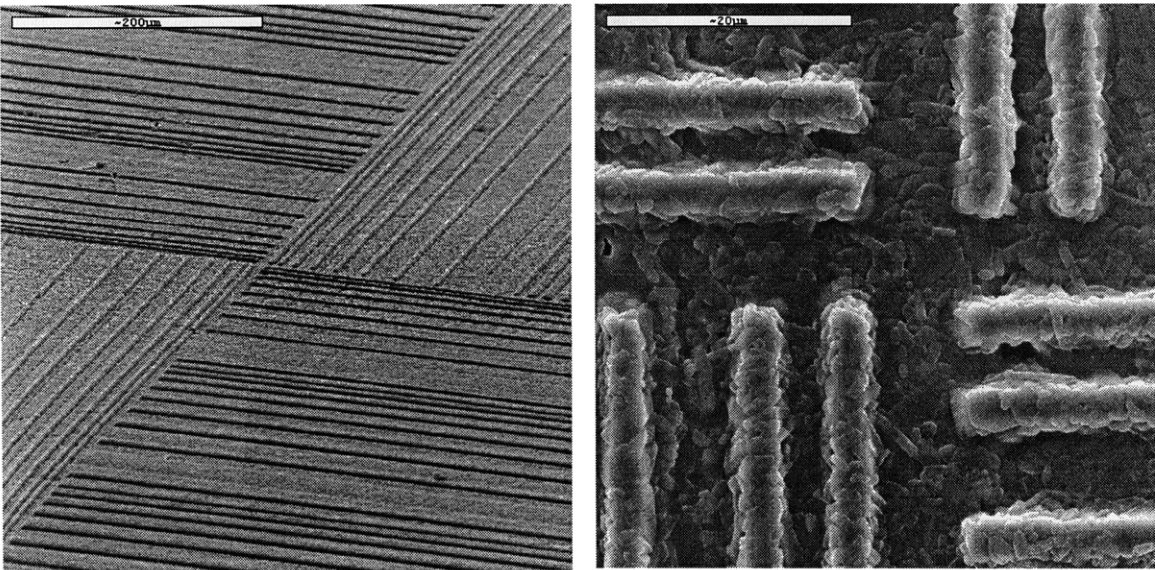


Figure 3-20 Fired Alumina Lines Forming Textured Ceramic

The limits of the micromolding technique were not only dependent on how small a feature could be patterned in wax. Minimum feature size was also limited by the sintered grain size of the ceramic. Herein lies one of the drawbacks of this powder based process. Ceramic forming is unable of achieving features smaller than the base particle size of the working material. This is unlike high precision non-ceramic forming processes such a LIGA, where metal can be plated directly into a mold. The sintered size of the ceramic particles will ultimately determine the smallest feature available, regardless of how small a feature is molded. As such, the smallest practical particle size slurry should be used for maximum feature resolution and surface finish. A tradeoff between particle size and drying effects makes this an interesting design challenge. Sintering time and temperature must also be carefully controlled to control grain growth during firing.

This section has examined the capabilities and limitations of the process to create ceramic forms with micron scale features. Several different structures were successfully produced, demonstrating the capability of the process to produce complex high aspect ratio parts and to resolve features approaching sintered grain size. Features smaller than two microns were resolved, proving that very small dimensions were possible. Parts with aspect ratios of up to 7.5 were also successfully formed by this method. Determining factors in part resolution appeared to be the quality of the molds used and the fired grain size of the ceramic.

3.1.2 Part Quality

The quality of parts produced by the process is a true measure of its worth as a manufacturing tool. The process must be able to produce parts without defects in order for them to be placed in a MEMS or mesoscale device. Understanding the origin of part defects is essential to developing a reliable, consistent process. A variety of defects were observed during part production, most of which were common to all parts produced.

The major source of flaws in PZT fibers, as well as other parts produced by this process, were drying defects. During drying, solvent evaporates from a drying surface at a rate given by:

$$\dot{V}_e = k(p_v - p_A)$$

where k is a constant dependent on thermal and geometrical factors, p_v is the solvent vapor pressure, and p_A is the partial solvent pressure in the atmosphere. The evaporation rate per unit area is constant due to the continuous supply of fluid to the surface, hence this is called the Constant Rate Period (CRP) of drying. During the CRP, a liquid meniscus is located at the surface of the body, which is continuously fed from a supersaturated region central to the body. In order to maintain the least amount of surface energy in the system, fluid is constantly moving to the surface through capillary action to maintain the less energetic solid/liquid interface. As the supersaturated region is depleted, there is no longer a source of fluid to keep the surface saturated. Studies have shown that the point of maximum capillary stress occurs immediately after the supersaturated region has been depleted, leaving a 100% saturated drying plane that then begins to recede into the body. Capillary stress is inversely proportional to pore size, and is give by:

$$P = \frac{2\phi\gamma}{d}$$

where ϕ is a geometric packing factor, γ is the surface tension, and d is the pore diameter. It is at the point of maximum capillary stress when the electrostatic repulsion forces between dispersed particles are overcome, causing the particle network to shrink.³⁸ The dispersion state of the slurry, therefore, plays an important role in how the body deforms during drying.

Void formation is believed to be influenced by the dispersion state of the slurry. In a well dispersed slurry, a dense layer of particles is cast on the drying surface as moisture continues to be removed from the body. The corresponding loss of moisture is accompanied by a change in part volume due to particle packing at the drying surface.

This volumetric change is hindered by the hard dense layer and constrained by the mold, thus causing any volumetric change to occur opposite the drying surface. It is the large amount of shrinkage that occurs during drying of a dispersed slurry that causes a void to form. Figure 3-21 demonstrates this phenomena. This would explain the location of shrinkage voids seen opposite the cast surface of fibers (Figure 3-22) and in the center of pipette applied ceramics, both of which were made with well dispersed slurries.

A slurry that is not well dispersed, or flocculated, produces parts without shrinkage voids. In a flocculated slurry, the electrostatic forces between particles are weak, allowing the natural attractive forces (VanDer Walls) to cause the particles to form floccs. The resulting agglomerates cluster at the drying face, forming a structure with large pores that is significantly weaker than the dense solids layer formed by dispersed slurries. The weak structure allows uniform shrinkage throughout the body, allowing the original shape to be maintained. The large pore structure also results in less shrinkage of the body during drying. These are the same principles behind creating spherical particles during spray drying operations.³⁹

To test this theory, flocculated slurries were created and used to make micromolded parts. Alumina slurries were flocculated by adding CaCl_2 to increase the ionic strength of the slurry, thereby reducing the interparticle repulsive forces causing the slurry to flocculate. PZT slurries were flocculated by adjusting the amount of polymeric dispersant. Flocculation of slurries was verified through viscometry. Parts created with both flocculated and dispersed slurries are presented in Figure 3-23. A dramatic difference in formation of defects is immediately apparent between parts made from flocced and dispersed slurries. Unfortunately using flocculated slurries results in a lower green density due to the larger pores created during drying. Therefore there is a tradeoff between defect mitigation and green density.

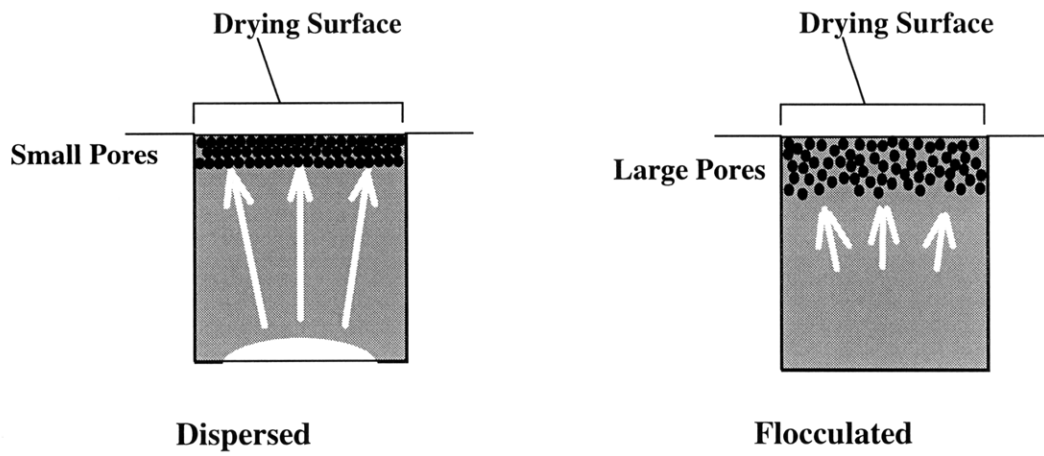


Figure 3-21 Void Formation Due to Shrinkage During Drying

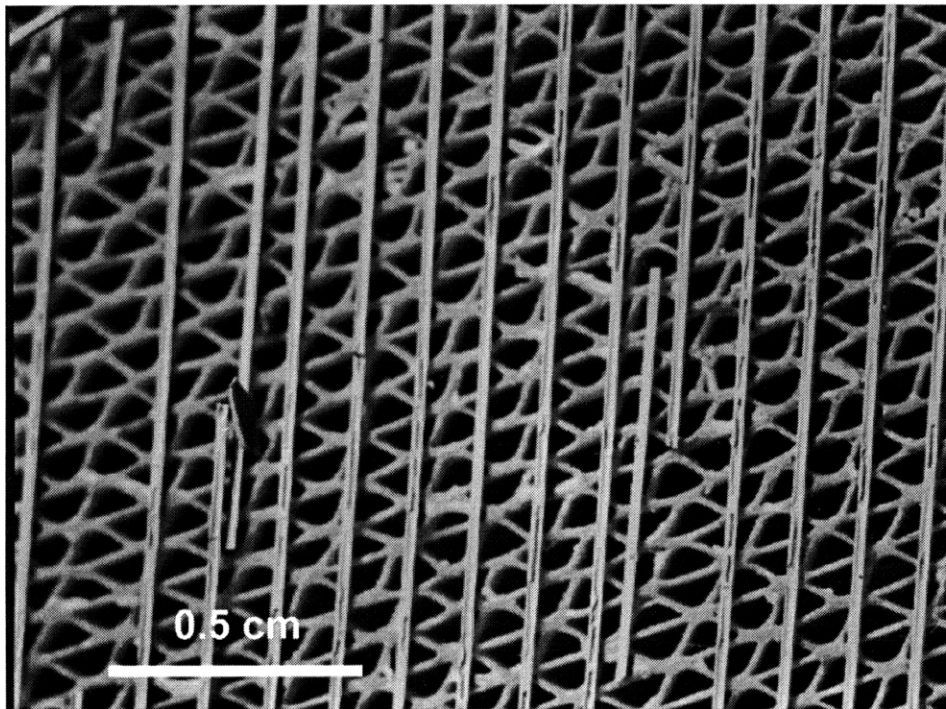
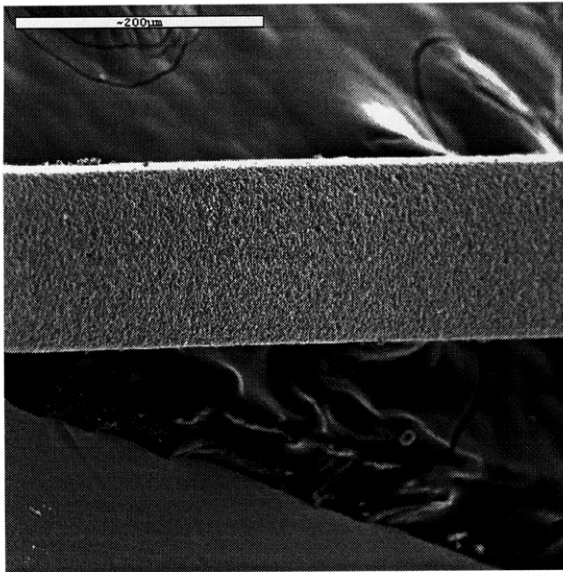


Figure 3-22 Square PZT Fibers with Shrinkage Voids⁴⁰

Flocculated



Dispersed

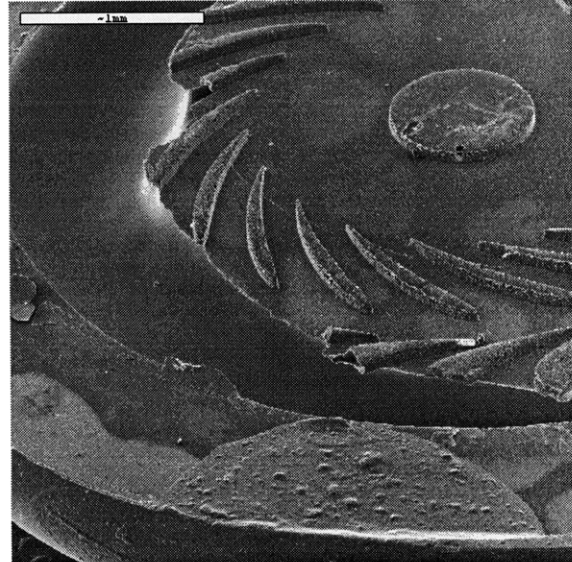
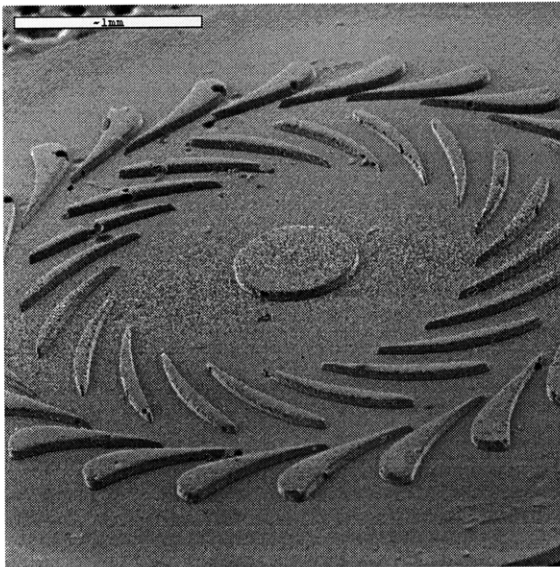
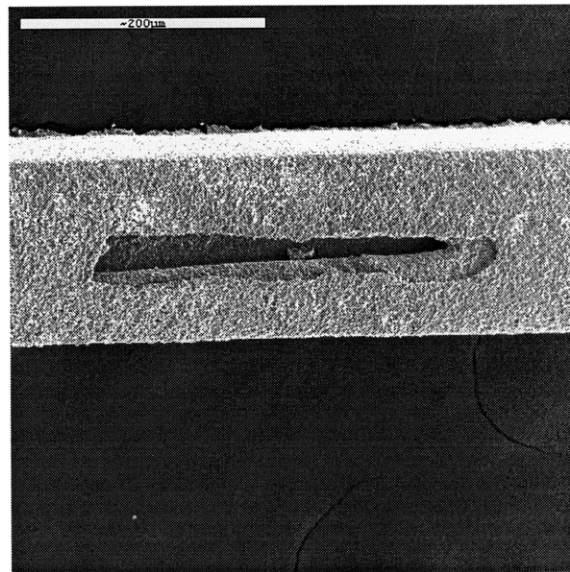


Figure 3-23 PZT Fibers and Alumina Micro Turbines Created From Flocculated and Dispersed Slurries

Other issues affecting part quality included warpage during firing (all parts), powder residue (PZT fibers) and mold wetting (micro turbines). The most pronounced warpage during sintering was observed in PZT fibers fired on a PZT powder bed. There were no constraints on the fibers as they sat on the PZT bed, therefore they were free to

deform during sintering. Deformation of the powder bed also occurred during firing, causing the fibers to warp and crack. Sintering also imparted some negligible warpage on the micro turbines and micro reactor parts, although this warpage was not quantified. Additionally, some of the PZT powder inevitably sintered to the fiber. Efforts to resolve these problems have recently centered on development of a micromolded setter (Figure 3-24), which has shown encouraging results in both straightening fibers and avoiding powder residue (Figure 3-25).⁴⁰

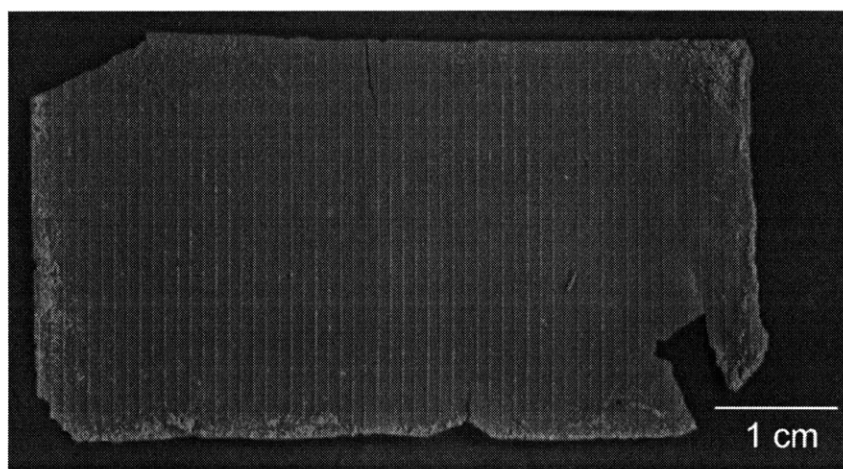


Figure 3-24 Micromolded PZT Setter⁴⁰

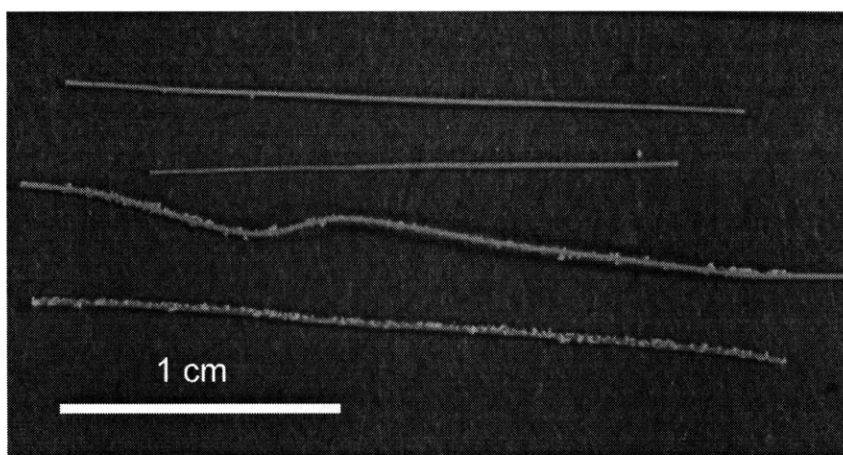
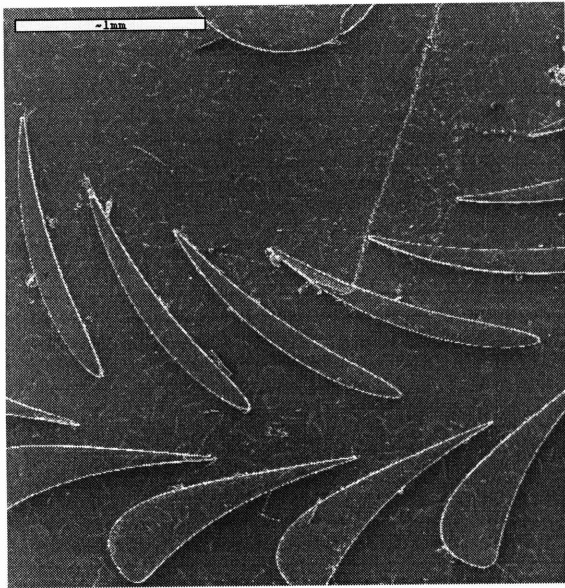


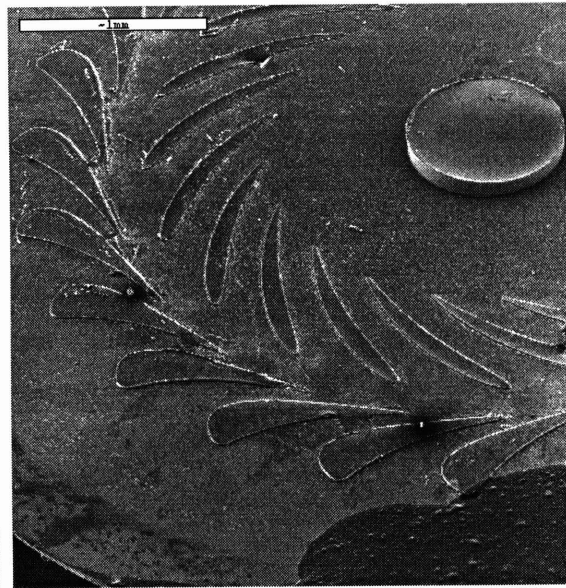
Figure 3-25 PZT Fibers a) Fired on Micromolded Setter (top) and b) PZT Powder Bed (bottom)⁴⁰

Wetting of the wax molds also posed a problem, especially when using aqueous slurries. Alumina slurries made with different solvent systems were used to create micro turbines. Figure 3-26 shows several micro turbines and the contact angles of their respective slurry solvents. Turbines produced with slurries containing low contact angle solvents produced the best results, completely filling the features. A water and methanol slurry completely failed to fill the turbine blades, leaving only impressions of the blades in the alumina. Surfactants were added (0.002 g/ml Surfanol 104E) to improve wetting characteristics, although complete filling of deep features was not achieved. Since the best filling results have been with solvent based slurries, this suggests that a flocculated non-aqueous slurry would produce parts with complete filling and no drying defects. Investigations into different surfactant concentrations, as well as more compatible mold/slurry combinations will be the subject of future work.

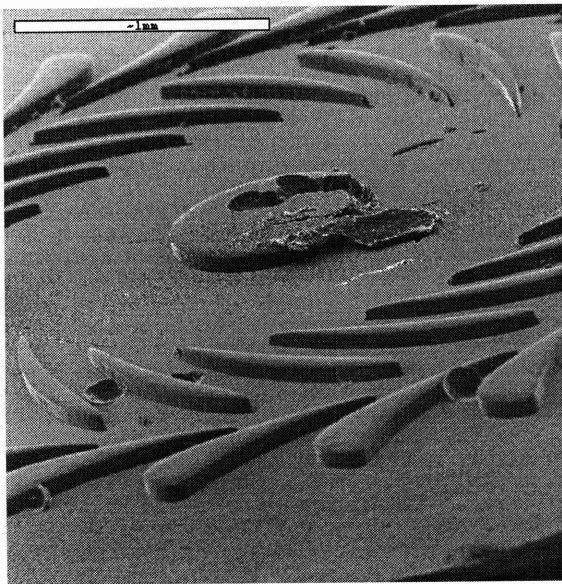
This section has examined several issues related to part quality. It has explained the source of major defects found in parts, and has exposed several areas in which improvement is needed. Adjustment of process parameters through an understanding of phenomena behind defect formation will lead to a process that can reliably produce mass quantities of perfect parts for MEMS and mesoscale devices.



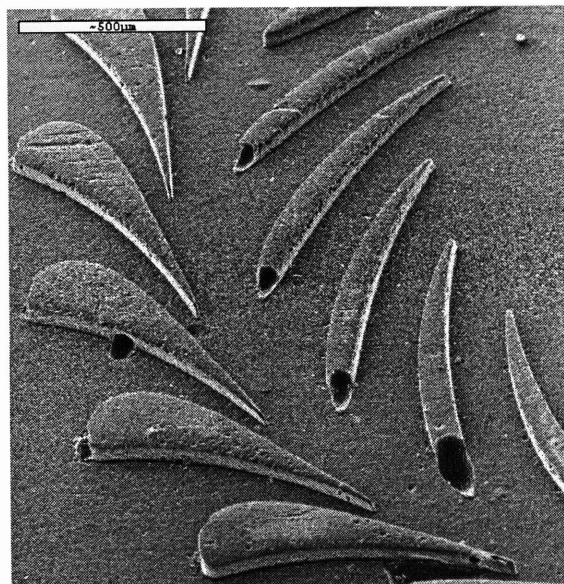
IPA < 15°



H₂O/Methanol = 85°



MEK/Ethanol = 20°



H₂O/Methanol/Surf = 57°

Figure 3-26 Effect of Contact Angle on Mold Filling

3.1.3 Yield

Not only must the process produce defect free part, but it must also be able to do so in large quantities. Determining the success rate of batch production was difficult due to the experimental nature of the slurries. Gaining an understanding of slurry drying characteristics made quantitative yield determinations difficult. However, several observations were made regarding yield and yield improvement. Process yield was largely a function of the part geometry, and each part had specific issues. Batch yields ranged from complete failure to complete success. Clearly yield improvement and consistency are areas for future work.

The yield of PZT fibers was initially poor, due to the non-sacrificial silicone molds being used. Yield improved once a switch to wax sacrificial molds was made. Initial attempts to melt the wax mold were performed on porous alumina. Fully intact continuous fibers were successfully melted out of the wax, however, the fibers tended to stick to the alumina, and were very difficult to remove without breaking. A razor blade was used to scrape the fibers off the substrate, but several continuous length fibers were broken this way. Yield was again improved when a honeycomb structure was used as a melting substrate. This structure provided enough support to prevent sagging and allowed a path for wax to be removed. Removal of the fibers from this substrate was much easier.

The fibers must be transferred to the firing crucible after wax melting. This was done with fine tweezers. Grabbing the green fibers directly usually resulted in breakage, so a “forklift” approach was taken (Figure 3-27). The tips of the tweezers were bent upward and used to forklift the fibers. This method greatly decreased breakage due to physical manipulation.

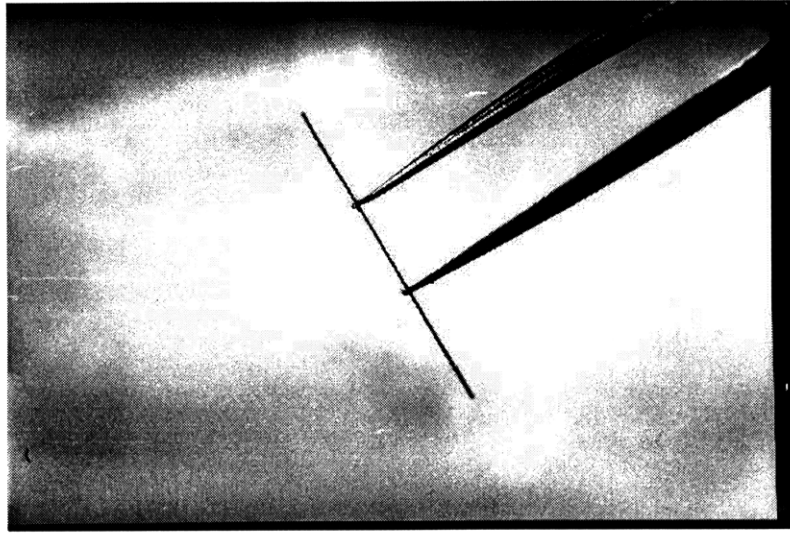


Figure 3-27 Fiber Handling with Forklift Tweezers

The alumina parts were not very sensitive to physical manipulation due to their larger dimensions. However, the small features on the micro turbines could easily be damaged if touched during handling. Removing the parts from the melting surface also posed a hazard, as any lateral forces could cause the blades to break. Investigation into stronger binder systems and different wax melting techniques should help prevent breakage due to manipulation.

Cracking of micro turbine and micro reactors typically occurred during drying, especially when using smaller particle size ceramics. Recalling that capillary stress is inversely proportional to pore diameter, a smaller particle size powder will have smaller pore sizes, hence have a larger tendency to crack during drying. Controlling the drying rate through usage of a humidity oven mitigated cracking during drying, as the decreased drying rate allowed stress gradients through the part to come into equilibrium. This method worked for aqueous slurries, however solvent based systems could be controlled in this manner. Utilizing a flocculated slurry also helped mitigate cracking. The larger pores created in a flocculated slurry resulted in lower capillary stresses. Subsequently, parts made from flocculated slurries did not need to be placed in a humidity oven.

Clearly there are several issues associated with making ceramic parts with a consistent yield. Before a quantitative measure of yield can be made with confidence, several process related issues should first be resolved. Improvements in process performance, handling techniques, and slurry characteristics will provide methods to improve part yield.

3.1.4 Dimensional Stability

Understanding the dimensional changes across mold steps is critical to designing precision parts. Examination of the different process steps revealed that some changes in dimension occurred between the original design and the final part. Additionally, firing of ceramics inherently involves shrinkage, and mold designs should be made with this in mind.

Measurements of original silicon etchings, silicone master molds, wax molds, and fired parts (created from the same slurries used to make the micro turbines) yielded information regarding dimensional changes across process steps. A test pattern of squares was etched in silicon using CCl_4 to a depth of two microns (Figure 3-28). The features were photographed using an optical microscope at a magnification of 750X, focusing on the bottom edge of the features. Each feature was measured with a hand held digital micrometer three times from edge to edge horizontally, removing and replacing the micrometer from the picture between every measurement. The three measurements were averaged to determine the dimension of the feature. Measurements were also taken across a second length scale (a row of five features) in the same manner. Table 3-1 and Table 3-2 lists the dimensional changes measured across the process steps.

Measurement of green parts were not conducted for a variety of reasons. Measurements had to be taken either after wax melting or binder burnout, which resulted in inaccuracies due to wax uptake into the part, wax residue on the part, or shrinkage during binder burnout. Therefore, it was assumed that the green part retains the same

dimensions of the wax mold, hence dimensional changes were reported between wax and fired ceramic parts.

There was considerable difficulty in accurately measuring features with micron scale accuracy. Errors were minimized by photographing features at the highest possible magnification, and by measuring each feature three time. Error was introduced every time the micrometer was placed on the photograph for measurement. Other errors were the result of poor photograph resolution, resulting from low contrast and focusing errors. Incident lighting was used to enhance photographic quality, however, it was still sometimes difficult to differentiate edges. Error was estimated by measuring features twenty times in each type of photograph used. The average error imposed by the micrometer was about 0.1 μm . Taking into account variations in contrast and focusing quality, the actual measurement error was estimated to be somewhere between 0.1 μm and 0.3 μm .

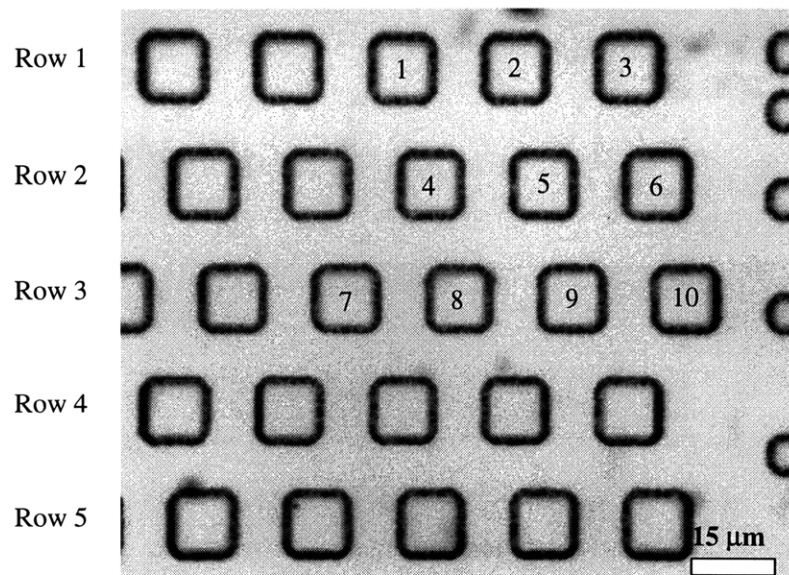


Figure 3-28 Silicon Array of 12 μm Squares

Square Number	Absolute Change (μm)			
	Silicon-Silicone	Silicone-Wax	Wax-Fired	Silicon-Fired
1	-0.2	-0.5	-1.9	-2.7
2	-0.2	-0.5	-2.0	-2.7
3	-0.2	-0.5	-2.1	-2.8
4	-0.4	-0.4	-2.0	-2.9
5	-0.3	-0.6	-2.2	-3.0
6	-0.1	-0.8	-1.9	-2.9
7	-0.9	-0.2	-2.0	-3.2
8	-0.2	-0.9	-2.0	-3.1
9	-0.3	-0.9	-1.9	-3.2
10	0.1	-0.8	-2.0	-2.8
Average Change (μm)	-0.3 ± 0.3	-0.6 ± 0.2	-2.0 ± 0.1	-2.9 ± 0.2
Average Change (%)	-2.1 ± 2.0	-4.6 ± 1.9	-17.1 ± 0.6	-22.8 ± 2.3

Table 3-1 Dimensional Changes Across Process Steps (12 μm Length Scale)

Row Number	Absolute Change (μm)			
	Silicon-Silicone	Silicone-Wax	Wax-Fired	Silicon-Fired
1	-0.2	-0.9	-14.0	-16.2
2	-0.3	-1.0	-14.8	-17.1
3	-0.1	-1.0	-14.3	-16.5
4	-0.5	-0.7	-14.4	-16.8
5	-0.6	-0.6	-14.2	-16.8
Average Change (μm)	-0.4 ± 0.4	-0.9 ± 0.19	-14.3 ± 0.3	-15.6 ± 0.3
Average Change (%)	-0.4 ± 0.4	-1.0 ± 0.20	-15.5 ± 0.3	-16.7 ± 0.3

Table 3-2 Dimensional Changes Across Process Steps (93 μm Length Scale)

Absolute and percent change were calculated for each 12 μm feature in this length set and averaged to determine the amount of expansion or shrinkage. The original features measured $12.8 \mu\text{m} \pm 0.2 \mu\text{m}$. Measurements indicated that an absolute shrinkage of $0.3 \mu\text{m} \pm 0.3$ ($2.1\% \pm 2.0$) occurred over each feature between silicone and silicone molds and $0.6 \mu\text{m} \pm 0.2$ ($4.6\% \pm 1.9$) silicone and wax molds. An absolute shrinkage of

2.0 $\mu\text{m} \pm 0.1$ (17.1% ± 0.6) was observed between green and fired states resulting in an overall silicon to fired shrinkage of 2.9 $\mu\text{m} \pm 0.2$ (22.8% ± 2.3) over a 12 μm length scale.

Measurements on the 12 μm length scale, while useful for examining changes across process steps, contained a large amount of relative error. Considering that the estimated error was about 2% of the dimensions being measured, and that large standard deviations were obtained for percent average changes, this length scale was not useful for determining dimensional variation when making multiple molds or parts. According to product literature, the silicone should be expected to shrink 0.6% during curing. Detecting a 0.6% change over a 12 μm feature would mean differentiating 0.05 μm on the micrometer, a value well inside the estimated error of the measurement method. It was believed that at this scale, variations in measurement were most likely due to errors in the technique rather than actual deviations in dimensions. The fact that shrinkage numbers did not approximate expected values, combined with the large standard deviations at this scale resulted in low confidence in results at these lengths.

Measurements across the larger length scale (93 μm) yielded much better results. An average absolute shrinkage between silicon and silicone of 0.4 $\mu\text{m} \pm 0.2$ (0.4% ± 0.2) was measured, a value more in line with the expected silicone shrinkage. Values between silicon and wax were determined to be 0.9 $\mu\text{m} \pm 0.1$ (1.0% ± 0.1), while wax to fired measurements indicated a shrinkage of 14.3 $\mu\text{m} \pm 0.3$ (15.5% ± 0.3). Overall shrinkage from silicon to fired part was 15.6 $\mu\text{m} \pm 0.3$ (16.7% ± 0.3).

Measurements at the 93 μm length scale approximated expected results well. At this scale, the measurement errors were only about 0.2 % of the length scale. Porosimetry was conducted on green and fired ceramics and indicated a porosity of 59.7% (accounting for binder) and 98.3% respectively. Expected linear shrinkage of 15.31% was calculated using the equation:

$$1 - \left(\frac{\rho_g}{\rho_f} \right)^{1/3}$$

where ρ_g and ρ_f are the green and fired densities. This corresponded closely to the average row shrinkage between wax and fired ceramic of 15.5%, and was reasonably close to the individual feature shrinkage of 17.1%. Since shrinkage during firing was a function of the green and fired densities of the slurry, it is important to note that these values will change depending on the dispersion state of the suspension. The increased confidence in measurements over the 93 μm range indicated that any variation among separate parts could be determined accurately.

Measurements of the reproducibility of the process were performed on wax molds and fired parts. Silicone molding was not measured for reproducibility, as shrinkage was predictable from product literature, and the dimensional changes associated with curing were very close to the measurement error. Therefore, any deviation across silicone molds would most likely be below the detectable limit.

Since shrinkage data for wax molds was not available, measurements were made over five different molds to determine mold reproducibility. Changes in dimension between several different wax molds and the silicone mold are presented in Table 3-3. Ideally, dimensions from mold to mold would be exactly identical. The largest standard deviation across molds was found in Row 2, with a deviation of $\pm 0.2 \mu\text{m}$. Since this was within the estimated measurement error, this suggested that when making several molds from one silicone mold, over a 93 μm area dimensions could be reproduced to within $\pm 0.2 \mu\text{m}$. Actual and expected dimensions were also compared. Expected change was calculated based on the value of 1.0% shrinkage determined earlier. Figure 3-29 shows that over five different molds, dimensions over a 93 μm area could be predicted confidently to within $\pm 0.3 \mu\text{m}$, again within measurement error. This indicated that, if there was any variation among wax molds, it was below the detectable limit.

Five ceramic parts were produced and measured across the 93 μm length scale to determine final part dimension predictability. Dimensional changes across the parts are presented in Table 3-4. The largest dimensional deviation over parts was observed in row 3, with a standard deviation of $\pm 0.8 \mu\text{m}$. Ideally, there would be no fluctuation in

dimensions of a row from part to part. Based on an average expected silicon to fired shrinkage of 16.8%, final part dimensions between original silicon etching and fired ceramic fell within a $\pm 0.8 \mu\text{m}$ range over a $93 \mu\text{m}$ area (Figure 3-30), indicating that variation of part dimensions occurs during this phase of the process. Not surprisingly, this means that the ceramic forming step was limiting dimensional stability.

Mold Number	Absolute Change (μm)		
	Row 1	Row 2	Row 3
1	-0.8	-0.7	-0.9
2	-0.8	-0.7	-1.2
3	-0.9	-0.6	-1.1
4	-0.8	-1.0	-1.2
5	-0.9	-1.0	-1.0
Average Change (μm)	-0.9 ± 0.04	-0.8 ± 0.2	-1.1 ± 0.1
Expected Change (μm)	-0.9	-0.9	-0.9

Table 3-3 Dimensional Changes Across Multiple Molds Over $93 \mu\text{m}$

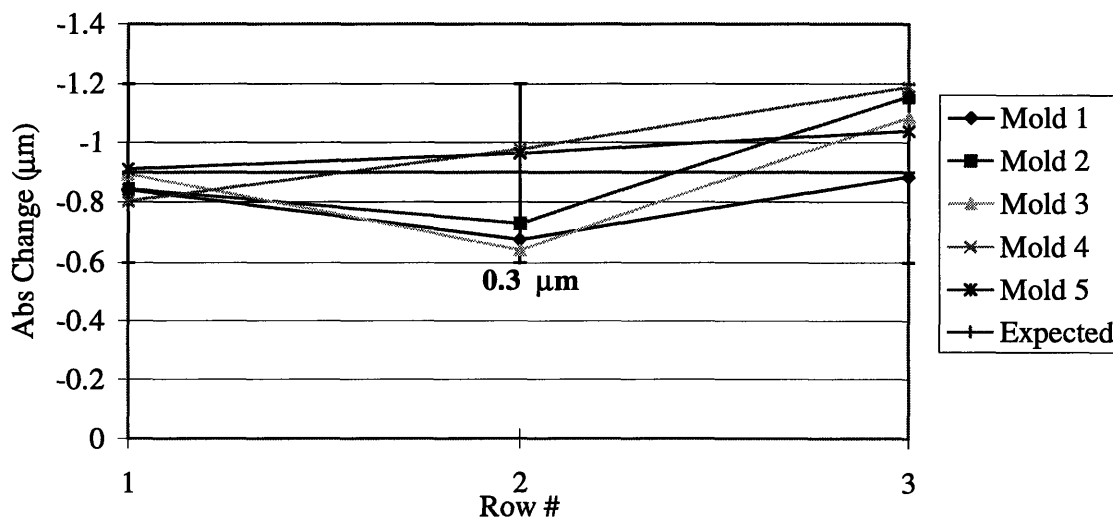


Figure 3-29 Actual and Expected Change Across Several Wax Molds Over $93 \mu\text{m}$

Part #	Absolute Change (μm)				
	Row 1	Row 2	Row 3	Row 4	Row 5
1	-15.2	-16.0	-15.4	-15.7	-15.8
2	-16.1	-15.1	-15.6	-16.0	-15.2
3	-16.0	-16.0	-16.3	-15.5	-16.1
4	-15.1	-15.6	-14.8	-15.6	-16.1
5	-15.8	-15.9	-16.5	-16.6	-16.6
Avg. Chng. (μm)	-15.6 ± 0.5	-15.7 ± 0.5	-15.7 ± 0.8	-15.8 ± 0.4	-16.0 ± 0.5
Avg. Chng. (%)	-16.7 ± 0.5	-16.8 ± 0.4	-16.7 ± 0.6	-16.8 ± 0.3	-17.0 ± 0.5
Exp. Chng. (μm)	15.6	-15.6	-15.7	-15.6	-15.68

Table 3-4 Dimensional Change Across Fired Parts Over 93 μm

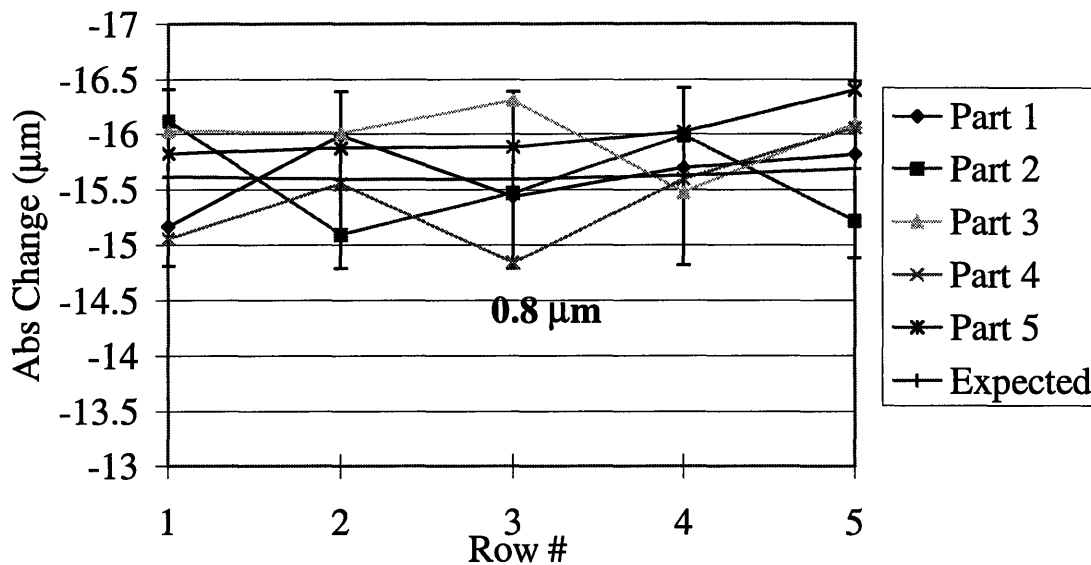


Figure 3-30 Actual and Expected Change Across Several Fired Parts Over 93 μm

Several factors contributed to the dimensional instabilities across the process. Unfortunately, accurate measurement of micron sized features was difficult and entailed a considerable amount of error. Because of this, dimensional stability across silicone and wax process steps was undetectable, as fluctuations appeared to be below the measurement error. Deviations in ceramic parts, however, were detectable, making the

ceramic processing step the limiting factor in predicting final part dimensions. This was not surprising, as there have historically been several issues regarding reproducibility in ceramic processing. Factors influencing shrinkage from green to fired states include the green density of the part, which is a function of dispersion state, drying conditions, and particle size distribution. Other factors contributing to shrinkage instabilities include sintering time and temperature.

Reasonable values for dimensional change were determined for the different process steps, although the measurement techniques used had a relative amount of uncertainty. Stability of the process up to the wax mold was determined to be predictable to within the estimated measurement errors (0.1 – 0.3 μm). A more accurate measurement technique is necessary to quantify stability of these steps further. Ceramic stability was found to be $\pm 0.8 \mu\text{m}$ over a 93 μm length scale. This translated into a non dimensional shrinkage of $8.6 \times 10^{-3} \mu\text{m}/\mu\text{m}$. This value extrapolated to the mesoscale would result in a variation of 86 μm over a 10000 μm length. This would suggest that the process was stable on the micron scale, but might be too unstable for a mesoscale device. Measurements over larger length scales should be performed to confirm stability at larger dimensions.

While the values obtained contained considerable amounts of errors, designers should be able to predict final part dimensions based on consistent slurry characteristics, processing conditions and silicon etching dimensions to within $\pm 0.8 \mu\text{m}$ over a 93 μm scale. Since ceramic processing was the limiting factor in reproducibility, optimizing processing conditions should result in a reduction of this value. This will allow designers to predict shrinkage and design accordingly to achieve the desired part dimensions.

3.2 Conclusion

This chapter has examined several aspects of the micromolding process which were important to understanding the mechanisms behind part defect formation. It has also examined the capabilities and limitations inherent in producing ceramic parts on a micron scale. Lastly, several design parameters have been established which will allow future users of the process to tailor their designs and achieve precise part dimensions.

Chapter 4

4.1 Cost Analysis

Cost is an important facet of part production. Production costs must be on a level where mass production is a viable option. A barrier to full scale production exists if the process is cost prohibitive. This section examines the major costs associated with making a ceramic part using the microforming process, namely tooling production.

This analysis focused on the tool production portion of the micromolding process, assuming that once a micromold was made, the actual ceramic forming process was the same. This was compared to the cost of a LIGA run, a technique that has proven to be capable of making high aspect micromolds for forming applications, but at a very high cost.

4.1.1 LIGA Processing

The high cost of facilities required to generate synchronous x-ray radiation is a barrier to wide scale LIGA mold production. Processing is done in a multi-user environment since only a few sources are available in the US. Multi-user processes are scheduled runs where several people share beam time and a common mask. LIGA processing is currently available to the public through a multi-user service such as the LIGA Multi-User MEMS Processes (LIGAMUMPs) provided by MCNC in Research Triangle Park, NC. This DARPA supported program sells 6.5 mm by 9 mm die sites with five dies delivered for \$900. A typical LIGA run has 20 dies on a 4" wafer. This process produces a 200 μm high nickel form, and is limited to minimum line widths of 20 μm and aspect ratios of 10.⁴¹

4.1.2 Deep RIE Processing

Processing prices for the MIT Microsystems Technology Laboratory were obtained and used in this analysis. Various clean room processing steps are priced in process units, each unit being \$5.75. Costs for a typical DRIE run of one 4" wafer with 20 dies is compared on a die by die basis to LIGA. Table 4-1 provides an estimated breakdown of the costs associated in producing a 4" wafer (staff produced costs are used to include labor). Only processing steps which incur costs are included in the table. The cost of the photolithography mask was considered negligible, as it could be used many times. It was assumed that a photolithography mask for LIGA would cost the same, although the x-ray mask used in the synchrotron represented an additional cost of \$5000. This amount was factored into the public selling price, but still represented a capital investment beyond that required for the micromolding process.⁴²

Process Step/Material	Step Cost (1 unit =\$5.75)	Per Wafer Cost	Per Die Cost
Photo Aligner	9 / Wafer	\$51.75	\$2.59
Developer	32 / 25 Wafers	\$7.36	\$.37
STS Etcher	30 / Wafer	\$172.50	\$8.63
Total		\$231.61	\$11.59

Table 4-1 Clean Room Costs for a Typical DRIE Process Run

4.2 Cost Comparison

A LIGA run costing \$900 for five dies translated into a cost of \$180 per die. Processing of a 4" wafer in the MTL facilities was estimated to cost \$231.61 per wafer. With 20 dies per wafer, a die cost of \$11.59 was realized for a savings of almost 94%. It should also be noted that both the LIGAMUMPS program and the MTL are supported by DARPA to offset the high costs. This comparison was made on a single wafer basis, and

processing costs can be expected to drop dramatically in a bulk manufacturing environment.

Deep RIE processing can be used to produce micromolds for ceramic forming at a significant cost savings. The process has demonstrated the ability to produce complex high aspect ratio molds, which can be used to make ceramic microforms. Not only is Deep RIE less expensive, but is also compatible with current processing methods, and can utilize the current industry infrastructure.

Chapter 5

5.1 Future work

A process for making ceramic parts with micron scale features has been developed which uses basic photolithography techniques. This process was inexpensive in comparison to other forming processes, and was relatively simple to perform. It has evolved from a crude forming technique to a viable alternative for making MEMS components, although the process still has room for improvement. There is still much work to be done before this process can have commercial potential.

5.2 Process Improvement

The micromolding process has demonstrated the ability to make ceramic parts, although there are still many issues which need to be resolved. The process must undergo refinement before it will be capable of producing parts on a large scale. Work is required in the area of quality control, yield improvement, and scale up.

5.2.1 Quality Control

A full understanding of defect formation is necessary to produce high quality parts. Defects observed in PZT fibers demonstrated that a well dispersed slurry will create shrinkage voids in the green parts. Experiments have shown that slurry properties can greatly affect the outcome of the final part, from defect formation to dimensional stability. A partially flocced slurry has been observed to perform better than a well dispersed one. Observations have also been made that indicate that solvent based slurries wet the molds better than aqueous ones. A complete investigation of the effect of slurry properties on part quality should be performed, determining the optimum balance of dispersion state and mold/slurry compatibility.

5.2.2 Yield Improvement

Improving part quality will be an important aspect of increasing yield, although another important advance will be in the refinement of process steps. The process can be made more efficient by eliminating handling steps and improving firing techniques. The ability to place the wax mold and cast part directly into the furnace for wax removal, binder burnout, and firing would resolve major part handling issues. This would eliminate the need to remove the part from the wax melt substrate and transfer it to the firing crucible. Elimination of physical handling steps should dramatically decrease breakage of green parts. While this is not as much an issue for parts with larger overall dimensions, small fragile pieces, such as PZT fibers, would greatly benefit from this improvement. Development of microsetters and firing schedules to reduce warpage will also increase yield of usable parts.⁴⁰

5.2.3 Scale Up

The process must be able to produce large quantities of product to become a viable manufacturing tool. Scaling up of the process is crucial to the commercial adoption as a forming technique. Several modifications could be made to the process to facilitate this.

A setup for continuously producing PZT fibers is proposed in Figure 5-1. Wax molds could be produced in a continuous fashion by using the silicone (or other material) master mold to emboss a steady feed of molding material. Such large molds could contain long lengths of fibers, or several thousands of small parts, into which a ceramic slurry could be continuously cast. This process would be very similar to a tape casting operation, except the carrier film would be the patterned wax mold. Several casting heads could be located in series to ensure complete filling of the molds. Large sections of filled wax molds could be placed in a furnace for wax melting, binder removal, and firing. This is but one approach that could be used to mass produce PZT fibers.

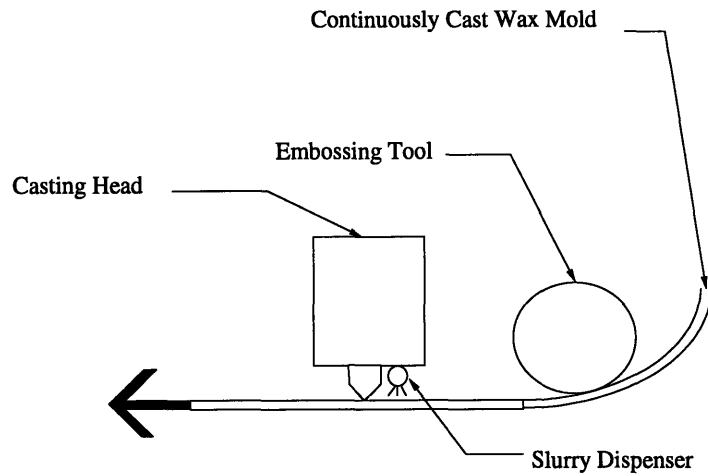
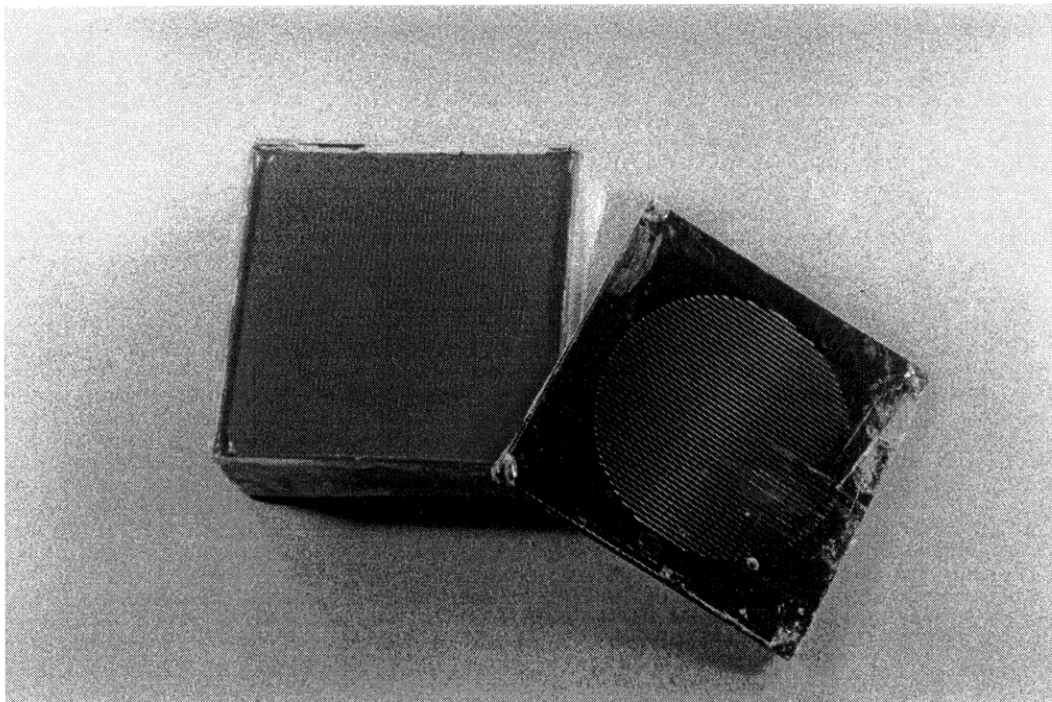


Figure 5-1 Proposed Continuous Casting Setup for PZT Fibers

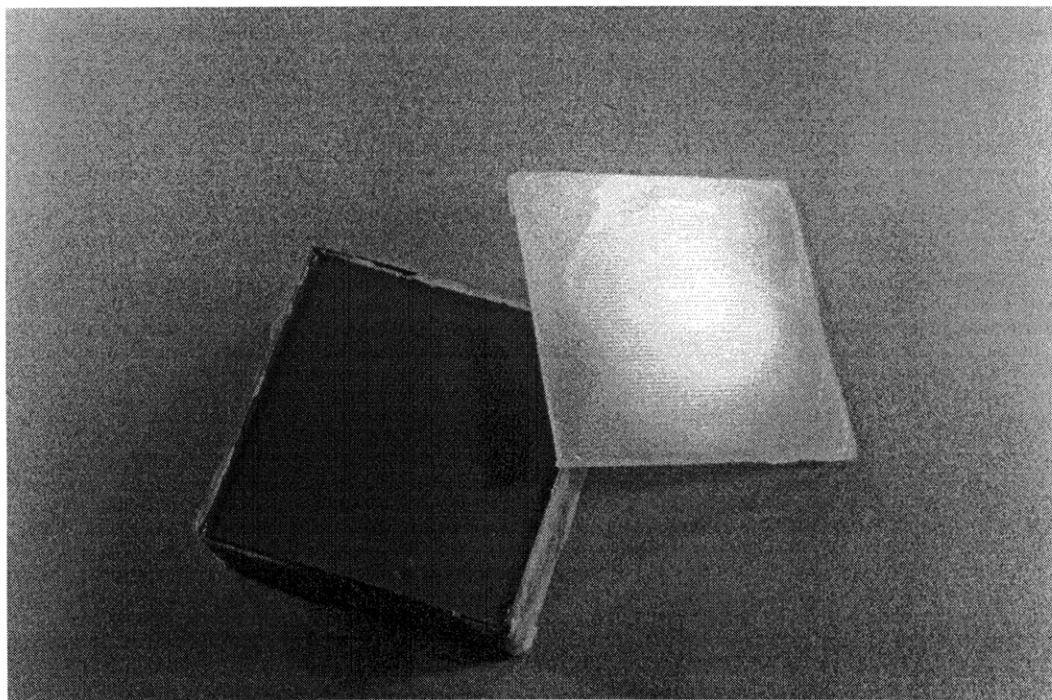
5.3 Conclusion

The micromolding process has demonstrated the ability to create MEMS and mesoscale ceramic parts with micron scale features through a series of mold transfers and slurry casting. This low cost, easy to perform method is competitive with other forming techniques being used to create ceramic parts with micron scale features. Reusable tooling, accurate reproduction, and dynamic flexibility give this process potential to evolve into a major forming avenue for MEMS and mesoscale components. Excellent results were obtained and basic phenomena understood. While there are still several developmental issues to be resolved, the microforming process shows much promise as a viable ceramic forming tool for MEMS and mesoscale applications.

Appendix A Micromold Tooling

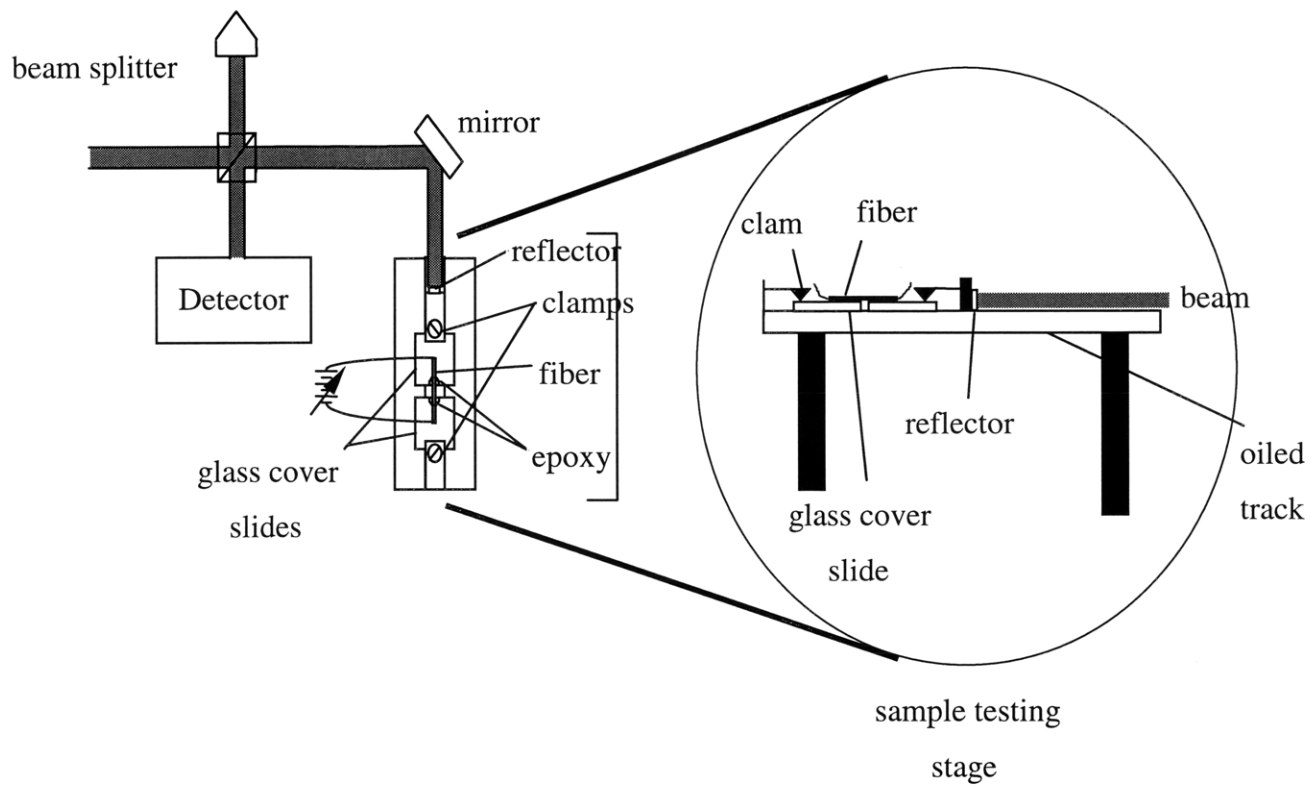


Silicone and Silicon Micromolds



Silicone and Wax Micromolds

Appendix B Fiber Testing Apparatus



Bibliography

- ¹ M. K. Raymond. "Making the Cut for Small Parts". *American Machinist*. Vol. 140, No. 2. Feb. 1996. pp. 40-1
- ² Analog Products – ADXL 50 Data Sheet. Analog Devices WWW Page. <http://products.analog.com/products/info.asp?product=ADXL50>
- ³ H. Wisniowski. "Analog Devices Puts Micromachines In Motion". Analog Devices WWW Page. 1998. <http://www.analog.com/iMEMS/mpd/xbckgdr4.html>
- ⁴ Rai-Choudhury, P. Ed. *Handbook of Microlithography, Micromachining, and Microfabrication*. Vol. 2. SPIE Optical Engineering Press, 1997.
- ⁵ Texas Instruments – Digital Light Processing. Texas Instruments WWW Page <http://www.ti.com/dlp/main.html>
- ⁶ L. A. Yoder. "The State of the Art in Projection Display: An Introduction to the Digital Light Processing (DLP™) Technology". Texas Instruments WWW Page, 1998. <http://www.ti.com/dlp/docs/business/resources/white/state/state.htm>
- ⁷ A. H. Epstein. "Micro Heat Engines, Gas Turbines, and Rockets –The MIT Microengine Project". Presented at MEMS Research and Applications in Microelectromechanical Systems, MIT. Cambridge, MA. Mar. 31- Apr. 1, 1998.
- ⁸ DARPA Mesoscale Machines for Military Applications. Announcement #:BAA98-21, Mar. 11, 1998. <http://www.darpa.mil/baa/baa98-21.htm>
- ⁹ R. W. Davis Jr., B. B. Kosicki, D. M. Boroson, and D. E. Kostishack. "Micro Air Vehicles for Optical Surveillance". *The Lincoln Lab Journal*. Vol. 9, No. 2, 1996, pp. 197-214.
- ¹⁰ P. Gravesen, J. Branebjerg, O. Jensen. *Journal of Micromechanical Microengineering*. Vol. 3, 1993. pp168-72.
- ¹¹ R. Srinivasan, I-M. Hsing, P. Berger, S. Firebaugh, K. Jensen, and M. Schmidt. "Micromachined Chemical Reactors for Heterogeneous Catalytic Partial Oxidation Reactions". Submitted to the *AICHE Journal*. May, 1997.
- ¹² M. Holmquist, R. Lundberg, T. Razzell, O. Sudre, L. Molliex, and J. Adlerborn. "Development of Ultra High Temperature Ceramic Composites for Gas Turbine Combustors". Presented at the International Gas Turbine & Aeroengine Congress & Exhibition. ASME 97-GT413, 1997.

-
- ¹³ M. vanRoode, W. D. Brentnall, K. O. Smith, B. D. Edwards, J. McClain, J. R. Price. "Ceramic Stationary Gas Turbine Development Program – Fourth Annual Summary". Presented at the International Gas Turbine & Aeroengine Congress & Exhibition. ASME 97-GT-317, 1997.
- ¹⁴ K.S. Chen. Department of Mechanical Engineering, MIT. Personal Correspondence, May 1998.
- ¹⁵ D. Richerson. *Modern Ceramic Engineering*. Second Edition, Marcel Dekker, Inc. 1992.
- ¹⁶ L. Weber, W. Ehrfeld, H. Ffeimuth, M. Lacher, H. Lehr, and B. Pech. "Micro Molding – A Powerful Tool for the Large Scale Production of Precise Microstructures". *Proceedings of the SPIE – The International Society for Optical Engineering*, Vol. 2879, pp. 156-67.
- ¹⁷ F. Mason. "MCs for Small, High-Precision Parts". *American Machinist*. Vol. 136, No. 9. Sept. 1992. pp. 65-8.
- ¹⁸ R. Ruprecht, T. Hanemann, V. Piottter, and J. HauBelt. "Injection Molding of LIGA and LIGA-similar Microstructures". *MID 96 Molded Interconnect Devices*. 2nd International Congress, Sept. 1996. pp. 265-74.
- ¹⁹ H. Ferimuth, V. Hessel, H. Kolle, M. Lacher, and W. Ehrfeld. "Formation of Complex Ceramic Miniaturized Structures by Pyrolysis of Poly(vinylsilazane)". *Journal of the American Ceramic Society*. Vol. 79, No. 6, June 1996. pp. 1457-65.
- ²⁰ R. Knitter, E. Gunther, U. Maciejewski, C. Odemer, and Karlsrukr. "Preparation of Ceramic Microstructures". *Ceramic Forum International : CFI : Berichte der DKG*. Vol. 71, No. 9, 1994. pp. 549-56.
- ²¹ Costello, K. Chand Kare Technical Ceramics. Personal correspondence, Apr. 1998.
- ²² B. Beuschens. Westford Laser Services Inc. Personal correspondence. Mar. 1998.
- ²³ C. Van Hoy, A. Barda, M. Griffith, and J. W. Halloran. "Microfabrication of Ceramics by Co-extrusion". *Journal of the American Ceramic Society*. Vol. 81, No. 1, Jan. 1998. pp. 152-58.
- ²⁴ J. Bride, S. Baskaran, N. Taylor, J. Halloran, W. Juan, S. Pang, and M. O'Donnell. "Photolithographic Micromolding of Ceramics Using Plasma Etched Polyimide Patterns". *Applied Physics Letters*. Vol. 63, No. 24, Dec. 1993. pp. 3379-81.

-
- ²⁵ MEMS TechNet: Deep Si RIE. MEMS Technology Applications Center WWW Page. <http://mems.mcnc.org/technet/deeprie.html>
- ²⁶ J. Bhardwaj, H. Ashraf, and A. McQuarrie. "Dry Silicon Etching for MEMS". Presented at the Symposium on Microstructures and Microfabricated Systems at the Annual Meeting of the Electrochemical Society. Montreal, Quebec, Canada. May 4-9, 1997.
- ²⁷ A. A. Ayón, C. C. Lin, R. A. Braff, M. A. Schmidt, R. Bayt, and H. H. Swain. "Etching Characteristics and Profile Control in a Time Multiplexed Inductively Coupled Plasma Etcher". To be presented at 1998 solid state sensor and actuator workshop, Hilton Head, South Carolina, June 1998.
- ²⁸ MicroElectroMechanical Systems. Surface Technologies Systems WWW Page. Courtesy of the MEMS Technology Applications Center at MCNC. <http://www.stsystems.com/mems.html#mems>
- ²⁹ S. Limb, D. Edell, E. Gleason, and K. Gleason. "Pulsed Plasma-Enhanced Chemical Vapor Deposition from Hexafluoropropylene Oxide: Film Composition Study". *Journal of Applied Polymer Science*. Vol. 67, No. 8, Feb. 1998. pp. 1489-502.
- ³⁰ A. Bent. "Active Fiber Composites for Structural Actuation". Ph.D. Thesis, Massachusetts Institute of Technology, 1997.
- ³¹ M. Pasucci. CeraNova Corporation, Hopedale, MA. Personal correspondence, May 1998.
- ³² W. Coburn. Staveley Sensors, East Hartford, CT. Personal correspondence, May 1998.
- ³³ A. Prazan. MIT Summer UROP Project, 1997.
- ³⁴ C. Hiwa, A. Baba, and T. Nakagawa. "Strength of Composites with Fibers Having Expanded Ends". *Journal of the Society of Materials Science, Japan*. Vol. 41, No. 464, May 1992. pp. 687-93.
- ³⁵ K-S. Chen. Department of Mechanical Engineering, MIT. Personal Correspondence, Mar. 1998.
- ³⁶ S. Firebaugh. Department of Electrical Engineering and Computer Science, MIT. Personal Correspondence, Mar. 1998.

-
- ³⁷ S. Fan, P. Villeneuve, J. Joannopoulos. "Large Omnidirectional Band Gaps in Metallodielectric Photonic Crystals". *Physical Review*. Vol. 54, No. 6, Oct. 1996. pp. 11264-11251.
- ³⁸ R. Chiu and M. Cima. "Drying of Granular Ceramic Films: II Drying Stress and Saturation Uniformity." *Journal of the American Ceramics Society*. Vol. 76, No. 11. Nov. 1993. pp 2769-2777.
- ³⁹ H. Takahashi, N. Shinohara, M. Okumiya. "Influence of Slurry Flocculation on the Character and Compaction of Spray-Dried Silicon Nitride Granules". *Journal of the American Ceramics Society*. Vol. 78, No. 4. Apr. 1995. pp. 903-908.
- ⁴⁰ M. Tupper, M. Rosenthal, A Prazan, M. Cima. Unpublished results.
- ⁴¹ Multi-User LIGA at MCNC WWW Page. Jan. 1998. <http://mems.mcnc.org/liga3.html>
- ⁴² A. Cowen. MCNC Center. Personal Correspondence. Mar. 1998.